**Tomás Rosa Calmeiro**

Bachelor of Science in Biology

# Atomic force microscopy assisted with electron and ion beam microscopy for the direct measurement of biostructures and DNA samples

Dissertation to obtain a Master degree in Biotechnology

Supervisors: Tito Busani, Research Professor, University of New Mexico

José Ricardo Ramos Franco Tavares, Assistant Professor, Universidade Nova de Lisboa

Jury:

President: Pedro Miguel Ribeiro Viana Baptista, Associate Professor

External Examiner: Peter Jonathan Eaton, Associate Researcher

FACULDADE DE CIÊNCIAS E TECNOLOGIA
UNIVERSIDADE NOVA DE LISBOA

**September 2013**

**Tomás Rosa Calmeiro**

Bachelor of Science in Biology

# Atomic force microscopy assisted with electron and ion beam microscopy for the direct measurement of biostructures and DNA samples

Dissertation to obtain a Master degree in Biotechnology

Supervisors: Tito Busani, Research Professor, University of New Mexico

José Ricardo Ramos Franco Tavares, Assistant Professor, Universidade Nova de Lisboa

Jury:

President: Pedro Miguel Ribeiro Viana Baptista, Associate Professor

External Examiner: Peter Jonathan Eaton, Associate Researcher

FACULDADE DE CIÊNCIAS E TECNOLOGIA
UNIVERSIDADE NOVA DE LISBOA

**September 2013**

**Atomic force microscopy assisted with electron and ion beam microscopy for the direct measurement of biostructures and DNA samples**

## Resumo

Nesta dissertação apresenta-se estudos no campo da biotecnologia através de microscopia de força atómica (AFM), uma técnica normalmente associada a ciências de materiais. Apresenta-se, com especial destaque elementos de biologia molecular e bionanotecnologia. Analisou-se ADN, insulina e enzimas de restrição como objectos isolados, a fim de documentar propriedades como morfologia ou comportamento, e também no contexto das interacções entre si. Analisou-se com especial atenção a interacção entre ADN e a endonuclease EcoRV. O estudo de nanopartículas de ouro pretendeu estabelecer uma relação entre a funcionalização desta e a medição do aumento do diâmetro médio por AFM. Dada a natureza destes objectos de estudo, modificaram-se e avaliaram-se tanto protocolos de imobilização como de preparação, considerando medições ao ar ou em líquido. Para alcançar o objectivo de desenvolver medidas com maior sensibilidade e resolução aumentada, modificaram-se pontas de AFM através de revestimentos metálicos e microscopia electrónica de varrimento assistida com focagem de feixe de iões. Testes feitos com estas pontas confirmaram o sucesso das modificações e que estas estavam funcionais, confirmando-se isto através da aquisição de medidas e imagens mais sensíveis e de qualidade superior, quando comparadas com pontas que não foram modificadas.



Palavras-chave: Microscopia de força atómica, AFM, bionanotecnologia, interacções DNA-proteína, modificações de pontas de AFM, Focagem de feixes de iões

## Abstract

Studies of atomic force microscopy (AFM), a technique commonly associated with material sciences, in the field of biotechnology, with special emphasis on molecular biology and bionanotechnology elements, are presented herein. DNA, insulin and restriction enzymes were analysed as isolated objects, in order to document properties like morphology and behaviour, and also on the interactions between each other. The interaction between DNA and the EcoRV restriction endonuclease was especially highlighted. Gold nanoparticles were also studied in an attempt to establish a relationship between functionalization and average diameter shifts, as perceived by AFM. Given the nature of these objects of study, both immobilization and preparation protocols were modified and evaluated, considering measurements in air or in liquid. To serve the objective of developing probes with higher sensitivity and resolution, especially for liquid measurements, AFM cantilevers were modified through metallic coatings and scanning electron microscopy assisted with focused ion beam (SEM-FIB). Tests performed with these probes confirmed that the modifications were successful, the probes are functional and can aid in the production of better quality images, through the acquisition of sharper data in comparison with non-modified probes.



Keywords: Atomic Force Microscopy, AFM, bionanotechnology, DNA-protein interaction, AFM probe modifications, Focused Ion Beam

# Table of contents

Resumo ..... III

Abstract ..... V

Acknowledgments ..... XIX

Abbreviation list ..... XXI

1. Motivation and objectives of this dissertation ..... 1

1.1. Motivation for microscopy developments ..... 1

1.2. Objective of the experimental work of this dissertation ..... 3

2. Nanotechnology in biological sciences: analytical tools ..... 5

2.1. Microscope types, basic physics of operation and limitations ..... 5

2.2. Beyond visible light: Electron Microscopes ..... 6

2.3. The Scanning Electron Microscope and its potentialities ..... 7

2.3.1. Focused ion beam ..... 10

2.4. The first Scanning Probe Microscope ..... 11

2.5. Atomic Force Microscopy: origins, instrumentation, basic principles of operation, advantages and disadvantages ..... 12

2.5.1. Origins of the AFM ..... 12

2.5.2. Instrumentation ..... 12

2.5.2.1. Piezoelectric actuators ..... 13

2.5.2.2. Force transducers ..... 14

2.5.2.3. Feedback control ..... 14

2.5.2.4. Force Curves ..... 15

2.5.3. Channels of acquisition ..... 15

2.5.4. The probe ..... 16

2.5.5. Artefacts ..... 17

2.5.6. Main advantages over microscopy techniques ..... 19

2.5.7. AFM Contact Mode ..... 20

2.5.8. AFM Non-contact and Intermittent Contact Modes ..... 21

3. Atomic Force Microscopy applied to DNA, proteins DNA-protein and nanoparticle-protein interactions .....25

3.1. AFM in liquid media and force spectroscopy .....25

3.2. Phase mapping versus topographic mapping: why is it so useful in biological sample imaging?.....28

3.3. AFM tip modifications and relation to resolution of an AFM.....30

4. Modification of AFM probes.....35

4.1. Focused ion beam milling to enhance lateral resolution .....35

4.1.1. Contact mode tip modification with FIB SEM.....35

4.1.2. Lateral resolution results and comparison.....37

4.1.3. Gold-Palladium coating of tips and horizontal resolution comparison.....39

4.1.4. Gold-palladium coating of AFM probe backside to enhance photodiode detection 40

5. AFM comparison studies – Insulin and gold nanoparticle conjugates .....43

5.1. AFM measurement and analysis of amyloid insulin .....43

5.1.1. Overview on insulin and rationale for selecting this hormone .....43

5.1.2. Results of AFM measurements and analysis.....44

5.1.3. Discussion and comparison between air and liquid acquisition .....46

5.2. AFM measurements of uncoated and functionalized gold nanoparticles .....47

5.2.1. Gold nanoparticles and their application to bionanotechnology.....47

5.2.2. Development of AFM measurement protocol.....48

5.2.3. Results of gold nanoparticle measurements: average height shifts.....50

5.2.4. Discussion of gold nanoparticle results.....52

6. AFM measurements of DNA.....55

6.1. HRPII plasmid DNA.....55

6.2. DNA preparation for AFM measurements.....55

6.3. Results of DNA measurements.....56

6.3.1. Plasmid conformation and first comparison between topography and phase acquisition .....56

6.3.2. Morphology and dimensions of DNA: width vs. height, topography vs. phase, high resolution imaging and plasmid sequence length prediction ..... 59

6.4. Discussion of DNA results ..... 61

6.5. Comparison between single (ssDNA) and double stranded DNA (dsDNA) imaging under AFM ..... 64

6.5.1. Difference between ssDNA and dsDNA and preparation for AFM ..... 64

6.5.2. Results and discussion of ssDNA imaging ..... 65

6.6. Measurements of plasmid DNA undergoing EcoRV digestion ..... 67

6.6.1. Overview on restriction enzymes, on EcoRV and objective ..... 67

6.6.2. Preparation of the DNA-EcoRV measurement ..... 68

6.6.3. Results of the DNA-EcoRV reaction ..... 70

6.7. Discussion ..... 75

7. Conclusions ..... 77

8. Future prospects ..... 81

9. References ..... 83

I. Appendix ..... i

a. Material and methods ..... i

i. General information on equipment, operation and facilities ..... i

ii. AFM probe index ..... ii

iii. AFM probe modifications ..... ii

iv. Insulin measurement conditions ..... ii

v. Material and methods of gold nanoparticle functionalization ..... iii

vi. Material and methods of DNA related experiments ..... iii

# Index of equations

Equation 2.1 – Resolution of a system dependent from wavelength. .....5
Equation 2.2 - Equation for Hooke's Law .....20
Equation 2.3 - Equations for amplitude and resonance frequency shifts.....22
Equation 3.1 Simplified equation of Bustamante *et al.* for a simple spherical tip shape 32
Equation 3.2 Prediction of the width of a structure with a Rs radius when measured with a tip with Rp radius. .....32

## Index of Figures

Figure 2.1 – Basic schematic and components of operation of a SEM. .....8

Figure 2.2 - Schematic of the interactions between elements that give birth to secondary electrons (SE), backscattered electrons (BSE) and emission of X-rays (X-ray) in SEM imaging. Orange circles represent electrons while the grey circles the atom nucleus. .....10

Figure 2.3 – Diagram of FIB milling of a surface (exemplified as an AFM probe) by sputtering with a focused ion beam. The collision of the ion beam with the surface results in the sputtering of surface atoms, together with beam atoms and secondary electrons. .....11

Figure 2.4 – Simplistic schematic of an AFM's using an optical lever as force transducer. .....13

Figure 2.5 – Simplified force-distance curve for the interaction of an AFM probe and a sample. .....15

Figure 2.6 – Topographic (A), amplitude (B) and phase (C) images of the surface of a human hair. .....16

Figure 2.7 – Schematic of a chip with an AFM probe. The chip can be locked in the AFM and the cantilever is left protruding, with the probe ready to interact with the sample. ....16

Figure 2.8 – Tip related artefacts and their effects on image quality. Because images are convolutions of tip geometry, when a tip fractures in unexpected manners, it can produce odd features, such as spherical structures becoming triangular (A). Contaminations on the sample can also be dragged by the tip, leading to images with both good quality and bad quality sections alternated (B). If a tip picks up contaminants or breaks in two, resulting in two structures touching the sample at the same time, this can lead to the appearance of multiple images of the same feature (C) compared to an image clear of artefacts (D). .....18

Figure 2.9 – Examples of drift. Both the spherical nanoparticles (A) and the spherical liposomes (B) appear as elongated features. .....19

Figure 3.1 – Thermal capture of an Olympus BC-AC40TS both in air and liquid. The main resonant peak shifts from approximately 100 kHz to 25 kHz and a broadening in the peak (lower Q factor) occurs. .....27

Figure 3.2 – Force curve acquired by inward force spectroscopy on a protein, with detail of the effect on cantilever bending at near setpoint zero (squared area). Setpoint zero refers to the height from the sample at which the feedback control acknowledges the standard tip-sample distance for imaging and switches the *z*-axis control on. In this case, its refers to the height in which net attractive forces were first detected. .....28

Figure 3.3 – Effect of changing different wave variables compared to the original wave signal. The waves in the bottom are overlapped with the standard wave (which also appears

above them) and have similar parameters, except for amplitude, frequency and phase, respectively. .....29

Figure 3.4 – Difference between topographic and phase imaging. The scale on the topographic image (A) was selected using the automatic scaling given by the AFM software. It can be seen that no DNA can be observed due to the existence of features several times larger than its height, which mask it. However, using phase imaging (B) makes it possible to observe subtle DNA molecules in the same area. .....30

Figure 3.5 - Simulation of aliasing of the UNL logo. The first image is the original, the second one averages the colour value of each 4 pixels into 1, the third one each 16 pixels into one and the fourth each 64 pixels into one. .....33

Figure 4.1 - Scanning electron microscope image of AFM probes after milling with the focused ion beam. .....36

Figure 4.2 – 3D rendering of the FIB generated comparison feature. .....37

Figure 4.3 - Results of operation with FIB milled probe. Topographic image of the comparison feature when done with an unmodified probe (A) and with the FIB milled probe (B) and respective height profiles.....38

Figure 4.4 – Elemental maps of the probe's tip by EDS. A: Elemental map of silicon. B: Elemental map of gold. .....39

Figure 4.5 - Images produced by unmodified and coated probes were done in the same area of a silicon surface, marked with a red rectangle (A). Topographic images of this area done with an unmodified probe (B) and with a coated probe (C), as well as amplitude imaging done with an unmodified probe (D) and with a coated probe (E) are presented together with RMS values. .....40

Figure 4.6 - Comparison between topographic images of DNA molecules done with an uncoated probe (A) and a probe with its backside coated (B).....41

Figure 5.1 - A: Topographic image of amyloid insulin, both in aggregate and in fibril form. B: stretched insulin fibrils.....44

Figure 5.2 – Topographic image and height profile example of the structural periodicity observed in insulin fibrils acquired in air. .....45

Figure 5.3 – Height profile of an insulin fibril measured in air.....45

Figure 5.4 – Comparison of box plots of insulin widths and heights measured in air and in liquid media. .....45

Figure 5.5 - Insulin fibrils measured in liquid. Red arrows mark the structural periodicity. .....46

Figure 5.6 One of the many citrate crystals that grew from the deposited nanoparticle solution (A). These masked the nanoparticles but in some situations it was possible to detect spherical particles entrenched in the crystal using phase imaging (arrows on B). .....50

Figure 5.7 - Examples of topographic imaging of different batches of conjugates. .....51
Figure 5.8 - Box plots of nanoconjugate diameter distributions as measured by the three indicated methods.....52
Figure 6.1 - Topographic image of DNA molecule acquired in liquid with Olympus TR800PB probe.....57
Figure 6.2 - Topographic image of several HRPII plasmids (A) and detail of one of these molecules where the circular configuration can be seen (B). .....58
Figure 6.3 - Schematic on the reason why DNA, being a cylindrical molecule, appears with different values when acquired on the *z* axis (height) and on the *x0y* plane (width) due to convolution effects. .....58
Figure 6.4 - A clear difference in the sharpness of the DNA boundaries can be seen when comparing between topographic acquisition (left image) and phase acquisition (right image). .....59
Figure 6.5 - Topography of a DNA molecule where a pattern repetition can be observed. .....60
Figure 6.6 – Box-plot of the distance between crests measured on the DNA molecule. 61
Figure 6.7 – Images of a DNA molecule with the areas selected for pitch distance studies marked. These were used to produce the height profiles and the box-plot graph. .....61
Figure 6.8 – Average width values measured for the different probes used in the experiment in nanometres. 'Average res.' refers to AC160TS probes, 'High res. unmod' to the unmodified SSS-NCH and 'High res. mod' to the gold-palladium coated SSS-NCH. Topography and phase refers to the channels in which the measurements were obtained. .....64
Figure 6.9 - Topographic images of aggregated ssDNA molecules as a result of DNA melting and intra and inter-strand homology. In A, a detail of the condensed structure can be seen while in B several DNA aggregates can be observed. .....65
Figure 6.10 Phase imaging of ssDNA condensing around contaminants. These appeared both as long and thin objects with boundaries in white (A) and globular objects (B, pointed by arrows). .....66
Figure 6.11 Topographic images of DNA plasmids and EcoRV units, marked as white arrows. As can be seen by the lower magnification (A) and higher magnification image (B), EcoRV units appear as bright dots which can be both associated with DNA or unbound on the substrate. .....70
Figure 6.12 EcoRV units seem to have rough surfaces, both when measured in the topographic channel (A) and in the phase channel (B). Background was removed to aid in the observation of differences on the EcoRV unit, shortening the height scale in the process. .....71

Figure 6.14 – Phase image (A) and diagram (B) of the DNA-EcoRV conjugate. The red arrow in the phase image marks the zone where DNA was cleaved and the white one the location of the EcoRV unit. .....72

Figure 6.13 Topographic (A) and phase (B) imaging of an EcoRV aggregate resting against the substrate. .....72

Figure 6.15 – Examples of possible DNA-EcoRV cleavage complexes. The squared area in images A and B shows the areas which generated images C and D. Bend angle measurements were done in these, as represented by the yellow lines in images G, H, I and J. Images. E and F represent schematics of these complexes. .....74

Figure I.1 – Microscope equipment used in this dissertation's experiments: the AFM Asylum Research MFP-3D Stand Alone(A) and the dual beam SEM-FIB Zeiss Airuga (B). ..... i

Figure I.2 – Transmission electron microscope image of the gold nanoparticles before functionalization..... iv

## Index of tables

Table 5.1 - Means and standard deviations of nanoparticle conjugate diameters as calculated by the indicated methods and difference between mean values obtained for AuNP-MUA and AuNP-MUA-BSA conjugates. All values are in nanometres. .....51

Table I.1 – Specifications of AFM probes used in this dissertation as advertised by manufacturers. ..... ii

## Acknowledgments

To Tito Busani for taking me as his student, for teaching me the basics of AFM operation and instrumentation, for answering all the questions, for standing by me when I needed, for reviewing the dissertation, especially the parts related to physics, and overall for being a friend with whom many hours were spent in the laboratory.

To Ricardo Franco for taking me as his student, for planning the biotechnological component of the dissertation together with me and Tito, and for sharing his remarkable know-how in bionanotechnology. I am also thankful for the exhaustive reviewing and corrections of the dissertation, especially in the biological oriented experiments.

To Joana Vaz Pinto for selflessly finding the time and availability to review some chapters of this dissertation, pointing some mistakes, making some suggestions and answering and explaining some more advanced doubts in Physics. Thank you for the time working together and for sharing your invaluable knowledge with a permanent smile on your lips.

To Inês Gomes, João Luz and Tiago Monteiro, from Bionano@requimte, for the good times in their company and for their aid in the nanoparticle functionalization and DNA isolation.

To Ann-Katrinn Awizio and Friedhelm Freiss from AtomicForce F&E GmbH (Asylum Research) for the outstanding and joyful support, for taking the time to teach me liquid mode operation, force spectroscopy and advanced AFM modes, as well as answering all the weird questions of an AFM initiate without laughing.

To Pedro Viana Baptista for allowing me to extract DNA in his laboratory (Centro de Investigação em Genética Molecular Humana, FCT-UNL). My thanks also go to Pedro Pedrosa and Bruno Viegas for guiding me throughout the original DNA extraction protocol whenever I needed.

To Elvira Fortunato, for allowing me unrestricted access to the facilities of CENIMAT/I3N, especially to the atomic force microscope. I also wish to thank the rest of the CENIMAT/I3N crew for their warm welcoming and for receiving me as one of them.

To Sara, because actions speak louder than words.

To Family, for always being there, it doesn't matter if I did or didn't need it. Thanks for the blind support throughout all these years and for making me who I am (deal with it!). Thanks to Simão, for randomly waking up at 4 am and, upon realizing I am awake, happily strolling to me like it's the best moment of his entire week.

# Abbreviation list

AC – Alternate Contact

AFM – Atomic Force Microscope/Microscopy

AuNP(s) – Gold Nanoparticle(s)

BSA – Bovine Serum Albumin

BSE – Backscattered Electrons

DNA – Deoxyribonucleic Acid (ds – double stranded; ss – single stranded)

EDS – Energy Dispersive X-Ray Spectrometry

FIB – Focused Ion Beam

MEMS – Microelectromechanical systems

MUA – Mercaptoundecanoic Acid

PDB – Protein Data Bank

SE – Secondary Electrons

SEM – Scanning Electron Microscope/Microscopy

SPM – Scanning Probe Microscope/Microscopy

STM – Scanning Tunnelling Microscope/Microscopy

TEM – Transmission Electron Microscope/Microscopy

# 1. Motivation and objectives of this dissertation

## 1.1. Motivation for microscopy developments

In some science fields, such as pure mathematics, advances in knowledge and new findings can depend uniquely on the development of new theories and hypothesis. This particularity arises from their abstract nature or near independence of equipment. However, this is not true for all fields of study. Biology, especially some of its subdisciplines like microbiology or molecular biology, are flagrant cases of fields of study that have always been highly dependent of advances in other fields.

Only after some phenomena were discovered and some devices invented, it was possible for biologists to develop their own new methods and protocols to study their targets of interest. It's almost like saying that, in some situations, we must first wait for physicists, mathematicians or chemists to study, propose and develop novel methods of study and analysis before biologists have the proper tools to prove or disprove their own theories.

On another hand, curiosity is a defining attribute of the human species. Apart from biological reasons (such as the development of human intelligence derived from the evolution of the brain), it is the fundamental attribute responsible for the technological development achieved by humanity throughout its period of existence. The wish of seeing and understanding both unseen phenomena and objects, be it what lies far away in the night sky or what makes up everyday objects, are possibly among the oldest desires of mankind. To fulfil this wish, many devices and methods throughout history were proposed and used, allowing studying what the eye cannot see.

This desire of seeing what is so small the eye cannot discern has been present throughout the entire history of biology, and is linked to one of its defining inventions: the microscope. This milestone invention was fundamental in several findings such as the discoveries of unicellular organisms by van Leeuwenhoek in the 17$^{th}$ century, or that cells divided to originate new ones during mitosis, by researchers such as Remak, Kölliker or Flemming in the 19$^{th}$ century.

There are some examples that, in some circumstances, biologists may have to wait before their proposed theories can finally be visually or analytically confirmed. For example, although some had already hypothesized the existence of organisms small enough to be seen with the naked eye, centuries would have to pass before visual, unequivocal evidence of the existence of bacteria could be presented with the invention of the microscope. A more recent but similar example that also shows the dependence from advances in other areas is the discovery of viruses. Pasteur, in the 19$^{th}$ century, had already proposed that rabies were produced by a

pathogen too small to be seen with an optical microscope and several scientists backed this assertion throughout decades through indirect methods, since existing optical microscopes didn't allow seeing more than very small undetailed bodies. Only in 1931, with the invention of the electron microscope, microbiologists had the tools to finally obtain visual confirmation of the existence of virus and to study their structure and morphology, allowing their cataloguing and establishing connections with so many diseases[1–4].

The objective of this dissertation and, by extension, the laboratory worked developed with it, was beyond acquiring the skills needed for atomic force microscopy operation and preparation, especially oriented at biological fields. The great objective of studies that gather several areas of study is to bring together - as has been done by others with great success and benefits to research and industry - the knowledge and know-how of two very distinct areas of study. Although investigation of "pure disciplines" must be respected and fomented, it is also undeniable that many advances in science arise from interface studies where the best of what each field has to offer can be gathered. This way, it becomes possible to merge the potentialities of more than one area, what has the possibility of improving the approaches to phenomena and our understanding of them, as well as the amount of methods to study them. For that reason, nanoscale phenomena and devices are some of the objects of study in which most of the attention rests on, due to their novelty and ground breaking implications for future generations and technology[5].

Over the next decades, nanotechnology and the areas which emerged out of it, such as bionanotechnology, will surely grow to occupy a place in society far greater than what it occupies today, what arises from its potential of explaining and exploring phenomena that up to now are not perfectly understood or, while being, couldn't yet be integrated into devices that have everything to become ground breaking inventions. These possibilities lead some to defend that nanotechnology has the potential of ultimately transforming society in a way similar to the discovery of maritime trade routes or the industrial revolution[6].

It is also undeniable that, as has happened and still happens with most developments in biotechnology in general, bionanotechnology is a relatively young area of study full of potential but also experimentations that delve deep into new phenomena or into the manipulation of structures at nanometric scale, triggering novel phenomena. Many of these have not been thoroughly studied, meriting great attention and care with the possible future implications that the manipulation of these elements may hold, not only for humanity as for the entire biosphere. Several entities already underline the importance of supervision and regulation of nanotechnological developments[6,7].

Knowing this, it becomes of the utmost importance that there is equipment able to document and analyse how nanodevices and their constituents operate, how they influence the media surrounding them and also how classic elements of other areas, ranging from metal wires to nucleic acids, behave when conjugated with these novel structures as far as on the atomic level. This is why there is interest in the development of protocols and methods that allow pushing the boundaries of the existing technology and aid in the understanding of phenomena that may possibly be the core of the operation of futuristic devices.

## 1.2. Objective of the experimental work of this dissertation

The overall objective of this dissertation rests, first of all, in the interest in the continuous development of methods and techniques that allow visualizing and understanding biological phenomena, both from a more morphological and classic point of view, such as cell imaging, down to more state of the art applications, such as single molecule interactions. Therefore, two main components - one more technical and another more research oriented, in which biological studies took place - are approached in this dissertation.

The technical component basically included learning how to operate the AFM, understanding its components, learning how to critically analyse images, especially on the differences between the types of information acquired, to grasp the concepts that explain differences in modes of operation and how resolution is affected by the AFM's elements. AFM on itself is not a very hard or demanding technique so it is relatively straightforward to learn the basics required to start producing simple, low magnification images, and to move to more challenging samples by building upon experience over time.

This training initially comprised learning basic modes of operation, such as standard alternate contact modes or contact mode in air. The aim was to move to more challenging modes, such as liquid mode operation or force spectroscopy, and even becoming familiar with methods and modes of operation that are less AFM biology oriented, which are often demanded in characterization jobs or projects.

The research oriented part, although far more biological oriented, also had experiments related with physical modifications of the AFM probe as means to improve resolution. Understanding and using common protocols of immobilization for the biomolecules studied throughout this dissertation's experiments, as well studying the dimension, structure and morphology of these biostructures, both when isolated and when reacting with one another were also considered key objectives. Liquid mode operation was also to be approached and the replicability of measurements done in it are to be compared with acquisition in air.

Insulin, DNA and the enzyme EcoRV were used, with each of these biostructures being analysed individually. However, due to the specificity and knowledge of the interaction between DNA and EcoRV enzymes, the dynamic interaction between these two was also focused in an attempt to establish the possibility of observing the cleavage mechanism with AFM.

Gold nanoparticles functionalized with different coatings, such as in the absence or presence of a BSA protein coating, were also studied as model for the use of gold nanoparticles functionalized with other elements, such as antibodies for diagnosis or treatment.

On the subject of probe modifications, two main objectives were approached in this dissertation: tip modification by focused ion beam and tip coating with nanometric metallic layers to protect tips from oxidation or enhance resolution.

The focused ion beam approach can be used to modify tips up to the scale of its resolution, which can routinely be as small as one nanometre. The modifications that were planned were projected for operation at larger scales than those used in most of the biological studies to be presented herein. However, these are intended to serve as clear indications of the positive effect that these modifications can have on measurements as well as how the development of this technique can lead to the fabrication of sharper and more sensitive tips, without needing expensive and less replicable functionalizations such as with carbon nanotubes. The determination of the use of coatings as a factor affecting the quality of the measurement, both positively and negatively, will also be approached.

Through all of this, it is desired that this dissertation serves as a document that reinforces the use of AFM as a, if not the, primary technique for high resolution imaging of biological structures, especially with the potential of characterizing interactions between them in real time and in their native media.

# 2. Nanotechnology in biological sciences: analytical tools

## 2.1. Microscope types, basic physics of operation and limitations

As of today, there are several types of microscopes operating in everyday research and industrial environments, from which three are more commonly used - the optical microscope, the electron microscope and the scanning probe microscope – although each of these spawn several subtypes of their own. Each one of these has its advantages and limitations, inherent to the way they are operated and the way they interact with the sample. For example, the optical microscope operates using light and can be as simple as a child's toy, while electron microscopes are expensive and complex, using electron beams instead of sunlight or light bulbs, and requiring controlled environments. The other main microscope type is the scanning probe microscope, in which sample interaction is undertaken by a sharp tip contacting or interacting at a nanometric distance with a sample's surface.

The operating limit of optical, and even of electron microscopes, is normally associated with the wavelength of the element that interacts with the sample, as happens in the case of the classical optical microscope. In most of the nowadays optical microscopes, a beam of white light is focused by optical lenses and transmitted through the sample. Due to different absorption behaviour of different materials before incident light, a contrasting image between transparent media and opaque or highly refractive media is produced. More complex microscopes, such as the scanning near-field optical microscope, have been developed, showing that the resolution limits dictated by visible light could be surpassed by using apertures smaller than the wavelength and acquiring the reflected light at such a close distance from the surface that it does not travel the necessary length to diffract. However, the fact is that the key of this design is the existence of a hollow needle collecting the light very close to the surface and not the cascade of magnifying lens popularly associated with a regular microscope[8,9].

The resolution limit of these images is not only determined by the wavelength, but also by the numerical aperture of the focusing lenses and observation media. Images acquired through this technique will start losing quality below resolutions of 400 nm, since that is the wavelength of violet light, while images below roughly 200 nm of resolution will be of bad quality, as determined by the Abbe diffraction limit equation, shown below[10].

$$d = \frac{\lambda}{2(n sin\theta)}$$

**Equation 2.1 – Resolution of a system dependent from wavelength.**

In the equation, $d$ is the minimum resolution possible to attain, *i.e.*, the smallest distance two points must have between each other to appear as separate features, $\lambda$ is the wavelength of

the beam of the incident wave, $n$ is the refractive index of the observation medium and $\theta$ the diffraction angle of the lens. The calculation of "$nsin\theta$" defines the value of the numerical aperture (NA)[11]. It can be, therefore, inferred from the equation that there are two ways of improving resolution knowing that there is a limit to diffraction angles: operating in media with higher refractive indexes, in order to increase numerical aperture, or using beams of smaller wavelengths, like ultraviolet light waves of other nature, like the mentioned electron waves[10,12]. This second method is precisely the one which was applied to electron microscopes in order to go beyond the resolution attained by visible light. In this type of microscopy, the traditional beam of visible light used in optical microscopes, with nanometric wavelengths, is replaced by an electron beam with a wavelength orders of magnitude below that, effectively pushing the resolution limit to values that can go as far as the ångstrom (100 pm) and the magnification to values in the range of the millionth[13].

## 2.2. Beyond visible light: Electron Microscopes

The most well-known electron microscopes are the scanning electron microscope (SEM) and the transmission electron microscope (TEM). The basics behind the operation of both microscopes are the same: an electron beam undergoing electromagnetic focusing is aimed at a sample, being the main difference the way through which detection of the sample occurs.

In a TEM, basically, the beam is transmitted through a thin slice of the sample, where elastic and inelastic scattering of electrons occur. These are then propagated through imaging lenses and into a detector opposed to the electron source[14]. On the other hand, detection on a SEM is not so straightforward: when the electron beam is accelerated towards the sample, the atoms on its surface will have their original electrons substituted by those in the beam or just be plainly deflected away from the sample, what will allow for different sample characteristics to be inferred and shown, after these electrons have been captured by detectors with different properties[8,15].

However, both these microscopes have disadvantages of their own. For example, to produce quality images, they must be operated in vacuum or else the electron beam will be dispersed by the particles naturally present in the atmosphere, meaning the amount of electrons and the energy they carry, when interacting with the sample, will be deficient to produce any image[15,16].

Another important disadvantage is that, under normal conditions of operation, it is impossible, or very challenging, to image insulating materials, since they tend to capture the electrons, instead of conducting them away to the ground of the stage. When this happens, the sample surface becomes charged in such a way that the amount of electrons start acting as an

electric shield, deflecting incident electrons on their own, leading to the observation of erratic features in the images.

Other disadvantage related to the incident electron beam is that this beam carries a high amount of energy with it. Therefore, many soft and organic materials can be damaged by the energy released from the interaction of radiation with matter. The result is usually an increase in the local temperature. Biological samples, from tree leaves to proteins or DNA in a buffer solution (which carries the issue of making an observation difficult or impossible in vacuum) are usually clearly damaged by those effects. It is possible to overcome some of these problems by coating the materials with a metallic, and therefore conducting, nanometric layer. However, when the purpose is observing, documenting and studying phenomena at nanometric scale, a layer of 10 nm of any coating material may mask, or even destroy, details that one wants to observe[10,15,17–19].

These limitations are some of the reasons why these microscopy techniques were out of bounds in many situations to biological and biomedical research, and as will be presented below, one of the reasons why scanning probe microscopy techniques, became such an interesting approach to research on biological samples.

## 2.3. The Scanning Electron Microscope and its potentialities

The first microscope using electrons as element of sample interaction was developed in 1931 by Max Knoll. Knoll's microscope proved that, although with worse magnification than a standard optical microscope, electrons could be used to obtain magnified images of samples, giving birth to the field of electron microscopy. However, the first microscope equipment worth of being qualified as a scanning electron microscope (SEM) was only developed by Mandred von Ardenne in 1937. This SEM was the first electron operated microscope to obtain high resolution by focusing an electron beam onto a surface and producing a raster image without chromatic aberrations[20]. Chromatic aberrations spoiled images in both optical and electron microscopes because lenses don't exhibit the same refractive indexes for all wavelengths, meaning a focused, unique wavelength element had to be used or else images produced would become blurry after a set magnification, like can be seen in the edges of items in deficiently focused photographs[21]. The resolution of the SEM respects the Abbe diffraction limit, meaning that in theory it can achieve 2 pm of resolution. However, other significant factors contribute in limiting the magnification of this microscope, such as beam diameter, interaction volume or signal-to-noise ratios, leading to real resolution values closer to 1 nm in average recent equipment[22,23].

When producing an image, the most common mode of sample interrogation is done by detecting the electrons ejected away from the outer shells of the atoms constituting the surface of the material under observation. These electrons are called secondary electrons, which lends name to this main mode of operation, offering resolutions up to half nanometre in the most powerful equipment. The other most known imaging mode is the backscattered electrons mode, which can also give insight on the different chemical compositions of surfaces[8].

As it has been just mentioned, the scanning electron microscope produces images at the cost of focusing electrons, which are accelerated with a given voltage away from a source. By extrapolating the position and behaviour of these electrons, it becomes possible to map topography or chemical differences through the use of detectors present in the sample chamber.

In most SEMs, the electron source, called the electron gun, relies on a tungsten or possibly lanthanum hexaboride filament, which is heated up until it becomes thermionically activated: when temperature is high enough to favour the emission of electrons. There is another type of electron emission, which relies on field emission, in which a needle emits electrons by setting a voltage bias near the electron source with an extractor, leading to electron extraction by quantum tunnelling. These sources must be monochromatic, *i.e.*, to emit an element of a single wavelength, in order to avoid the mentioned aberrations. These electrons are then electromagnetically focused in the electron column by a set of condenser lens, generating a beam as sharp as possible, since a thin and energetic beam is a requirement for high magnification imaging. The focused beam is then deflected by deflection coils mounted just before the opening to sample chamber, which allows for the beam to be aimed along the surface of the sample in order to produce a raster scanned image. The detectors lie inside the sample

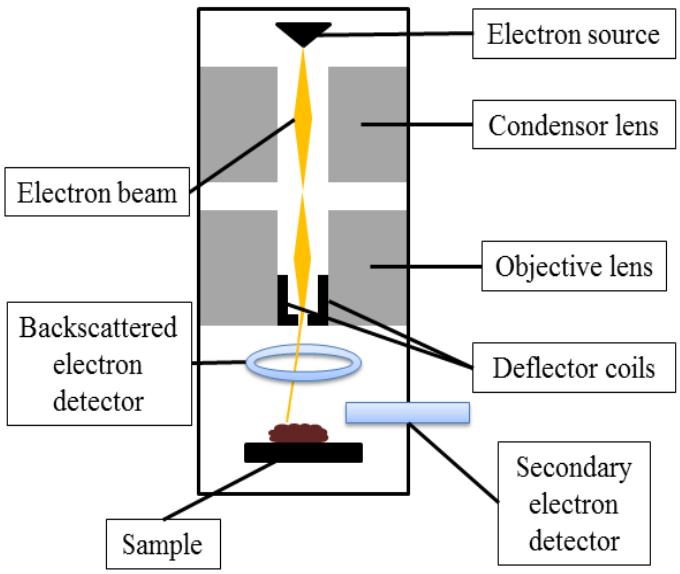


**Figure 2.1 – Basic schematic and components of operation of a SEM.**

chamber, strategically placed to favour the detection of the different types of electrons that are produced by the sample; or even electromagnetic radiation like X-rays. Secondary electrons are produced by inelastic scattering of the electron beam, *i. e.*, an electron which was ejected due to a collision with an incident electron in which there is no conservation of energy. These electrons are called low energy electrons because there is loss of kinetic energy related to collisions occurring when the electron travels through the atoms on its way to the surface. These ejected electrons normally originate from the k-shell of the atoms and must be attracted by electrical bias to the respective detector, because, although they carry enough energy to be ejected and cross some atoms, they cannot go further than few nanometres from the surface. After detection of electrons and steps of electrical amplification, it is possible to extrapolate their position and intensity of the signal in order to produce a contrasting image. This image depends on the amount of secondary electrons being emitted, allowing for a topographic image of the sample to be produced[15,20,24]. Figure 2.1 represents the basic instrumentation of a SEM.

On the other hand, backscattered electrons are produced by elastic scattering of the electrons. This mode of operation allows building a relative map of the elements on the sample surface, since higher atomic number atoms favour the generation of more backscattered electrons. The equipment used to detect this type of atoms does not need to make use of electric bias because, while secondary electrons originate from the sample and carry less energy, backscattered electrons originate from the electron beam and therefore have higher energy, being deflected back (hence backscattered) by the atoms and exiting the sample with enough strength to collide with the detector. The amount of backscattered or deflected electrons rise in proportion to the atomic number of an element's atoms because such elements have more massive nucleus, which deflect more electrons in comparison to lighter elements. This data will offer topographic data with less resolution; however it will be far more informative if the objective is to determine that there are different elements present in the sample surface. This type of information is also very interesting because it can be used in electron backscattering diffraction (EBSD), a technique in which backscattered electrons are diffracted following a pattern directly related to the crystalline orientation of the material under observation, allowing mapping and identifying the crystal system of a sample[15,25].

Other types of techniques that were of interest to this dissertation and which were used are energy-dispersive X-ray spectroscopy (EDS) and focused ion beam (FIB). Energy-dispersive X-ray spectroscopy is a technique that allows the analysis of the elements constituting a sample and to produce an element map of the different chemical elements that compose it. It is based on the principle that when an electron beam interacts with the atoms on the surface of the sample, there is a chance that an electron orbiting the inner electron shells of a ground state atom will be ejected. In this situation, the vacant position left behind will be

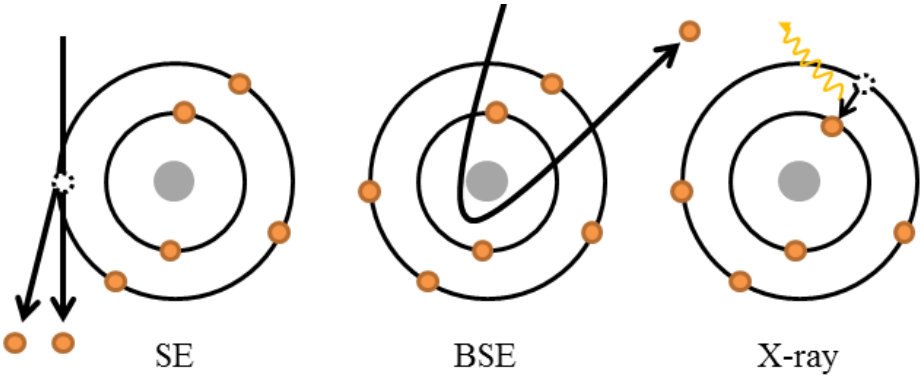


**Figure 2.2 - Schematic of the interactions between elements that give birth to secondary electrons (SE), backscattered electrons (BSE) and emission of X-rays (X-ray) in SEM imaging. Orange circles represent electrons while the grey circles the atom nucleus.**

occupied by a higher energy electron orbiting in the outer electron shell, which will lose the excess energy when moving to the inner shell through the emission of an X-ray photon. The energy carried by this photon is specific for the atom and for the shell the electron originates from and, therefore, with the appropriate detector, it is possible to measure the number and energy of X-ray emissions and to determine with high precision what elements constitute the sample and where they are located[15].

### 2.3.1. Focused ion beam

The technique of focused ion beam (FIB) is discussed together with the SEM because, although this is not an electron microscope since the sample interacting element are ions, the fact is that they are similar pieces of equipment, in which sample interrogation and detection is based on the same principles. Many SEMs incorporate FIB columns in their machinery, constituting two-beam systems and allowing, besides standard SEM imaging, to collect other data or to nanofabricate structures by depositing new atoms, or sputtering original ones away from a surface[8,15,26].

This technique relies on the use of a liquefied gallium source covering a tungsten tip. Through the use of a field emission extractor, an electric field capable of ionizing gallium is generated. These ions can then be accelerated towards a sample with nanometric precision, what can have different outcomes intimately related with the desired application[27]. These can be used for micro and nanofabrication, which can follow both a top-down and a bottom-up approach. For the former, its destructive properties can be used to mill and sharpen features or create precise patterns by removing the atoms of a material off a surface, such as when sharpening an AFM probe in order to enhance its resolution (Figure 2.3), an interesting possibility approached in this dissertation. For the latter, its constructive properties can be used in order to deposit atoms on the surface and fabricate structures. By injecting a precursor gas to form a film containing the element we are interested in depositing, the FIB beam can be used to dissociate and breakdown this film, forming thin, precise deposits that can be used in the fine construction

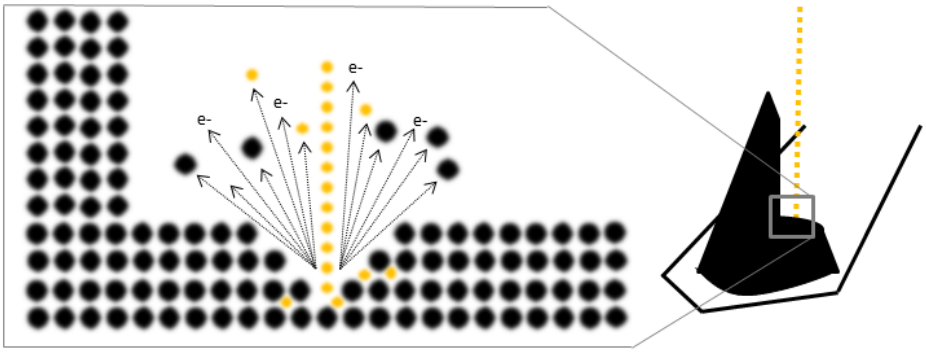


**Figure 2.3 – Diagram of FIB milling of a surface (exemplified as an AFM probe) by sputtering with a focused ion beam. The collision of the ion beam with the surface results in the sputtering of surface atoms, together with beam atoms and secondary electrons.**

of microcircuits, for example. FIB systems can also be used to modify the surface, such as by implanting beam atoms in it or be used for surface interrogation and analysis, because of the emission of secondary electrons as in SEM and also for surface characterization, such as in grain size measurements, since ions are channelled in different directions in relation to the grain sizes of the material and the angle of incidence, allowing the generation of 3D images micrometres into the material[27–29].

## 2.4. The first Scanning Probe Microscope

The invention of the scanning tunnelling microscope (STM) in 1981 by Gerd Binnig and Heinrich Rohrer at IBM Zürich, gave birth to a new type of microscope that didn't fit into the already existing categories of optical microscopy or electron microscopy. This microscope was dubbed the first type of scanning probe microscope ever created, becoming a breakthrough in the field of microscopy for a variety of reasons related to, for example, the way it interacted with the sample associated with the magnifications and resolutions it allowed to attain.

The fundamental characteristic that defines scanning probe microscopy is that the images of a sample are generated by the interaction between it and a probe (a needle or a sharp tip), instead of with electromagnetic waves. For the first time, the limit of a microscope was not defined by phenomena like diffraction of light, the length of the wave used in its operation or lens apertures, but by how sharp a probing item can be and the sensitivity of the feedback circuit that monitors its movement.

Scanning probe microscopy spawned many different microscopy techniques, but the two most widely used and known are two: scanning tunnelling microscopy (STM) and atomic force microscopy (AFM). In scanning tunnelling microscopes, which can routinely achieve true atomic resolution, surface detection is done by closely approaching a conducting tip to a surface in which both are under a chosen electric current and voltage: the difference of the applied voltage between both is known. When the distance between the tip and sample is extremely small, *i. e.*, roughly half nanometre, the voltage bias is enough to allow electrons to tunnel

through the gap between the two by quantum tunnelling. Knowing this, it is possible to map the surface of a sample by crossing the detected changes in electric current over the voltage applied and the position of the tip over time[30,31].

## 2.5. Atomic Force Microscopy: origins, instrumentation, basic principles of operation, advantages and disadvantages

### 2.5.1. Origins of the AFM

The first device that can be tracked as the ancestor of the atomic force microscope is the stylus profilometer, invented in 1921 by Schmalz. This "microscope" obtained information on a surface by dragging a probe, like a cantilever with a sharp tip, along a sample surface in a raster fashion. This allowed to obtain several profile lines that when merged together would make a projection of the topography of a surface. This was achieved by setting a cantilever probe on a fixed position with its tip touching the surface and then using a stage to move the sample horizontally. These cantilevers would bend and twist as they encountered the features of the moving surface and by using a light beam aimed at a mirror on the cantilever, it was possible to record the changes in cantilever position using photographic paper, since height shifts would change the mirror position and divert the beam to different locations. However, the forces applied to the cantilever meant that it could bend or crash against large features, leading to cantilever damage, diminishing resolution, or damaging the sample. One proposed solution for such issues was to oscillate the cantilever above the sample, lowering the forces involved in the probe-sample contact while still keeping surface tracking possible, a proposal that was ultimately introduced in AFM[31,32].

### 2.5.2. Instrumentation

It can be said that an atomic force microscope is almost like a very sensitive and fine-tuned profilometer because both stand on the same principle of dragging a tip on a surface to measure it. However, while profilometers only measure the difference in height when the probe is in contact, the AFM measures the interaction forces between the sample and the tip, besides the possibility of detecting several properties due to a far more complex instrumentation.

The fundamental concepts involved in its instrumentation are three: piezoelectric transducers, force transducers and feedback control. Piezoelectric materials have the property of changing their dimensions when an electric potential is applied to them and *vice versa*, with typical sensitivity going as low as ångstromic changes per volt. The inclusion of these elements in the stage (*xy* plane) and the cantilever holder (*z* axis) allows to control with astonishing precision the movement of the sample below the probe, as well as how high this probe needs to be to interact with the surface satisfactorily. This vertical interaction can be detected by force transducers, which normally consist in an optical lever system similar to profilometer's, which

must have sensitivity beyond 1 nN, allowing registering the intensity of the force between a probe and a sample.

The last fundamental element is feedback control, which monitors and registers such force values and feeds commands to the piezoelectric actuators in order for them to dilate or compress and keep the tip interaction force at a pre-set value. Simply put, when the sample moves under the probe and a feature appears that would bend the cantilever up or down, the force transducer will detect a sudden raise or decrease of force and redirect this information to the actuators, so that the *z* axis actuator can move the tip away, before it crashes the surface, or bring it closer so it can keep on tracking at the same distance and same net force (Figure 2.4)[32–34]. While this, it can also generate reference signals which can be compared with the received signals and used to generate images.

### 2.5.2.1. Piezoelectric actuators

The precision scan of a sample is only possible because of the use of piezoelectric elements throughout the three axis of operation of the AFM. Different voltage values can be fed to these elements in order to generate precise movements, not only to move the sample in regards to the probe, the *x*-*y* plane, but also on the *z* axis, fundamental to maintain the probe-sample interaction at a fixed value. This can be achieved by using piezoelectric ceramics such as amorphous lead barium titanate ($PbBaTiO_3$) or lead zirconate titanate ($Pb[Zr_xTi_{1-x}]O_3$ with $0<x<1$), which can be formulated to have smaller coefficients of expansion but higher linearity and *vice versa*, hence the respective definitions of hard and soft ceramics. These elements can limit how fast an AFM can operate because the rate at which they can do contraction and extension cycles defines how quick the sample can be scanned. It is desired that these exhibit

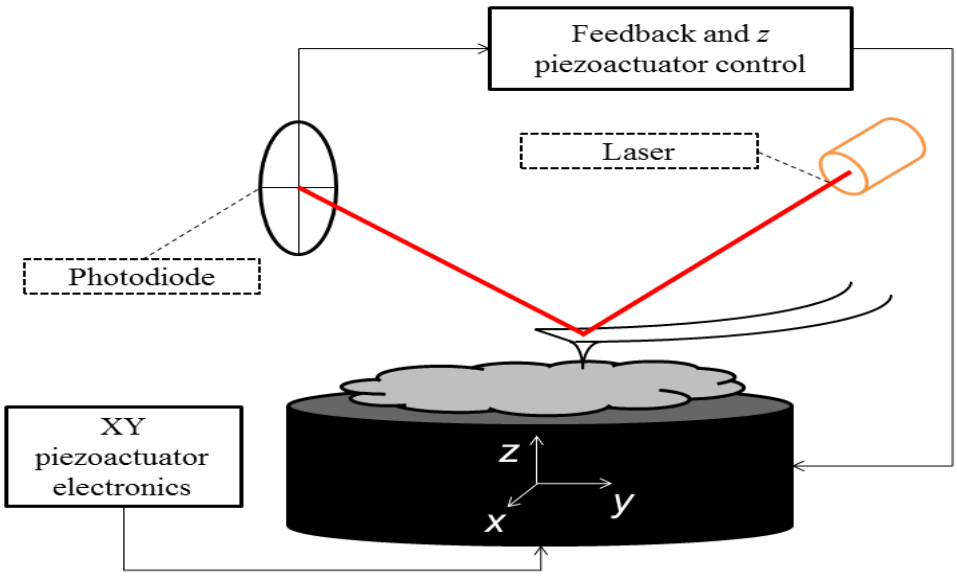


**Figure 2.4 – Simplistic schematic of an AFM's using an optical lever as force transducer.**

linearity between applied voltage and dimension changes at all times and in all conditions, however, this is not always true as discussed in the Artefacts section below[33].

#### 2.5.2.2. Force transducers

Force transducers are the elements responsible for detecting shifts in the force exerted on the probe's tip. Although it is deducible that they must be extremely sensible in order to detect variations smaller than the nanometre in the *z* axis, their precision is also required so that force differences can be detected long before they become enough to damage a tip, especially in modes of operation in which the probe enters repulsive regime. In this case, very small variation in tip-sample distance will generate large force differences, due to the steepness of the force curve in the repulsive regime, as will be explained in the 'Force curves' section below.

Originally, cantilever deflection was detected relying on STM electronics and an STM probe. However, AFMs using this method, along with others such as relying on interferometers or piezoelectric principles, are a minority compared to those relying on the principle of the optical lever, due to the high sensitivity of this method associated to its simplistic design as well as the ease and cost advantage of producing AFM probes with reflective coats. The only downsides are that these coatings may lead to non-reproducibility and the alignment, if manual, may be time consuming and, if done incorrectly, may give rise to image artefacts[33,35,36].

The optical lever works on the principle that the reflective back of a probe can reflect a laser beam from an emitter to the centre of a photodiode. This photodiode has, for example, four quadrants, which will produce voltage proportional to the amount of light that they receive. When the probe is deflected or twists, the beam will move away from the centre and into one of the quadrants, generating an electric potential that, when detected, can be used to deduce information from the surface such as height or lateral deflection similar to the photographic paper of the profilometer[37].

#### 2.5.2.3. Feedback control

The reason why an AFM scan can attain such magnifications is also related to a fine feedback system which can almost instantly collect the information obtained by the force sensors, process it, and generate signals to control the elements fundamental to the scan, such as piezoelectric actuators. At the same time as this data is processed to generate an appropriate response to changes in topography, the difference between the inputted and the outputted signals throughout the various channels can be registered. These signals include and are not limited to, for example, *z* voltage and error signal, amplitude and phase in the case the cantilever is being oscillated, voltage bias between cantilever and sample in case of conductive AFM,

etc… The difference in these signals can then be translated by appropriate software and form maps of the surface of the sample.

#### 2.5.2.4. Force Curves

The force between the probe and the surface plays a defining role in atomic force microscopy and is intimately related with certain types of operation. When the distance between a probe and the surface starts to decrease, at first a cantilever just stays in its relaxed position. However, as the cantilever distance starts to shrink to values on the range of the few hundreds of nanometres, attractive forces (van der Waals or capillary effects, for example) start to play a considerable role and the probe will be snapped in the direction of the surface. However, as the distance keeps decreasing, net repulsive forces (for example, from the convergence of electron clouds) will start to dominate this interaction and the tip will be bent back away from the sample with increasing strength in relation to how small the gap becomes (Figure 2.5). This principle is transversal to all AFM modes of operation and is exploited in several modes of imaging, while also explaining certain outcomes of operating in certain modes (like why probes are more prone to damage in contact mode operation)[38].

### 2.5.3. Channels of acquisition

When operating an AFM, it is common for it to output more than just one type of signal, such as topography. For example, in contact mode, while the topographic image of the surface is generated using the *z* piezoactuator voltage signal, the AFM can also collect its error signal (how much it was being deflected before the feedback circuit corrected the height) or the lateral deflection of the cantilever (how the interaction with the surface made it bend laterally). In oscillating modes, the same thing can be done, allowing to visualize topography as well as, for example, alterations in the frequency, amplitude or phase of the cantilever oscillation, as represented in Figure 2.6. This allows obtaining several readings of the sample at the same time.

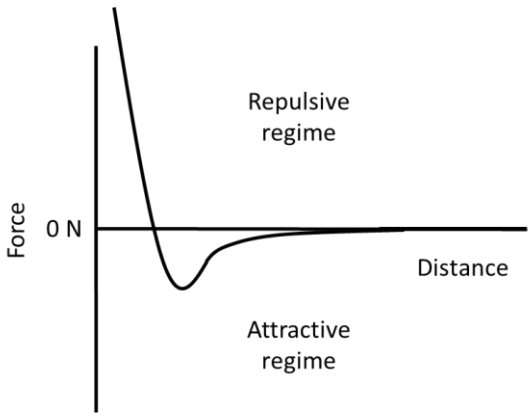


**Figure 2.5 – Simplified force-distance curve for the interaction of an AFM probe and a sample.**

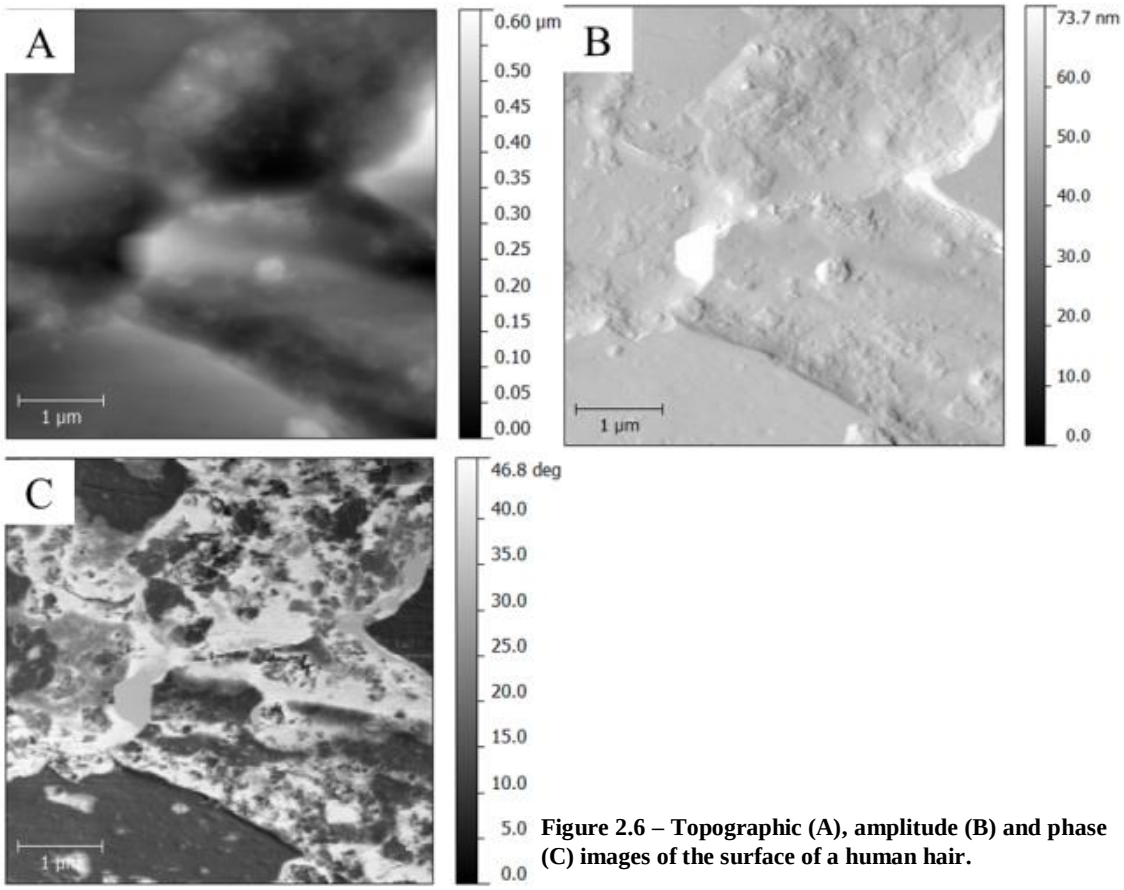


**Figure 2.6 – Topographic (A), amplitude (B) and phase (C) images of the surface of a human hair.**

### 2.5.4. The probe

Although every single circuit or element present in the AFM is important for it to deliver what is demanded of it, there is not a more fundamental element to create a good measurement than the AFM probe. The probe is of the utmost importance for an AFM measurement because, in most cases, it will be its properties determining the quality of a measurement, since it is the element responsible of collecting the information *in situ*. There are no perfect probes and even excellent probes will produce some artefacts, which are presented in the section below (2.5.5), in certain conditions[39]. However, probes from the same fabricant are expected to be homogeneous and to operate under the same conditions, being expected of them to behave in a precise and replicable way, allowing an experienced operator or any experienced person who analyses the images to read beyond these artefacts.

For ease of manipulation, because probes are disposable and are easily replaced, these

**Figure 2.7 – Schematic of a chip with an AFM probe. The chip can be locked in the AFM and the cantilever is left protruding, with the probe ready to interact with the sample.**

are sold on standardized substrate chips. These chips have the cantilevers, which carry the probe, protruding from one of its sides (Figure 2.7). Probes are fabricated relying on MEMS technologies and there are two main groups of probes: silicon nitride probes, more flexible and often with a triangular shape and a square pyramidal probe and also silicon probes, stiffer and usually rectangular, with triangular pyramidal or conical probes. Contact mode oriented probes usually have low (on the range of the few dozen kilohertz) resonant frequencies, spring constants below 1 N/m and are fabricated from silicon or silicon nitride ($Si_3N_4$). Alternate contact probes are stiffer, with spring constants which can be of several dozen newton per meter, and have higher resonant frequencies, which in the most recently developed biology oriented can be as high as 1.5 MHz, although general purpose probes are commonly oscillated in values between 70 and 400 kHz. They are normally only fabricated out of silicon[32,33,40].

Probes are normally modified with coatings to increase the voltage generated by the photodiode and, therefore, the sensitivity of the measurement. However, these can be extensively modified, as will be focused with more detail on Chapter 3.3. The probes used in this dissertation's experiments and their main characteristics can be seen in Table I.1 of Appendix I.a.ii.

### 2.5.5. Artefacts

An artefact is a feature that appears during a scan which is not real. While in some situations these may be obvious to the operator, in other situations they can be subtle and mislead, requiring some experience to detect them. West and Starostina consider that there are four primary sources of artefacts: the probe, the scanner elements, the image processing and external vibrations, although other also exist[41].

Probe related artefacts originate from the fact that images generated by AFM are convolutions of the tip geometry and the features of the sample. This can lead to different situations like small protruding structures appearing larger than they are in reality, while holes in the surface will appear smaller in width and depth because the tip cannot penetrate in it. Alterations in probe geometry due to bluntness, tip contamination or cracking of the tip, forming a double tip can also introduce several unreal features on the images (Figure 2.8).

Scanner elements can also affect the quality of acquisition because piezoelectric elements are not infallible when it comes to the precision of its movement. Phenomena like thermal drift, hysteresis or creep are vulgarly associated with AFM and can degrade image quality (Figure 2.9). Thermal drift is related to the heating of the equipment during operation, affecting the linearity of piezoelectric expansion and contraction due to changes in the environmental conditions for which parameters were initially tuned. Hysteresis and creep are similar non-linear phenomena that relates on the fact that electronic components do not always

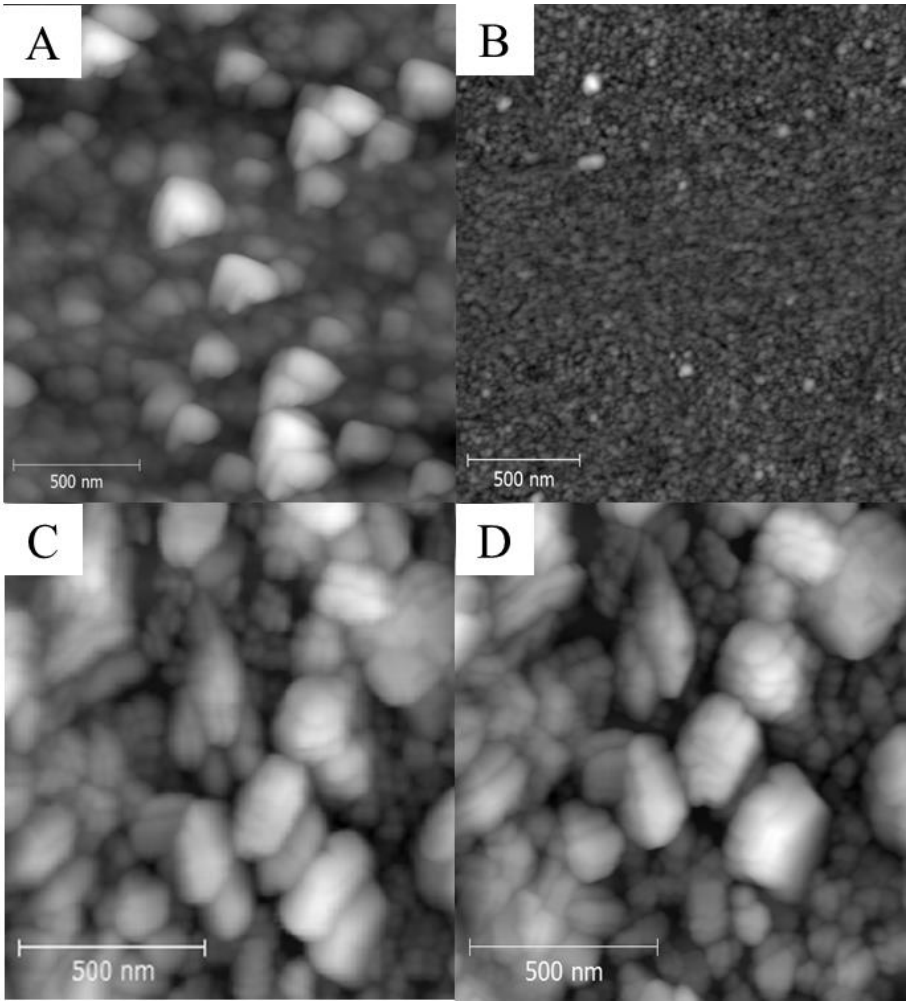


**Figure 2.8 – Tip related artefacts and their effects on image quality. Because images are convolutions of tip geometry, when a tip fractures in unexpected manners, it can produce odd features, such as spherical structures becoming triangular (A). Contaminations on the sample can also be dragged by the tip, leading to images with both good quality and bad quality sections alternated (B). If a tip picks up contaminants or breaks in two, resulting in two structures touching the sample at the same time, this can lead to the appearance of multiple images of the same feature (C) compared to an image clear of artefacts (D).**

follow the same behaviour pattern when doing symmetric movements, what can be due to inherent characteristics, such as the age or operation hours of a system or acquired due to outside factors, like temperature. Hysteresis relates to the principle that any piezoelectric element tends to maintain the state it is in, in a principle that can be compared to inertia. This means that the voltage needed to generate a specific change in dimension, may not be enough to produce the same change in other situations or, on the other hand, may be excessive. Creep is a similar phenomenon that derives from the fact that when a sudden change in voltage is applied to a piezoelectric actuator, the response behaviour may not be totally linear: there can exist a lagging period before it exhibits motion or, in the opposite case, there can exist situations that after the voltage input has been interrupted, the element keeps on behaving as if it was still under the effect of that input, although this is rare in the most common closed-loop operation (with XY correction engaged)[42].

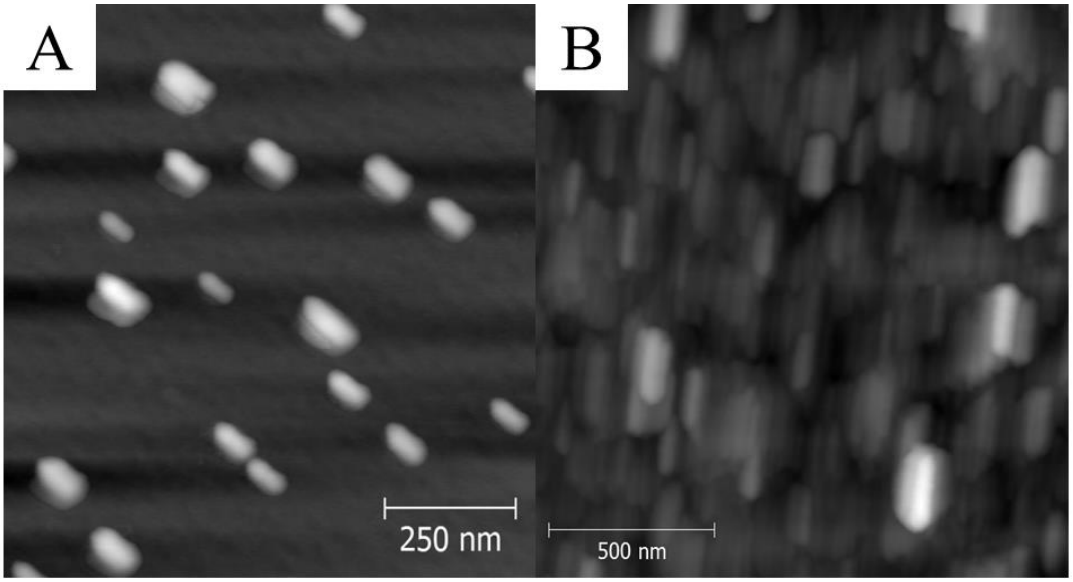


**Figure 2.9 – Examples of drift. Both the spherical nanoparticles (A) and the spherical liposomes (B) appear as elongated features.**

Others can relate to scan conditions such as speed: when the probe is traveling too quickly over the sample and encounters a plateau feature, the tip may bounce over the edge for a small distance after climbing its wall and then fall off the other edge in a parabolic trajectory, instead of following the two 90º bends in both locations.

Other key issues are constant noise and vibrations, which can originate from an acoustic source, such as people talking, or from the ground, like if the AFM is set on a room next to a busy corridor. This can affect the measurements, especially high resolution ones, because it can interfere with the precise tip-sample distance or the probe oscillation, possible leading to the tip bouncing and bumping the surface, what may lead to a quick loss of sharpness and, by default, loss of resolution or even tip damage. Although there is a limit beyond no device can isolate an AFM from outside interference, there are anti-vibration tables and stands that can help in countering many of these interferences when used together with acoustic isolating chambers. Many of these artefacts may be corrected with AFM software, which normally carries correction, data and image manipulation modes. However, care must be taken when using these because if they are used without consideration, they may introduce artefacts of their own in images[41].

### 2.5.6. Main advantages over microscopy techniques

Atomic force microscopes have several advantages of their own. Actually, if one was to sum its most important advantages in one simple sentence, it would be that atomic force microscopes allow ångstromic resolutions (in the range of the atomic lattice) without any special need of controlled environments. This means that it is a relatively cheap technique, for a modern, regular AFM able of such resolutions can cost as few as 25 thousand dollars, while capable of analysing almost all samples on demand without needing anything more than an anti-

vibration stand, an acoustic box and a desktop computer. Regular commercial AFMs do not need expensive vacuum or temperature solutions, since regular measurements (which are already beyond the resolution of most SEMs and weaker TEMs) of the most common samples can be done at room temperature and pressure, without needing to coat the sample, or even in liquid media, which is not something as trivial for SEM and TEM operation[8,33,43].

### 2.5.7. AFM Contact Mode

Contact mode AFM is the classical mode of operating an AFM since it resembles a stylus profilometer until the point piezoelectric and force actuators, coupled with feedback control, step into operation. It was the first mode of operation to be developed and applied to material sciences.

Contact mode operation relies on long and rigid AFM probes, with low spring constants and low resonant frequency, being dragged along the surface at a distance where the net forces applied to the tip are repulsive. The forces applied to the surface are pretty straightforward to define, since they are given by Hooke's Law, where $F$ is the force applied, $k$ the force constant or stiffness and $D$ the deflection in meters:

$$F = -kD$$

**Equation 2.2 - Equation for Hooke's Law**

Because of the strength of the repulsive force compared to interatomic forces, two things can happen if a tip is forced onto a surface: either it breaks or the atoms in the surface move away. This means that the forces applied to the surface are beyond what many materials can support, meaning that contact mode AFM can be a destructive technique to softer samples: most biological structures or even polymers are normally off bounds for contact mode AFM because the sample cannot sustain the forces applied to it, especially because the capillary forces between tip and sample in contact mode, due to the existence of a thin nanometric water layer in the surface, also originate greater forces against the sample. However, there are many reports of contact mode measurements done of these samples, especially when there is interest in doing submolecular scale images, and curiously, doing them in liquid can lower the capillary forces applied and produce better images by not upsetting the sample and the probe so much[33].

This means that while alternate-contact mode probes normally have a longer operation life, contact mode tips become worn and unfit for measurements earlier, since they tend to lose their sharpness faster, leading to earlier appearances of image artefacts in the measurements[44].

Nevertheless, it is an important technique for research and industrial environments that deal with rigid materials, like metals or semiconductors.

Common acquisition channels are:

Topography, which produces a height map of the surface;

Deflection, which produces a map of the slope on each point of the sample (the error of the measurement on each point), lending a more realistic look to the measurement, *i.e.*, showing it as our eyes would perceive it if they could see at such magnifications and;

Lateral forces, which create a friction map out of the twisting of the probe along its longitudinal axis, as perceived by the photodiode sensor.

Other important and widely used modes of operation are electric and conductivity measurements, which make use of special stages to measure the capability a sample has to conduct electric current. By building a circuit using the stage, the sample, the AFM head and the tip, a voltage bias can be applied between the tip and the stage, meaning that the resistivity the sample has to conduct energy through it can be evaluated. This is normally done by making a map showing the conductivity of the entire scanned area of the sample when at a set voltage bias, or by picking isolated points in the sample and evaluating its ability to conduct current when under an array of voltages, thus producing current-voltage or I-V curves[32,33,38,45].

These I-V curves can help understanding at micro and nanometric scale how a sample behaves from the electric point of view, what becomes especially important in studies which focus the development of structures at these scales with the ability to respond before electric impulses, such as new generation transistors or nanowires.

### 2.5.8. AFM Non-contact and Intermittent Contact Modes

Non-contact mode and intermittent contact modes are also known by other names like alternate or tapping mode, although sometimes they do not correctly refer to the mode being used. This last denomination – tapping mode - is actually the most common one, becoming the way of calling any non-contact mode of operation by many AFM operators. However, since it was patented by Veeco Instruments, Inc., calling tapping mode AFM to this mode of operation had to be omitted from official communications due to trademark reasons, what sometimes generates some confusion.

In these AFM modes of operation, probes are shorter and stiffer, therefore having higher spring constants. These properties allow them to be oscillated as high as hundreds and thousands of kilohertz while the sample is scanned, what allows operation at high frequencies, an important property because probe resonance frequency also plays a role in defining the resolution of the system.

Free resonance frequency ($w_0$) is dependent from factors such as the function of the cantilever mass ($c$) its spring constant ($k$) and the quality factor ($Q$) when much greater than 1. Knowing the free amplitude ($A_0$) and considering additional forces ($f'$) produced by the interaction with the sample, it is possible to calculate the produced frequency shifts ($\Delta w$) in the cantilever dynamics and the new values of resonance frequency ($w_0'$) and amplitude ($A$) (Equation 2.3)[46].

$$A = \frac{A_0\left(\frac{w_0}{w}\right)}{\sqrt{1 + Q^2\left(\frac{w}{w_0} - \frac{w_0}{w}\right)^2}} \text{ and } \Delta w = w_0' - w_0 \text{ where } w_0' = c\sqrt{k - f'} \text{ and } w_0 = c\sqrt{k}$$

**Equation 2.3 - Equations for amplitude and resonance frequency shifts**

Unlike contact mode, probes are kept at a higher distance from the sample surface, but still under the effect of intermolecular forces. The fundamental difference between non-contact and intermittent contact rests on the amplitude range. Non-contact operation uses small oscillation amplitudes, around ten nanometres, what allows for the tip to stay inside the attractive regime throughout the entire scan. This means that while this mode of operation can be very conservative to tip wear because the chances of tip damage are greatly reduced, it can also produce deficient imaging if not set correctly, due to the tip not penetrating the nanometric contamination layer that covers a sample. Intermittent contact, on the other hand, is associated with oscillations that can be as wide as one hundred nanometres. This means that the probe will be driven through both the attractive and repulsive regime on the same oscillation cycle, what has the advantage of eliminating lateral forces while in the repulsive regime, something that is not possible in contact mode AFM, and also of penetrating the contamination layer and feeling the sample directly, eliminating some interference and allowing to sense other properties. However, this mode of operation leads to greater more tip wear and damage chance than non-contact mode due to the effective contact with the sample[33].

Common channels of acquisition for these modes of operation are topography, amplitude and phase. Topographic acquisition is based on the same principle as in contact mode with amplitude being the error signal, similar to deflection. Because amplitude records the same type of data as deflection - the slope on each point – this allows to have the same visual effect that was as described in the contact mode chapter.

The other usually used channel of acquisition, which will be discussed in a chapter below, is phase imaging. This is an especially important and interesting channel because, unlike other measurements which suffer from tip convolution artefacts, the data collected by this channel derives from how properties of the sample surface affect the oscillation of the tip. Since this interaction is normally done between the atoms in the very end of the probe and the atoms

in the sample, when the targeted sample has very small widths, like DNA strands, this method becomes more interesting to determine the dimensions of the molecule and even repetitive patterns, since different structures provoke different effects upon tip oscillation even when the measurements are starting to border the resolution limits of the AFM.

These operation modes are highly favoured for the observation of soft and fragile samples, which tend to deform upon contact or which can be destroyed by stronger interactions, like living cells, that may become punctured by a contact mode probe. It is also considered to be a far less destructive technique and with higher sensitivity in some cases, since that, in theory, there is never true contact between the tip and the sample and therefore lesser chances of modifying it. These are the main reasons of non-contact AFM being such a popular operation mode in life science environments, polymer applications or single-molecule studies[47,48].

# 3. Atomic Force Microscopy applied to DNA, proteins DNA-protein and nanoparticle-protein interactions

## 3.1. AFM in liquid media and force spectroscopy

The atomic force microscope, which as a scanning probe microscope had been traditionally associated with physics and material science, became over time a tool for research in the fields of medicine, biology and biochemistry. In coherence with this, many probe fabrication companies sell probes that are specific for measuring in liquid, or can be adapted to different conditions like contact mode in air and tapping mode in liquid. Many AFM manufacturers already have equipment specifically oriented to biological samples as well, and release software prepared for measurement in liquid media and/or measurements done on biological samples, many going beyond basic topography[33,49].

These potentialities are what drew life science research towards the AFM: the possibility of observing life molecules and cells in their natural state or in a protecting buffer solution with unprecedented resolution, without worrying about damage or complex preparation protocols that would be necessary for the same observations in electron microscopes. Biostructures and biomolecules are hard, if not impossible, to observe in standard electron microscope equipment due to incompatibility with liquid media and the insulating properties of these elements or vacuum operation. Another interesting potentiality which will be approached in this essay is the prospect of using the liquid media as support for the occurrence of biological reactions during the scan. Hopefully, this will allow in the future for real time measurements of molecular biology phenomena, like polymerase chain reactions, as a standard and common mode of operation. This would allow for a different and visual approach to some of the greatest milestones in the history of biological research, making possible to document dynamic behaviours in real time[50,51].

Many life molecules can be dried and observed in air and, actually, in some situations, like in the observation of an enzyme, the inexistence of water can sometimes aid the enzyme in keeping its original structure and therefore produce a more realistic observation, since the amount of energy needed to denature a protein or allow it to change its structure is lowered by the presence of water[52]. However, the interest in the possibility of doing liquid AFM rests on the chance of documenting phenomena and reactions in the same conditions as they occur inside living organisms, or simply to observe molecules and structures in less disruptive conditions. Furthermore, depending on AFM development and its speed when scanning an area, time lapse images and real time imaging of single molecule interactions can become a reality in near future. One interesting examples of time lapse imaging of phenomena is the accompanying of the twisting and folding of DNA structures, as recently done by Jiang *et al*[53].

There is not one specific type of aqueous medium in order to operate an AFM in liquid, and this works as an advantage in observations because, as long as the medium is free from solid contaminations, in theory, any type of liquid would be fit. Obviously, the most used liquid is water, since it is a basic and logic choice with the single objective of keeping a structure or molecule hydrated during a scan, but many of the usual biology buffers can (and should) be used, especially if they have a specific end that can aid in preparing the object of study and therefore, producing better images[51].

There are already many published results concerning the observation of structures and molecules in aqueous media. A single search on science literature search engines, or even web search engines, will turn out many results of single protein images and DNA strands, but they normally are simple images focusing more morphology than interactions between these structures or life molecules, when this is precisely one of the most interesting promises of operating an AFM in liquid[50].

However, imaging in liquid is not as trivial as imaging in air. The first drawbacks arise during the tuning of the instrument. The liquid is known to damp the effects of the cantilever excitation, leading to a shift of the cantilever peak frequency to lower values (up to four times less) and also broadening the main resonance peak (smaller quality factor - *Q*), meaning that for the same input signal in air, the output result will be less pronounced when operating in aqueous media. These differences can be seen by doing a thermal capture (Figure 3.1) of the cantilever. A thermal capture consists in evaluating the probe's mechanical (deflection) response to thermal agitations, such as Brownian motion of the molecules that make up the measurement media. By plotting the frequency spectrum of this response, it becomes possible to estimate the cantilever spring constant, what then gives fundamental information to the tuning of the probe, aiding in selecting a resonance peak where the probe is the most responsive to alterations in the sample[54,55].

Due to this, the amount of energy needed to drive an AFM probe in liquid is greater, meaning that higher drive voltages must be used. These are often one order of magnitude above the range of drive voltages used in air operation, which are commonly on the range of the dozens of millivolts. It can be also happen that when the cantilever is driven, the liquid surrounding it also resonates and starts vibrating, leading to the appearance of false resonance peaks which can lead to a weak tuning and therefore weak imaging[48,56].

Liquid media opens many possibilities that are out of bounds for other microscopy techniques, but it has some limitations. The possibility of operating in liquid media at resolutions similar to those attained in air is extremely attractive and would shed more light on many reactions and interactions that occur between biomolecules and bioconjugates inside

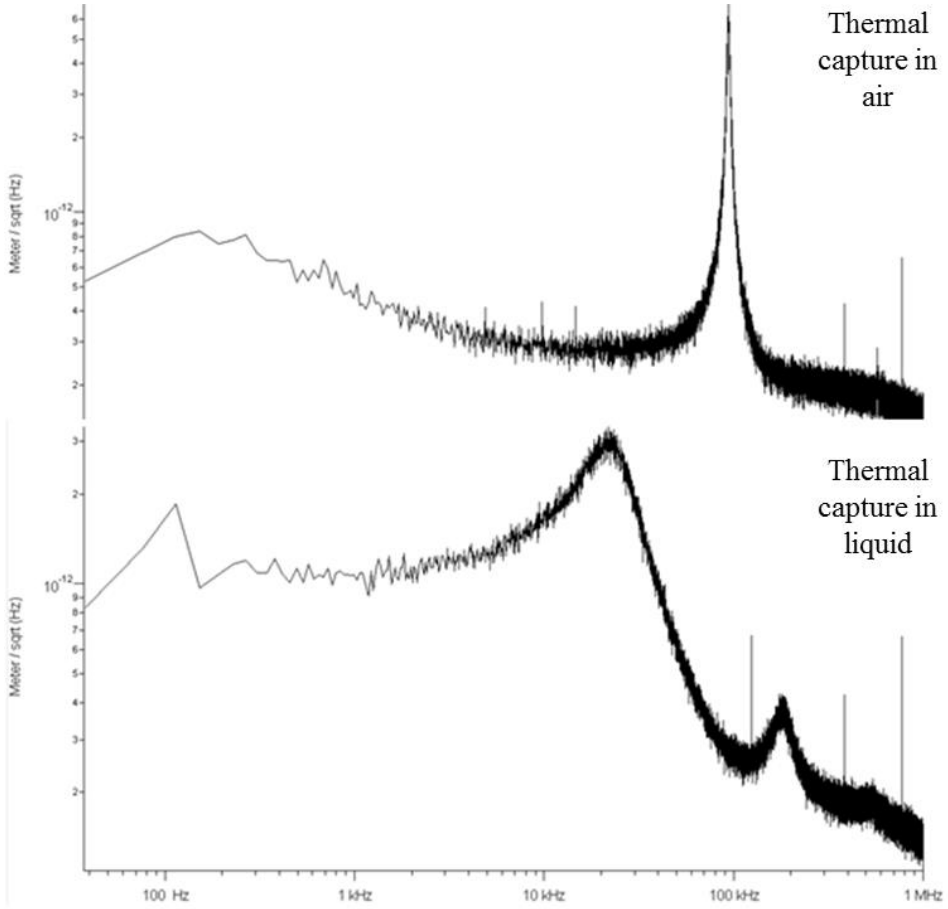


**Figure 3.1 – Thermal capture of an Olympus BC-AC40TS both in air and liquid. The main resonant peak shifts from approximately 100 kHz to 25 kHz and a broadening in the peak (lower Q factor) occurs.**

living cells. It would also allow measuring and analysing phenomena and characterizing key elements of biosensors *in situ*, which rely on biomolecules or phenomena related with biology to operate, some of which are nanotechnology inspired. Although several advances such as liquid cells and specific probes have been developed, the values of resolution that are possible to achieve on demand, *i.e.* without specific conditions of operation, preparation or imaging (room temperature and pressure, inside a drop of liquid, *etc*…), can easily fall behind those of operation in air or vacuum. Actually, many of the true atomic resolution images produced with an AFM in which outstanding results were produced (such as single molecule imaging with picometric resolution), would be impossible to apply on an observation with the objective of producing measurements on a biomolecule in a native or at least friendly medium, since many require vacuum or cryogenic solutions[57,58].

Another interesting mode of operation that can be applied to biological samples is force spectroscopy, which focuses on measuring the strength of the interaction between the AFM probe and the sample. The notion of the cantilever-tip interaction force curve is fundamental to this mode, as can be seen from the similarities between the Figure 2.5 schematic and Figure 3.2, a real force curve obtained with the AFM, in which the attractive and repulsive regime can clearly be differentiated.

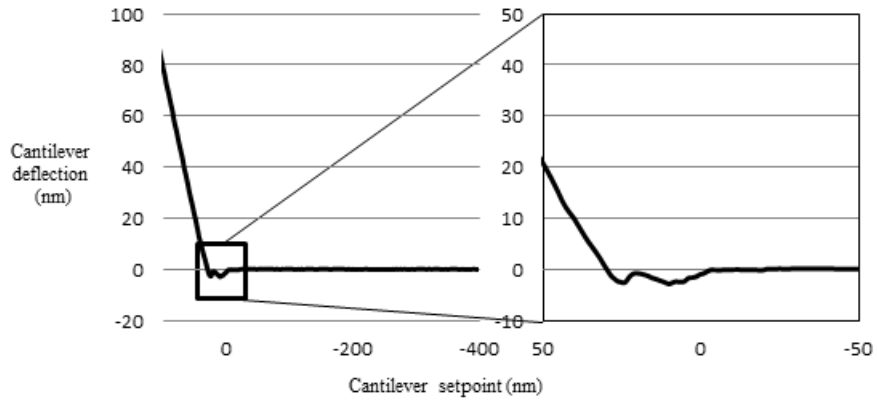


**Figure 3.2 – Force curve acquired by inward force spectroscopy on a protein, with detail of the effect on cantilever bending at near setpoint zero (squared area). Setpoint zero refers to the height from the sample at which the feedback control acknowledges the standard tip-sample distance for imaging and switches the *z*-axis control on. In this case, its refers to the height in which net attractive forces were first detected.**

Although this mode was not approached in this dissertation, it merits mentioning due to the interesting applications in biostructures, such as measuring the strength of the inter domain bonds that keep a protein assembled, by pulling an amino acid sequence in its surface away from it. The force needed to unfold the quaternary structure into an amino acid chain can be predicted by this method. It is also possible to do the contrary: compressing the biostructure and evaluating the resistance to deformation and the conditions in which it occurs. Unlike the most common modes, which rely on raster scanning the sample surface, this mode is one-dimensional since it involves selecting points on the sample, approaching the probe to that specific location and acquiring force curves. This can, therefore, be used to evaluate the mechanical properties of biomolecules and their resistance to unfolding and denaturation scenarios[59–62].

## 3.2. Phase mapping versus topographic mapping: why is it so useful in biological sample imaging?

The phase offset or phase difference between two similar waves relates to the delay in time that exists between them. The same way that two waves with a given frequency may have different amplitudes and *vice versa*, the phase is another property that can be studied and measured (Figure 3.3). Phase offset information is normally given in degrees. A wave with a phase of 0 degrees will overlap the original signal while a wave with 180 degrees of phase will appear as an inverse signal. The phase channel of an AFM shows how the sample properties interfere with the probe oscillation, by measuring anomalies in the measured sinusoidal signal of the probe when compared to a reference signal. However, it can also be a source of many artefacts, requiring correct interpretation.

It becomes clear from this small explanation that phase imaging depends on the AFM probe being oscillated, and that therefore this channel of acquisition relies on an alternate contact mode of operation. It is considered to be a non-topographic mode of acquisition since that, up to a certain extent, the type of acquired information is almost independent from

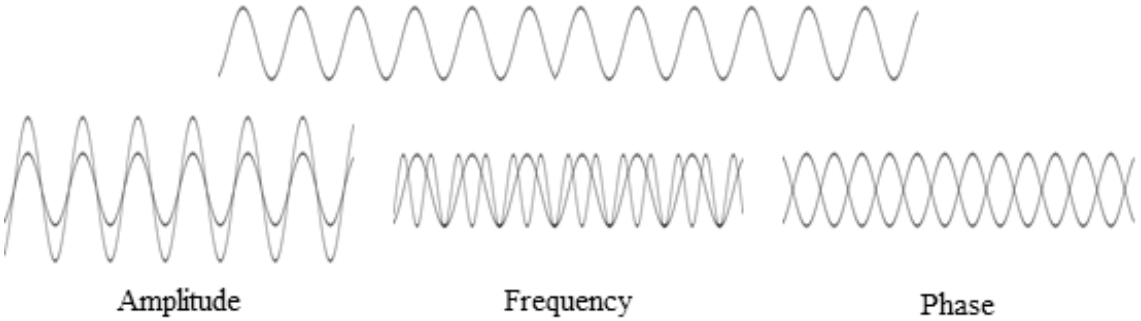


**Figure 3.3 – Effect of changing different wave variables compared to the original wave signal. The waves in the bottom are overlapped with the standard wave (which also appears above them) and have similar parameters, except for amplitude, frequency and phase, respectively.**

topography and relies heavily on physical and mechanical properties of the sample (the exception are large slopes, since lower contact areas of the tip with the sample can affect phase readings in a discreet way)[33].

These readings are qualitative by nature, meaning that one can differentiate materials on a substrate, but not point what elements compose it without prior knowledge of the sample, like through EDS analysis using a SEM. The oscillation of the probe can be affected by a series of factors such as composition, adhesion, friction and viscoelastic properties of the sample, which act upon the very end of the AFM tip. Basically, differentiation between areas is done because, to the same input, different results are presented by materials with different properties. An analogy to help in visualizing this phenomenon happens when wet and dry sand are stepped by the same person: the resulting footprint can be very different because although they are the same material, the viscoelastic properties are different[63,64]

This has the advantage of producing results that, by not relying exclusively on topographic elements, are less dependent of tip convolution effects and therefore can aid in producing sharper measurements of the features of a sample, helping to point, in a precise manner, where different materials lie on a substrate which can be similar from a topographic point of view[39].

Polymer chains, DNA strands and single molecules are the kind of sample which will not generate clear differences on topographic modes due to their small heights, even in comparison to the substrate roughness, perhaps even giving the impression that, when using larger scan areas in an attempt to find a suitable scan area, there is nothing to study in that area. However, paying attention to the phase signal can be a way to easily detect patterns and structures, aiding in the mapping of these and allowing sharper imaging because where the height of an object of study may represent dozens or hundred times the height scale, the phase signal obtained from the background and from that element may be different enough to allow detecting different structures, such as in Figure 3.4, where the DNA molecules that are

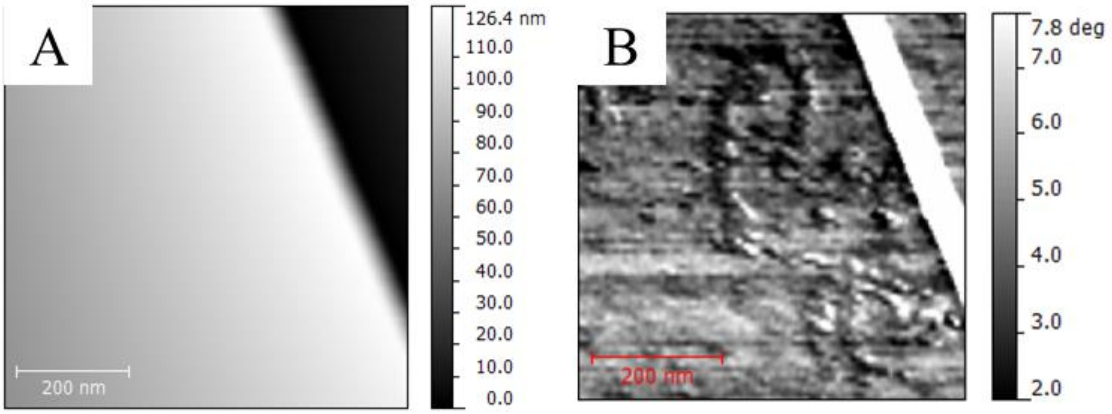


**Figure 3.4 – Difference between topographic and phase imaging. The scale on the topographic image (A) was selected using the automatic scaling given by the AFM software. It can be seen that no DNA can be observed due to the existence of features several times larger than its height, which mask it. However, using phase imaging (B) makes it possible to observe subtle DNA molecules in the same area.**

impossible to see in the topographic image, become less discreet in the higher sensitivity phase channel[65].

Samples of biological origin, be it larger targets like cells or nanometric life molecules, have very specific mechanical behaviours that can be used to distinguish between two seemingly similar structures, something that can go as far as allowing to differentiate cancer cells from healthy cells with a simple AFM scan. Because phase imaging data acquisition is strongly independent of topography, it becomes possible to use the data acquired through this channel to pinpoint the accurate location of specific types of molecules, their behaviour, patterns they exhibit, and to help understanding how these elements behave around other elements[39,66].

Basically, this is a very interesting channel of acquisition that offers and already delivered promises for biological measurements because where material or electronic engineers use the AFM to find defects, study electrical behaviour or to get roughness measurements, clearly focusing topographic acquisition, phase mapping focuses the nature and properties of a sample, how it affects the behaviour of an AFM probe, allowing the study of the properties of different samples like polymers, nucleic acids or cell walls, be it isolated on a substrate or undergoing reactions in a liquid and metabolism friendly buffer.

## 3.3. AFM tip modifications and relation to resolution of an AFM

One of the ways to pick a basic and cheap commercial AFM probe and bring it to another level of precision and resolution is by modifying the probe. Apart from the modifications approached in this thesis, there are many different approaches on this field: for example, electron-beam deposition or using carbon nanotubes on the tip of the probe[67,68]. Other modifications that aim more at improving force spectroscopy results consist in functionalizing the probe with a colloidal particle or even with specific molecules. While the first consists in

measuring the effects of compression on the sample, the second method makes use of functionalization with specific molecules. This allows to analyse single molecule interactions and evaluate the strength of the interaction between these two elements[69,70].

In this dissertation, focused ion beam microscopy is one of the approached procedures to modify AFM probes[71,72]. This can help, up to the precision of the FIB system, which modern equipment can take as far as 2.5 nanometres in low current, to sharpen a probe's slope, which normally borders the sixty degrees, up to virtually 90 degrees, therefore helping to eliminate some tip convolution effects and to enhance resolution[73].

Modifying the AFM probe with coatings is also a common approach that was studied. Many AFM probe companies produce coated probes for photodiode sensitivity reasons, however, liquid operation may justify tip coatings as well. Extreme pH operation and operating in liquids can in theory lead to the oxidation or reduction of the probe. This may seem trivial, but the real problem lies on the fact that this event leads to uncontrolled changes in tip radius during operation with that probe, making results very hard to replicate with the same probe, even in similar conditions.

As mentioned in the chapter on AFM probes, some artefacts may depend on the electronic components of the AFM, however other common artefacts are related with properties of the probe, such as its dimensions, which can lead to tip convolution phenomena when operating near the limit of magnification[41]

There are two main physical characteristics of an AFM tip which directly interfere with its lateral and horizontal resolution: tip radius and slope. Lateral resolution depends on the slope of the probe, since this affects the capability a tip has to measure very rough areas by going down on a deep but narrow depression between two ridges and resolving what lies on its bottom. Very sharp tips will be able to fit between the two ridges and measure the entire area behind them, no matter how deep, while larger tips won't fit because its sides will bump on the ridges before detecting the bottom and, although mapping the distance between those ridges well, inaccurate information of the area lying between them will always be displayed.

It is also true that horizontal resolution depends on the diameter of the tip, because it can be deduced that the smaller the tip is, the more specific and accurate will be the measurement of the area laying before it[33,68,74].

The equation below illustrates an approximation to the difficulties posed by tip convolution, in which $d$ is the minimum distance resolvable, $r$ the tip radius, and $h$ the height of the feature of interest.

$$d = 2\sqrt{2rh}$$

**Equation 3.1 Simplified equation of Bustamante *et al.* for a simple spherical tip shape**

For example, if a spherical tip has a radius of 20 nm and is being used to image a hypothetical structure with 1 nanometre of width but a height of 5 nanometres, these structures would have to be roughly 28 nanometres apart for the substrate between them be detected. This also means that these structures, although being rectangular, would appear as semispheres with radius of roughly 14 nanometres. It's clear that if a tip has one atom on its edge, it will for sure be able to distinguish different atoms on the sample, while if it has a tip made of a larger quantity of these particles, for example, enough to have 20 nanometres of radius, it will only be able to produce very sharp and defined images if the scan area is larger than some micrometres[49,75].

This previous equation was derived from another devised by Bustamante *et al*. in which it was predicted the width (*w*) of a structure under the AFM by knowing the probe's radius (*Rp*) and the structure radius (*Rs*)[76].

$$w = \frac{4(Rp + Rs)\sqrt{Rs(Rp - Rs)}}{Rp}$$

**Equation 3.2 Prediction of the width of a structure with a Rs radius when measured with a tip with Rp radius.**

Using DNA as example, which has roughly 2.5 nm of width and an average resolution probe with 10 nm of radius, the DNA chain would be expected to measure over 20 nm wide (21.65 nm), although this value would be shortened in phase mapping.

On the subject of resolution as well, the area of the probe that interacts with the sample is also determinant to the quality of the scan. If one attempted to scan a very small nanometric area with probes with several dozen nanometres of radius, it would be impossible to achieve atomic resolution. Make it the diameter of an hypothetical atom to be 100 pm. Any attempt to image at this scale would produce blurry and bad quality images in general because the outputted value, after the signal processing, only relates to the average of all the reading collected in each point of the scan area, what can result in aliasing of the sample[77]. The AFM resolution also depends of other factors, from the sensitivity of the piezoactuators to the force sensor, since these must be able to detect the smallest variations in the sample. However, if the probe used is unable to detect variations as small as those the force sensor and the data processing can measure, the resolution will be determined by it and not by electronics.

Aliasing means that the inputted signal was detected because one or some, but not all of its parameters, were of a value high or frequent enough to be detected (for example, the height


**Figure 3.5 - Simulation of aliasing of the UNL logo. The first image is the original, the second one averages the colour value of each 4 pixels into 1, the third one each 16 pixels into one and the fourth each 64 pixels into one.**

of a feature can be enough for the AFM to detect that change, but the frequency of the pattern such feature displays may be higher than the frequency of the AFM signal detection), which means that the produced image will show existent but inaccurate features[78]. An illustrative example of what aliasing consists of can be seen in Figure 3.5, where the detected signal would be colour and the aliased signal would be pixels per row (resolution).

This example, in which every image to the right of the other has less lines and columns, *i. e.* less resolution than the one before, easily illustrates why one of the most important scan parameters in hand with probe sharpness is the amount of lines and columns chosen during the scan. More points in an image mean that data collection by the AFM will happen more frequently and that, in theory, the more faithful the outputted image when compared to reality will be. This also explains why images of big scan areas can have more quality and allow for far greater zooming than images of very small scan areas but with less resolution, something that does not stand as always true when, for example, one looks at many images produced by electron microscopes[79].

The downside is that the time needed to complete a scan may suddenly change from under five minutes to entire hours, in the case of images with over one million points of samples requiring slower scan rates. The upside is that, hypothetically, it is possible to do an image of a dot which can be seen by the naked eye which can be zoomed up to the atomic lattice.

# 4. Modification of AFM probes

## 4.1. Focused ion beam milling to enhance lateral resolution

### 4.1.1. Contact mode tip modification with FIB SEM

Physical modifications were done in a scanning electron microscope by milling the probe tip using a focused gallium ion beam (FIB). The conditions are presented in the Appendix I.a.ii. These modifications had the objective of eroding the base of the tip in such a way that its slope could be reduced from values ranging the 65º to 60º, to values nearing the 90º in order to achieve maximum lateral resolution.

It was decided to use a contact mode probe rather than alternate-contact probes because contact mode probes are dragging along the surface all the time instead of oscillating, being more usually applied in studies that aim at larger scan areas where the objective is to map topography and obtain more realistic results in roughness[80,81]. Since the interest was focused on topography over other types of data acquisition, there was no need to select probes that could operate on other modes, which would be oscillating at a distance from the sample and are more sensible to variations of other nature, which were irrelevant to this study.

The probes were milled by locking the FIB beam on the probe's tip and selecting a ring area around it. The entire area but the very top of the tip, which is responsible for contacting with the sample and tracking the surface, was milled down several micrometres, in a procedure similar to one described by Konoplev *et al.*, what resulted in the probes seen in Figure 4.1[71].

Modified probes were then mounted onto the AFM and used on the same conditions of operation as the unmodified probes, in order to be easier to highlight differences. Two different samples were elected to be used in the study: an Asylum Research standard sample and a silica sample specifically designed and produced at the same time as the probes in the SEM-FIB, although only results done with the latter are presented. This sample had a group of features of different shapes and depths milled onto its surface, which were chosen specifically to raise the chance of seeing different behaviours between unmodified probes and probes with tips that had underwent dimension modification.

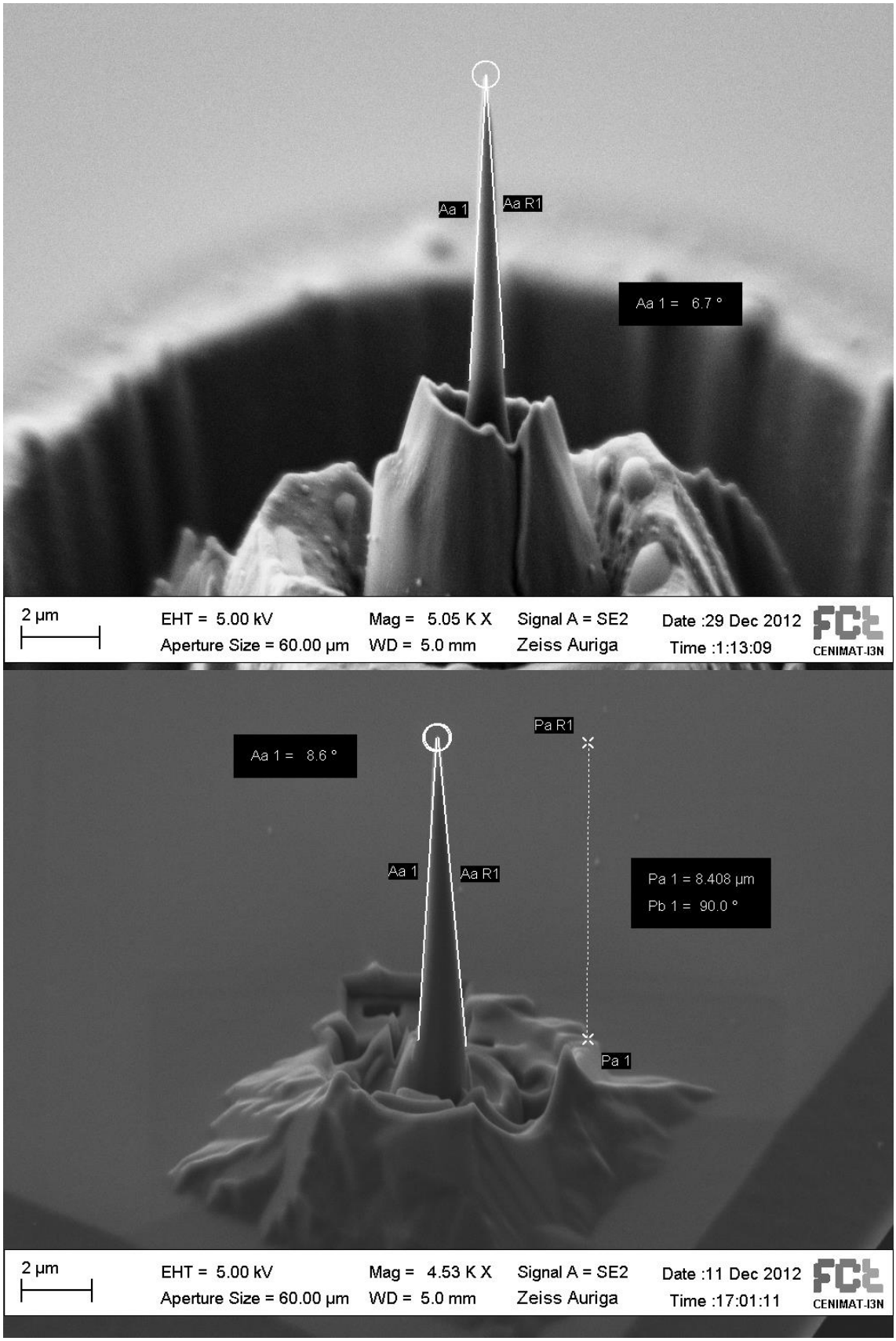


**Figure 4.1 - Scanning electron microscope image of AFM probes after milling with the focused ion beam.**

### 4.1.2. Lateral resolution results and comparison

The feature used to compare modified with unmodified tips was a comparison feature consisting in the shape of a trapezoid milled into a silicon substrate. This shape was milled under high electric current (5 nA at 30 KeV), what has the disadvantage of fabricating features with blunter edges due to smaller accuracy of the FIB gun, in order to quickly generate a 6 micrometre drop, which grew vertically by the smallest parallel side, and with a slopes towards the biggest parallel side (Figure 4.2). The drop size was chosen to be 6 μm because the voltage range of the *z* piezoactuator of the AFM (approximately 160 V) roughly translates into a range of action of 12 μm, meaning that since surface engagement is done with an applied voltage of 80V on the piezoactuator, the depth of such drop would be the maximum the AFM would be able to negotiate satisfactorily.

Figure 4.2 shows the 3D rendering of the comparison feature when analysed with the modified probes, while Figure 4.3 gathers topographic images (A and B) and height profiles, collected both with the FIB milled probe and the unmodified probe.

It can be seen that the steep vertical drop was shown as having a slope of roughly 59º, which is in agreement with the manufacturer specifications of a side angle with 25-30º (Figure 4.3A). Even more discrepant was the fact that the calculated depth of the trapezoid with the unmodified tip was approximated to be roughly 2.25 μm. It was also observed that that the deflection channel outputted completely constant values for the bottom of the trapezoid pit. This was a clear sign that the tip was never in contact with the surface, since a FIB milling, especially at high current, would never produce an atomically flat surface[82].

A new measurement session of the same feature was then done with the FIB milled

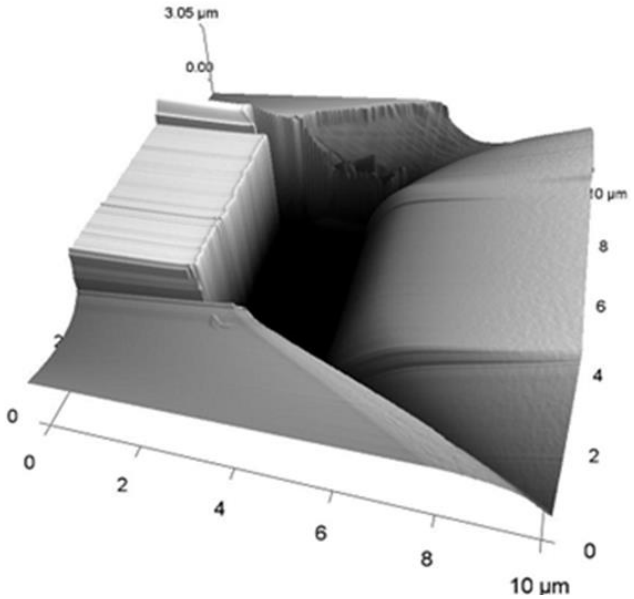


**Figure 4.2 – 3D rendering of the FIB generated comparison feature.**

probe, in which collected data showed a clear improvement in the ability to correctly measure the features when compared with unmodified versions: the vertical drop was now measured to have a slope with an angle few decimals above 88º and the depth of the pit, using the substrate surface as zero was now measured to be roughly the expected 6 µm, the value expected from the FIB milling (Figure 4.3B).

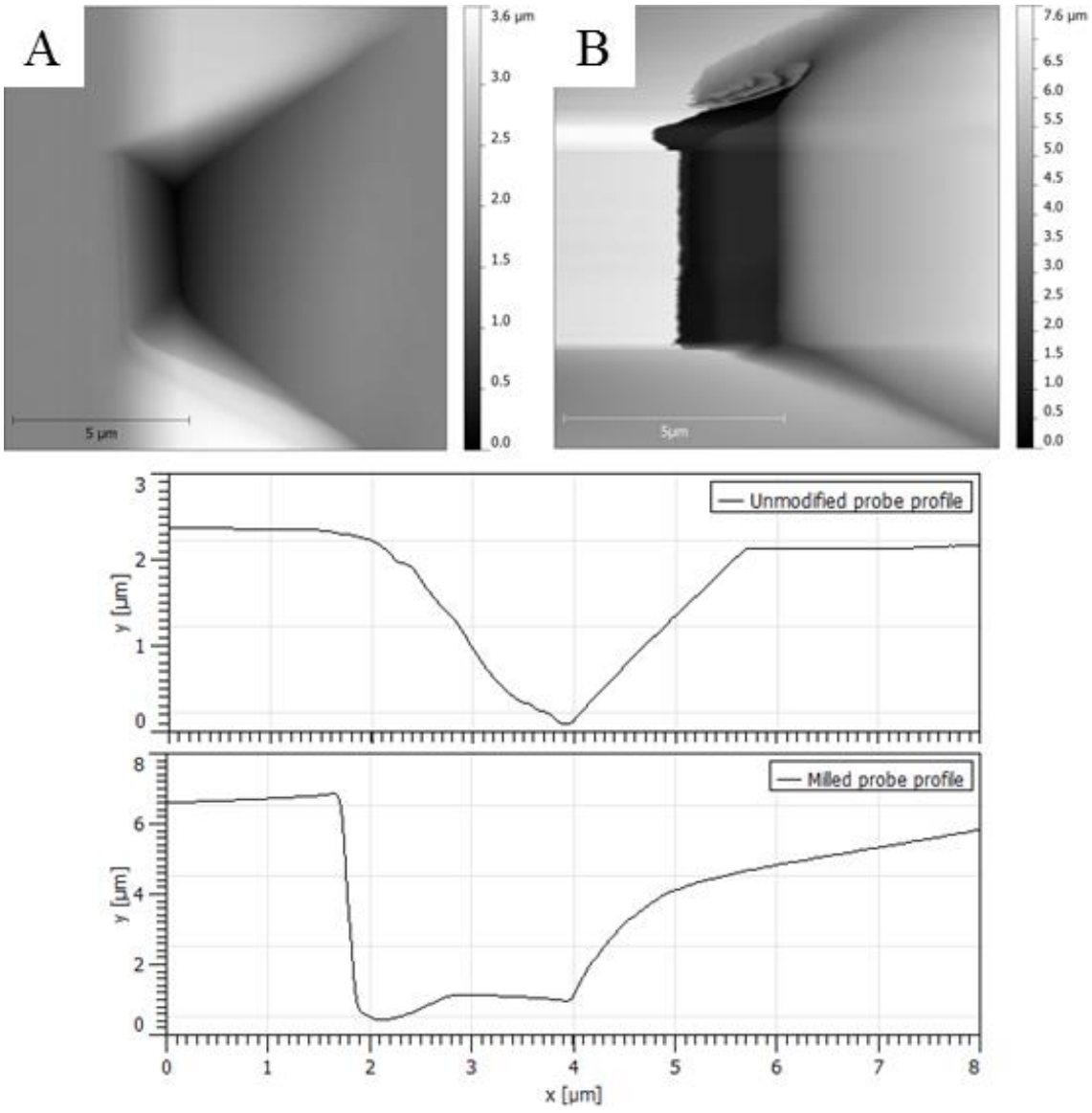


**Figure 4.3 - Results of operation with FIB milled probe. Topographic image of the comparison feature when done with an unmodified probe (A) and with the FIB milled probe (B) and respective height profiles**

### 4.1.3. Gold-Palladium coating of tips and horizontal resolution comparison

AFM probes were coated with a nanometric layer of gold-palladium in order to enhance reflectivity, and therefore the sensitivity of some of the measurements, and also to behave as chemical shield, since that silicon suffer redox reactions when used in liquid media or with biological samples, resulting in altered properties, especially in solutions with low or high pH.

The interest now was horizontal resolution and since the protective coating would be used in alternate contact operation, probes specific for this mode were modified instead, with the AC mode Tap300Al from Budgetsensors being selected for this study. After the deposition was complete, the modified tip was observed by SEM and submitted to EDS. The data (Figure 4.4) confirms the quality of the coating and the presence of gold.

The coated probe was then mounted onto the AFM and used to measure similar 1 μm areas of a comparison sample. The images obtained (Figure 4.5) show the results of topographic and amplitude acquisition of the same area. By visual inspection, the images appear to be extremely similar. The existence of subtle ridges, possibly a result of the FIB milling, can be seen in both images although with a small improvement in detail on the images produced with the unmodified probe. However, the height scale at which the images were done is small, even below the height scale of DNA molecules or single proteins. The roughness (RMS)* values obtained for unmodified probes were 124 pm and 75 pm for topography and amplitude, respectively, while gold-palladium coated probes showed 111 pm and 67 pm. As example, the RMS calculated for a topographic image of the atomic lattice of silicon was roughly 35 pm. The decreased RMS using the AuPd coated tip indicated that the radius of the probe is larger, as expected due to the deposition of the 8nm metallic layer.

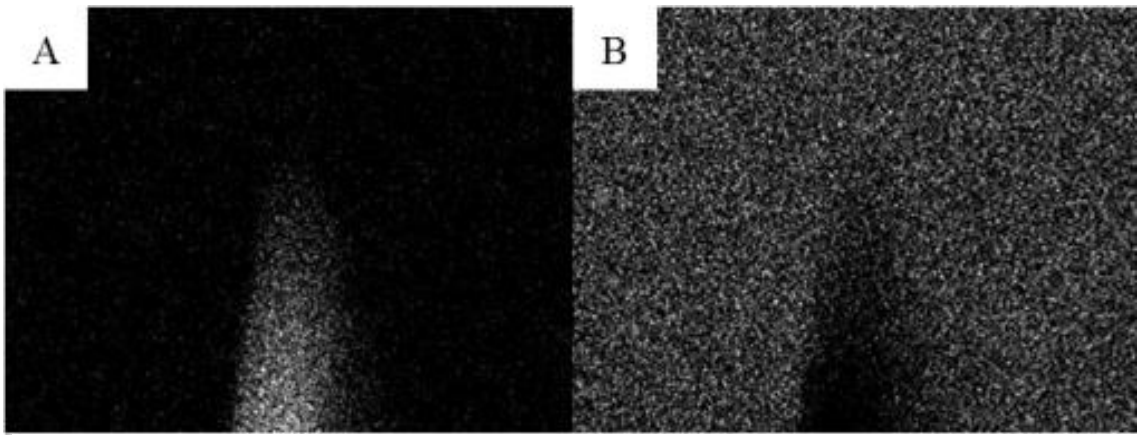


**Figure 4.4 – Elemental maps of the probe's tip by EDS. A: Elemental map of silicon. B: Elemental map of gold.**

* $R_{RMS} = \sqrt{\frac{1}{n}\sum_{i=1}^{n} {y_i}^2}$

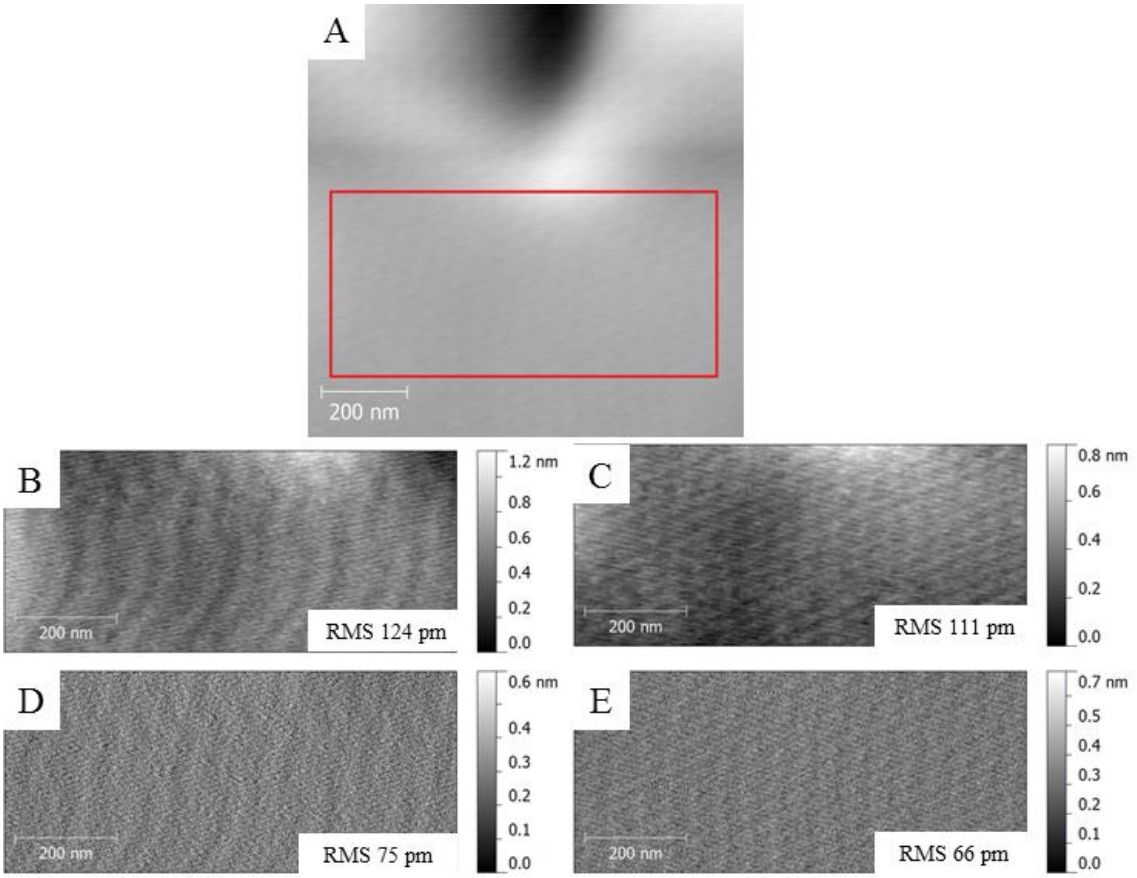


**Figure 4.5 - Images produced by unmodified and coated probes were done in the same area of a silicon surface, marked with a red rectangle (A). Topographic images of this area done with an unmodified probe (B) and with a coated probe (C), as well as amplitude imaging done with an unmodified probe (D) and with a coated probe (E) are presented together with RMS values.**

### 4.1.4. Gold-palladium coating of AFM probe backside to enhance photodiode detection

One of the disadvantages noted when using the probes which offer the highest resolution, such as the Nanoworld SSS-NCH probe, which was used on some of the AFM imaging on air of DNA and that can achieve atomic lattice resolution, is that they are normally sold without any special coating, *i. e.*, the reflection of the laser signal occurs straight on the silicon surface of the AFM probe.

This situation led to the paradox of having low cost probes with larger tip radius to reflect the laser beam with more intensity, meaning more sensitivity in the force transducer, than expensive and sharper probes. All the other alternate contact probes used already had a gold or aluminium coating, unlike this probe, resulting on the AFM photodiode producing voltage values that sometimes were below 3.5 milivolts, due to the fact the voltage generated is proportional to the amount of light the photodiode receives[33,83]. Coated probes regularly doubled this voltage value.

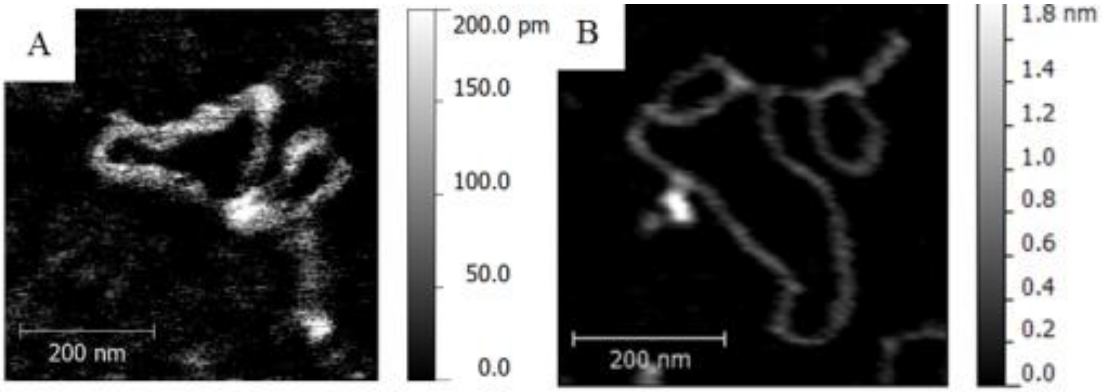


**Figure 4.6 - Comparison between topographic images of DNA molecules done with an uncoated probe (A) and a probe with its backside coated (B).**

It was thus decided to make an attempt at enhancing the probe reflectivity, while not compromising the resolution of the AFM probe, by only coating the cantilever side opposite to the tip. The coating was immediately determined to have increased the collected intensity of the beam by roughly 10% to 15%, since probe reflectivity shifted photodiode voltages from values ranging between 3.5 and 3.6 mV to values ranging between 4.0 and 4.1 mV. These values were obtained during the standard probe tuning procedures to start AFM measurements.

On the subject of AFM measurements using this probe, it was predictable that an SSS-NCH tip would produce more defined and less sluggish images than its cheaper and blunter counterparts, due to reduced tip radius. However, differences in results obtained with uncoated and coated probes were noted, especially on the topographic value, which depends entirely on the photodiode detection on the AFM used, as can be seen in Figure 4.6 where the difference in scale length is almost of one order of magnitude. The usage of these coated probes helped in the production of better contrasting images, what shows that backside coating of AFM probes seems to be an effective, quick and cheap way to enhance image acquisition in situations where the AFM probe used is not coated with a reflective layer.

# 5. AFM comparison studies – Insulin and gold nanoparticle conjugates

## 5.1. AFM measurement and analysis of amyloid insulin

### 5.1.1. Overview on insulin and rationale for selecting this hormone

Insulin was selected as the first biological molecule to be measured due to recommendation by the AFM manufacturer, since it is an extensively studied molecule in using AFM and SEM, allowing for the results to be compared and analysed in view of the existing literature. Insulin can also be measured both in air and liquid media, allowing for the liquid AFM training to be initiated with a molecule allowing a comparative analysis between images acquired in different media, in order to establish replicability.

This peptide hormone, produced by the beta cells of the islets of Langerhans in the pancreas of vertebrates, is stored as an hexamer during its production. However, only its monomeric form has the property of regulating blood sugar levels[84].

Misfolding or any other structural defect of any protein or hormone, may affect its solubility, which may lead to the appearance of fibril deposits in organs, a medical condition known as amyloidosis and which has been linked to the onset of neurodegenerative disorders such as Alzheimer or Parkinson's disease. Patients subjected to brain biopsies who were known to be suffering from these illnesses display deposits of insoluble amyloid proteins with a fibril like structure. These amyloid plaques affect the competences of the organ where they gather, especially the brain[85,86].

The insulin ready sample was donated by Atomic Force F&E GmbH, which chose to adsorb the insulin over a mica sheet, but without further information such as synthesis conditions or the expected insulin structure. However, it is known that conditions of synthesis and isolation, namely pH, can affect the way proteins will fold and therefore, what morphology they will exhibit. These structural changes should be evident by AFM or electron microscopy.

The pH of the medium chosen for the synthesis affects the chirality of insulin fibrils, since synthesis below pH 2.4 produces fibrils with a reversed (right) twist, while those synthetized in a medium with a higher pH will exhibit left hand twists, which should have a periodicity of 100 nanometres[87]. It is also documented that right and left hand fibrils can be distinguished because they do not share the same dimensions like width or height[87,88].

Methods and conditions of AFM operation and imaging can be seen in Appendix I.a.iv.

### 5.1.2. Results of AFM measurements and analysis

Measurements showed various structural forms of amyloid insulin, as well as the most reported form of insulin - the fibril form (Figure 5.1). Amyloid fibrils, which consistently stretched for more than one micrometre, were analysed to have widths of 38 ± 1.66 nm and to have heights of 4.06 ± 0.3 nm, with an example of a height profile at Figure 5.3, while it was also noted that in situations where fibrils overlapped, their height was roughly the expected value of 8 nanometres.

Measurements in liquid of insulin fibrils showed a small increase compared to width and height values obtained in air, with 43.6 ± 3.17 nm and 4.75 ± 0.44 respectively, which can be seen in Figure 5.4, along with the values acquired in air for comparison. Further observations in air had the objective of imaging the twists usually observed in insulin fibrils. These measurements coupled with image data analysis and width-height graph analysis showed the existence of a twist with a pitch of roughly 55 nanometres (Figure 5.2 and Figure 5.4). This structural periodicity was also observed in liquid, with image analysis pointing to similar values (Figure 5.5).

Another interesting feature observed that is coherent with the mechanism of formation of amyloid structures was that many insulin fibrils showed the tendency to aggregate, with several observed cases of fibrils adsorbed to each other, a feature that was predominantly observed in liquid media operation.

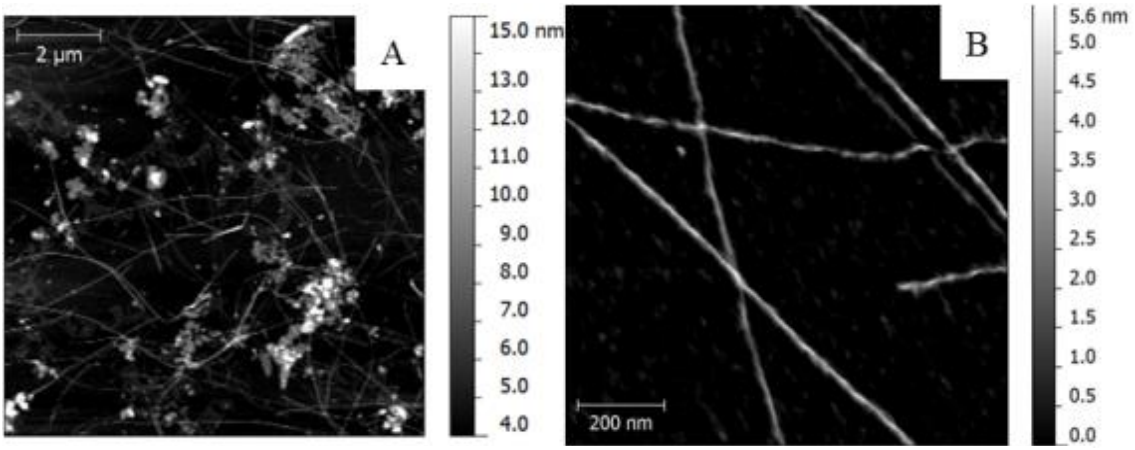


**Figure 5.1 - A: Topographic image of amyloid insulin, both in aggregate and in fibril form. B: stretched insulin fibrils.**

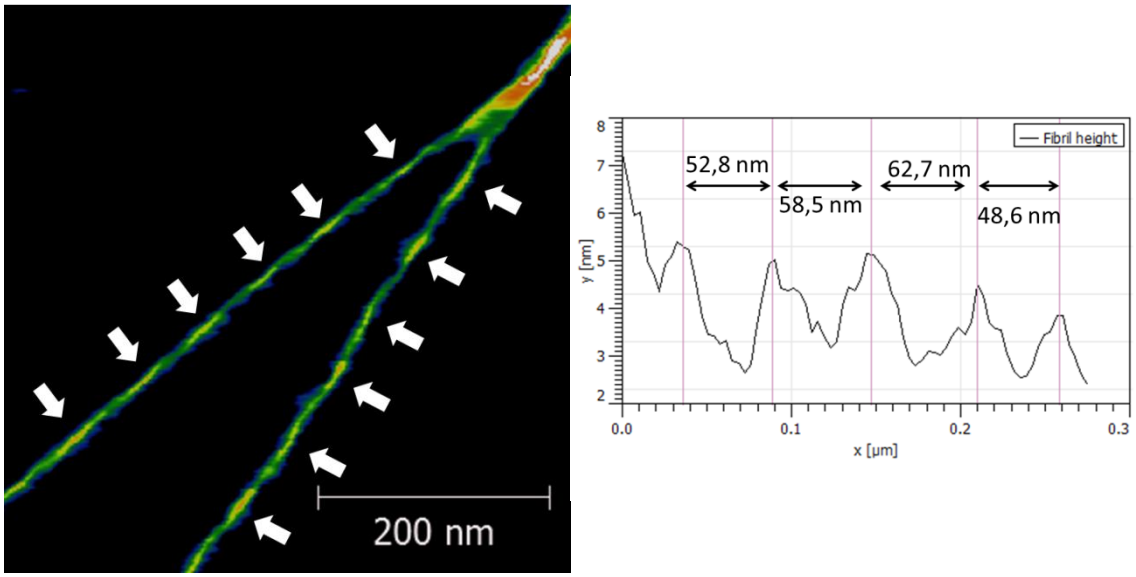


**Figure 5.2 – Topographic image and height profile example of the structural periodicity observed in insulin fibrils acquired in air.**

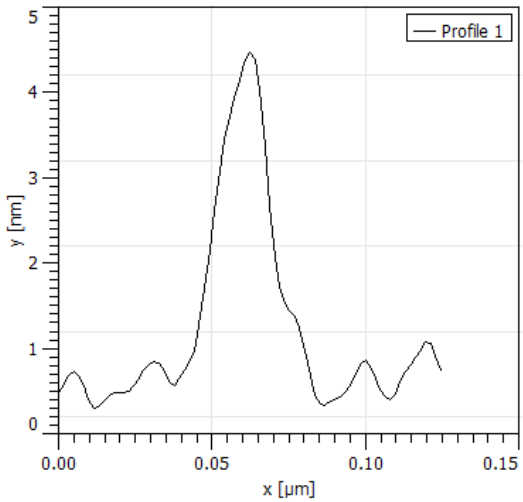


**Figure 5.3 – Height profile of an insulin fibril measured in air.**

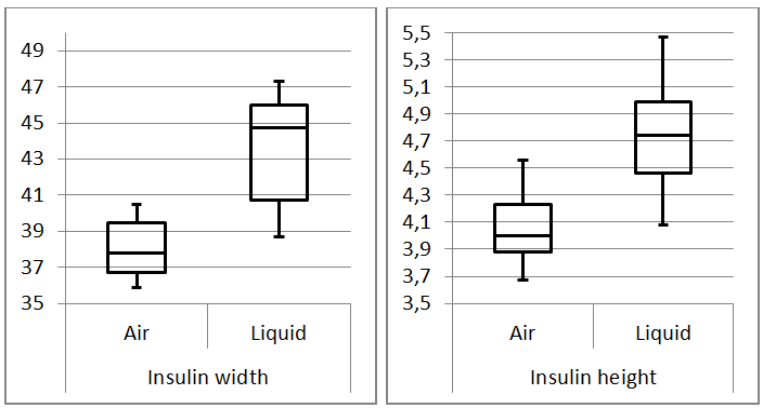


**Figure 5.4 – Comparison of box plots of insulin widths and heights measured in air and in liquid media.**

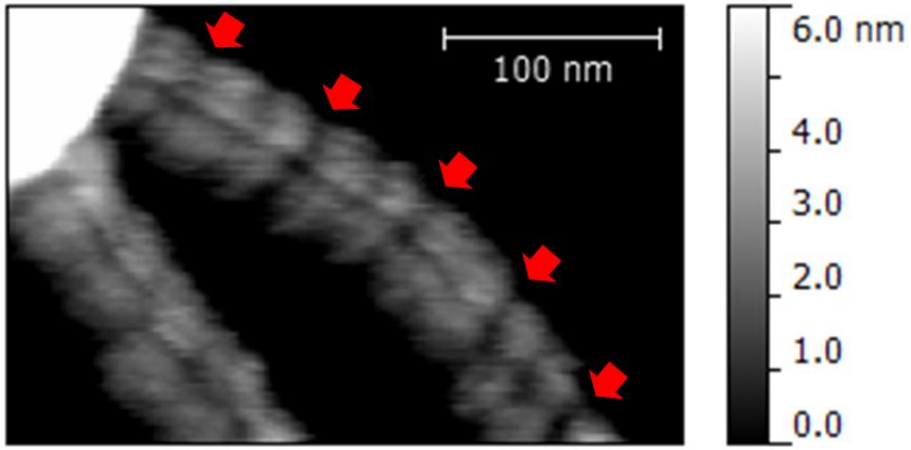


**Figure 5.5 - Insulin fibrils measured in liquid. Red arrows mark the structural periodicity.**

### 5.1.3. Discussion and comparison between air and liquid acquisition

As it has been briefly mentioned in the previous section, the results of measurements performed in liquid and in air are comparable and coherent with each other, albeit with few deviations that are not significant. Overall, AFM images collected through liquid media appear to be less sharp than those acquired in dry environment, an effect that possibly relates to two facts. First, the reduced sharpness of the liquid AFM probe used in this study, since its diameter is over four times larger the probe used in air operation. This size difference seems to have an obvious negative effect on the quality of the imaging due to tip convolution. Secondly, lower sensitivity due to interferences on the cantilever oscillation The fact that the AFM tip is immersed in a high density medium, like water or a reaction buffer, can result in images not as clear as expected, due to the tip being surrounded by a liquid which can interfere with the oscillation signal, especially due to a drop in the quality factor[56,89].

Data obtained in liquid medium was coherent with the measurements in air, because although they did not exactly match each other, they followed the line of expectancy of experiment's outcome. Indeed, liquid measurements indicated that the fibrils would be a small percentage wider and perhaps taller, since the probe used was less sensitive and blunter. Also, the contribution of water molecules in the volume and structure of may account for insulin appearing larger in liquid than in dried media experiments, although this also lowers the force needed to deform it[90,91].

It can be concluded that results obtained in liquid media had their dimensions inflated by a small margin –approximately 5 nm (15%) for width and 0.7 nm (17%) for height. However, one should not be too quick as to determine that this drop in the ability to read the molecule is exclusively related with the change in the medium. In fact, it should be taken into

consideration that the AFM probe used in liquid has a tip radius of 40 nm while the one used in air has a tip radius of only 9 nm. Through the application of the simplified equation derived from Bustamante *et al.*, it can be calculated that, in liquid, the insulin fibrils should not measure less than 40 nm while those in air could measure below this value, but not less than 20 nm. Insulin fibril widths measured in this experimented respected this prediction.

The periodicity described on these measurements of insulin, both from a visual and analytical standpoint and also imaging in both media, was also confirmed not to be an artefact, based on the existing literature. As mentioned before, the pH of the medium where the insulin fibrils are synthetized affects their chirality, leading to the formation of fibrils with different dimensions and characteristics. Kurouski *et al.*, through scanning electron microscopy and atomic force microscopy, have confirmed the existence of the same periodicity described in this work and have also studied the formation of fibrils in relation to the synthesis conditions. They have measured left hand twist fibrils, which originated from the aggregation of insulin monomers, and claim that they were 25 nanometre wide and 7 nm in height, values which were not found in the samples presented here. This type of fibrils was also reported to have a twisting with a distance of 100 nm. However, when analysing right hand twist fibrils, the authors claimed values of roughly 40 nm in width and 4 nm in height, although no indication on pitch distances for this type of fibril was given. These results are coherent with the results presented in the previous chapter and consistent with the data gathered in the CENIMAT/I3N equipment.

Surprisingly, it was also possible to demonstrate AFM's role as a key element in bionanotechnology by producing images that, almost two years after Atomic Force GmbH synthetized the fibrils in Germany, allowed determining some of the conditions of synthesis. In fact, it was possible to determine that the solution in which fibril aggregation was induced had a pH below 2.4 because not a single right hand twist fibril was observed while the study of insulin fibrils lasted. This result is an indication of how valuable an asset an AFM can represent in the field of nanocharacterization. Technical development of AFM and new hybrid modes should make it possible to routinely image and map specific amino acids in the near future, such as in the recent approach by Deckert-Gaudig *et al.* with tip-enhanced Raman scattering (TERS), underscoring the potential of recent methods of characterization of protein structures[86–88,92].

## 5.2. AFM measurements of uncoated and functionalized gold nanoparticles

### 5.2.1. Gold nanoparticles and their application to bionanotechnology

Being one of the core subjects of research in nanotechnology and the AFM one of the key instruments in this field, nanoparticle analysis and characterization is routinely approached through tapping or contact mode AFM, as is well described in the scientific literature[39,93,94].

Although nanoparticles were selected as a key element towards expanding the knowledge on AFM operation and its potential to biotechnology and bionanotechnology, the purpose of this training was beyond the simple measurements of the nanoparticles, but also to be able to use the analysis software to distinguish a naked gold nanoparticle from those that were functionalized with different capping agents. This could be done by establishing an average size shift in the different samples in trying to distinguish the presence of different molecules covering the nanoparticle. In theory, this would confirm the AFM as a useful tool when the objective is determining if the nanoparticles in a sample solution are functionalized with a high molecular weight capping agent (such as peptides or alkane thiols), or simply coated with a small and labile molecule such as citrate. Capping agents can be chosen by taking into account more than simply interrupting the growth of nanoparticles, since they can be selected having in mind the ability to confer specific properties to the nanoparticles, many of which are considered to be ground-breaking due to the possibility of being designed and engineered to develop and serve new applications for 21$^{st}$ century blossoming fields, such as bionanotechnology, biosensors and even theragnostics[95–98].

Gold nanoparticles were synthetized according to the method proposed by Turkevich *et al.* in 1951, the Turkevich or citrate reduction method[99]. This method stands on the principle of a solution of chloroauric acid being reduced by sodium citrate, although in practice other reducing agents can be used. Sodium citrate is known to react with gold ions ($Au^{3+}$) and reducing them into neutral gold atoms, which aggregate and precipitate, leading to the formation of monodisperse spherical nanoparticles with sizes directly related to the amount of capping agent used during the reaction and which will cover the growing nanoparticles, shielding them from further aggregation of gold atoms. This agent can either be citrate itself or any other component with the same function, from which there are many examples, ranging from proteins to organic compounds, or even DNA strands[99,100].

### 5.2.2. Development of AFM measurement protocol

The specific conditions of nanoparticle functionalization and preparation can be consulted in Appendix I.a.v. The results presented below were obtained by synthetizing a batch of monodispersed gold nanoparticles with average diameters of 13.9 ± 3.3 nanometres (Appendix Figure I.2). Mercaptoundecanoic acid (MUA) was used as a capping agent due to the presence of a thiol group in its molecular structure - $C_{11}H_{22}O_2S$ – which covalently binds to the surface of the gold nanoparticle[98]. BSA was selected as the protein to be electrostatically adsorbed to the surface of one of two groups of MUA functionalized nanoparticles in order to simulate functionalization with other proteins of interest, such as antibodies. Two separate groups were available for AFM analysis: one batch consisting of nanoparticles with MUA as

capping agent, and another batch of nanoparticles in similar conditions plus with electrostatically adsorbed BSA covering the entire nanoparticle.

The measurement protocol for the nanoconjugates was based on trial and error, by adapting procedures and protocols described in the existing literature and by developing them in accordance with the material at the laboratory's disposal. Due to the fact that the concentration values of the gold nanoparticle solutions used in AFM imaging in the study by Eaton *et al.* - which was elected as the main guideline for this study - were not given (only synthesis values), it was decided to deposit nanoconjugate solution, without any prior dilution or treatment, straight onto the substrate, which was selected to be freshly cleaved mica and evaluate how different concentrations of solution affected the measurements[101]. A drop of nanoparticle solution was deposited and left overnight on the substrate because no anchoring ligands were being used, meaning that any harsher method like rinsing the solution away or drying with a compressed nitrogen source, could compromise the deposition conditions or the sample stability and destroy the sample, especially if done straight after the deposition.

However, it was seen that the overnight evaporation of the solution liquid favoured the crystallization of citrate on the mica, originating fractal patterns that grew over the substrate and occupied large areas of the mica surface such as in Figure 5.6A. This unexpected feature makes it more difficult to distinguish nanoconjugates, although their presence can be detected in the phase channel (Figure 5.6B), but also raises the water potential of the surface, conferring the sample the ability to adsorb water molecules from its surroundings[102]. This meant that in spite of the sample being left to dry for periods longer than 12 hours, it would still retain humidity leading to the appearance of an even larger nanometric layer of water than the one previously mentioned in the previous chapters about AFM modes of operation, which interfered with the ability of the AFM to detect and to measure the surface with precision. In general, when the objective is not to image salts, their presence becomes an issue by forming large structures covering the target of interest and by favouring the adsorption of water due to the high water potential.

This issue was readily overcome by keeping the overnight drying step but doing so in vacuum, inside a desiccator in order to achieve higher rates of sample dehydration. The nanoparticle samples prepared following this way produced coherent measurements. These images showed aggregates of nanoparticles that gave clear evidence that the steps taken were improving the quality of the sample preparation and respective results.

The final batch underwent the same preparation as before. The only difference was a one to ten dilution beforehand to that there was background space between nanoparticles and even less salt particles and impurities, since they could compromise image quality.

Given the small diameter of the nanoparticles requiring operation at smaller scan areas, thermal drifting was regularly observed in scans. An attempt at lowering the rate of equipment heating by keeping insulation chamber of the AFM directly refrigerated with liquid nitrogen was done. However, this was dropped after some experiments since it was not producing the desired effect of making thermal drift less prominent. In reality, since electronic elements are more linear when there are no thermal gradients and the liquid nitrogen wasn't enough to compensate the heat produced by the AFM, its use only delayed the time required for the entire equipment to achieve thermal equilibrium and ensure that the temperature was mostly unaltered from the start to the end of the scan.

### 5.2.3. Results of gold nanoparticle measurements: average height shifts

Several images of each batch of nanoconjugates were produced, which showed the appearance of spherical structures that were enlarged on the *x0y* plane compared to the height scale. Some standard images where the nanoconjugates can be clearly seen are presented in Figure 5.7.

The existence of BSA covering the nanoparticles can be determined by evaluating the difference in height between BSA-conjugated and unconjugated nanoparticles. In order to do so, height dispersions of both batches of nanoparticles were plotted, involving data of over one thousand unconjugated nanoparticles and over three hundred and fifty BSA-conjugated nanoparticles in a method dubbed Standard, inspired in a protocol by the Nanotechnology Characterization Laboratory of the National Cancer Institute of the U.S.A[103]. Other two manual methods were tested for comparison and to evaluate the precision of the automatic and the

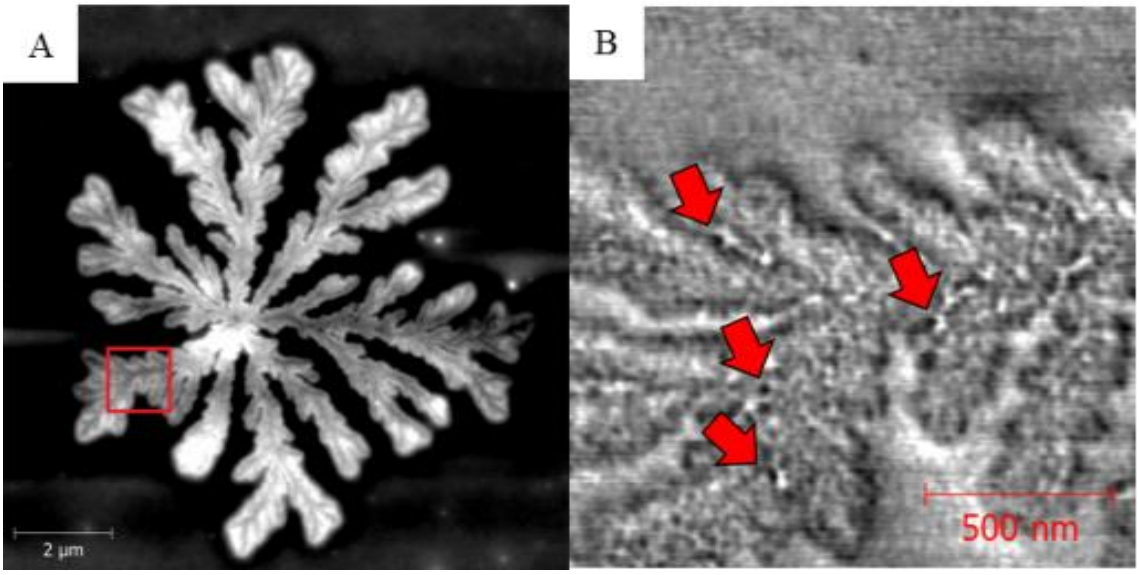


**Figure 5.6 One of the many citrate crystals that grew from the deposited nanoparticle solution (A). These masked the nanoparticles but in some situations it was possible to detect spherical particles entrenched in the crystal using phase imaging (arrows on B).**

manual selection of data, which were dubbed Manual One (M1) and Manual Two (M2). This first method relied on manually isolating the nanoparticle off the background and evaluating the average height of its points and the second on manually locking all the points above the smallest height value exhibited by a nanoparticle (or the vast majority where it became impossible to verify one by one) of each image, and averaging all the points above that *z* value.

The *z*-axis was selected in order to obtain diameter readings because this is the most sensitive axis of the AFM and also because, as was discussed above, nanoparticle dimensions on the *x0y* plane suffer more tip convolution effects, especially when the probe's tip diameter is larger than the object of study[104,105].

Values obtained by these measurements are presented in Table 5.1, which shows the average values obtained by each method and on each batch and also the difference between those means for each method applied.

**Table 5.1 - Means and standard deviations of nanoparticle conjugate diameters as calculated by the indicated methods and difference between mean values obtained for AuNP-MUA and AuNP-MUA-BSA conjugates. All values are in nanometres.**

| | **Standard** | **M1** | **M2** |
|---|---|---|---|
| **AuNP-MUA** | 8.46 ± 0.69 | 8.00 ± 0.48 | 9.63 ± 1.42 |
| **AuNP-MUA-BSA** | 10.57 ± 0.49 | 9.76 ± 1.34 | 11.21 ± 1.04 |
| **Mean difference** | 2.11 | 1.76 | 1.58 |

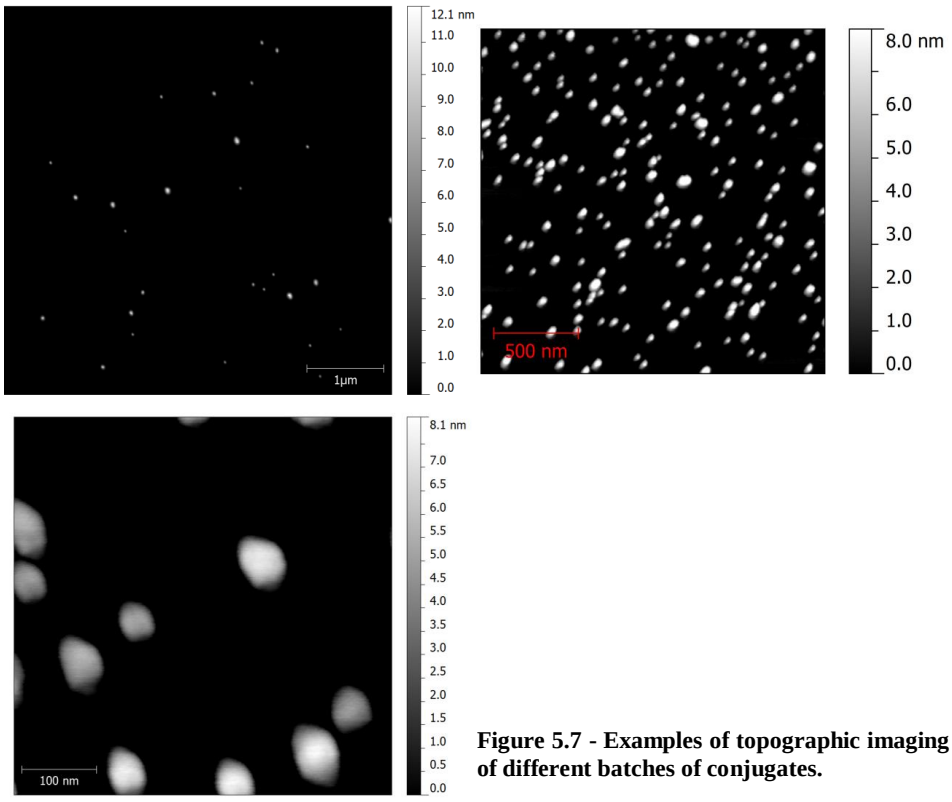


**Figure 5.7 - Examples of topographic imaging of different batches of conjugates.**

This data is also presented in Figure 5.8 which shows the distribution of the mean values obtained through analysis of the results, allowing to compare the dispersion of values obtained between different BSA-conjugates with the same method, and between the three methods.

From the graphs, it can be concluded that the three methods produced results coherent with the concept that BSA-conjugation would raise the nanoconjugates' height, and that there is a shift in the mean values that is as large as 2.11 nm, in the case of the most trustworthy Standard method. Manual methods show some overlapping values, but the tendency of BSA-conjugates to display larger values is nevertheless evident.

### 5.2.4. Discussion of gold nanoparticle results

Although TEM is indicated as a preferred technique for the characterization of metallic nanoparticles due to tip induced artefacts in AFM, there are, nevertheless, several experiments published concerning their AFM characterization, specially focusing the measurement of their diameter and diameter dispersions[104–109]. The article journal that was especially focused to compare with the results obtained was written by Gomes *et al.*, which suggests the use of height dispersions acquired by AFM to compare the same nanoparticles before and after functionalization with a protein[110].

The collected data suggests that BSA functionalization can be detected through AFM measurements and also that the introduction of different preparation protocols, especially the desiccator step, aided in doing so. The three methods used produced the expected results, with special note to the Standard method, in which dispersion intervals did not overlap. Similar results were obtained by Gomes *et al.*, in which functionalization of gold nanoparticles with a protein (horse heart cytochrome C) was also shown by AFM to produce a height increase when comparing to naked nanoparticles. The nanoparticles used by them were synthetized following the same method as the ones studied here. Analysis of Figure 5.8 shows that nearly all the

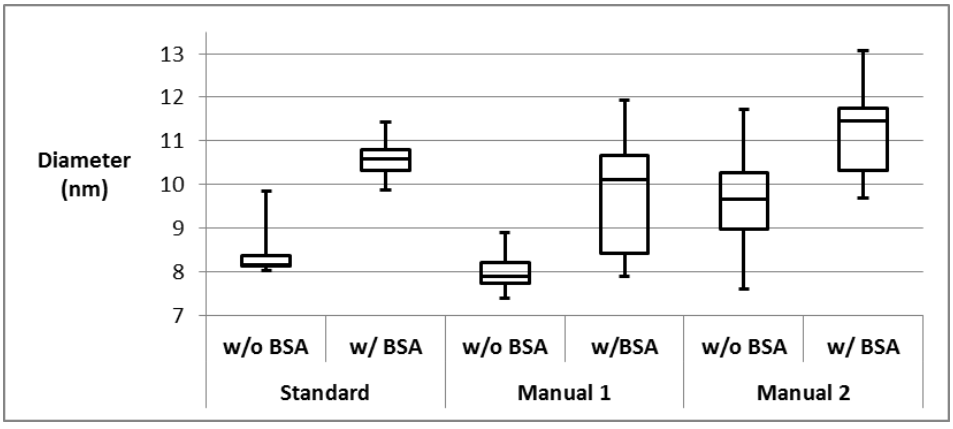


**Figure 5.8 - Box plots of nanoconjugate diameter distributions as measured by the three indicated methods.**

results for each method are coherent with the existence of a protein capping which increases particle diameter.

Knowing this, it was expected for the MUA-functionalized AuNPs to exhibit a diameter larger than the mean 8.46 nm. This same behaviour was observed with BSA containing conjugates, in which the expected height was to be more than the observed 10.57 nm. However, this can be explained with the existence of impurities in the nanoparticle solution that form a layer of debris, possibly salt, on the substrate after the drying or desiccation steps, contributing to a small but not negligible raise in the background, making nanoconjugates heights to show smaller values[111].

On the subject of the dispersions, the Standard method was the one which produced the most solid data, showing box-plots with small interquartile ranges, an indicator that the vast majority of the values are close to the mean, with few exceptions. The experiment was successful since the shift in height dispersions is clear when comparing both types of nanoconjugates, proving that nanoparticles with MUA and BSA do exhibit larger diameters than the ones only with MUA functionalization. Comparing to the shift reported by Gomes *et al.*, the shift observed with BSA-conjugates was larger, however BSA is a larger protein (63 kDa) than the horse heart cytochrome C (12 kDa) used on those experiments[112,113].

The other two methods used were included for comparison with the Standard method. It was expected for the manual methods to exhibit larger dispersion values because of their reliance on operator selection of data, more prone to errors. This assertion turned out to be correct, with Manual methods exhibiting, in general, large interquartile ranges, with observed values covering up to four nanometres of diameter – the double of the dispersion using the Standard method. Nevertheless, it is possible to observe a shift in mean and median as well as in the minimum and maximum values between the two nanoconjugate types under analysis, what is enough to claim that it is possible to distinguish the samples containing BSA from samples only containing MUA-functionalized AuNPs, although to achieve the same level of confidence as with the Standard method, the amount of images and time needed to produce them would be far greater.

In conclusion, the three methods have successfully shown the existence of differences in the constitution of both nanoconjugates, with mean and median diameters appearing larger in the presence of BSA-conjugated nanoparticles. Also, although the Manual dispersions cover several nanometres of diameter, it is noteworthy that in all situations without exception, the BSA-conjugates always had higher minimum observable values than those observed in conjugates with only MUA. The same behaviour was observed with maximum values,

indicating that in spite of some overlapping of interval of values, BSA-functionalized nanoparticles can never exhibit some values that nanoparticles without BSA can and *vice versa*.

# 6. AFM measurements of DNA

## 6.1. HRPII plasmid DNA

The organism elected to be used for the growth of DNA was an *Escherichia coli* strain containing the HRPII (Histidine Rich Protein II) overexpression plasmid, which was cultivated following growth protocols especially developed for plasmid DNA harvesting and extraction. The HRPII protein is produced only by *Plasmodium falciparum*, the agent responsible for the onset of falciparum malaria, during the infection of humans. Because of this specificity in protein production, HRPII became a target for the diagnosis of malaria[114,115].

Bacteria were grown in selective conditions to isolate those containing the HRPII plasmid. Plasmid extraction was done with an extraction kit fabricated by NZYTech (a more detailed protocol can be consulted in the Appendix I.a.vi.1)[116]. The usual steps of determining the success of extraction, yield or integrity by ultraviolet-visible spectrophotometry or agarose gel electrophoresis were not done since that these either were not determinant for the success of the measurements or could be determined by AFM imaging.

From this point, the DNA solution used to image DNA throughout this dissertation was stored at 4ºC and ready to be use at any time. No degradation of DNA in these conditions was observed up to six months.

## 6.2. DNA preparation for AFM measurements

One of the intrinsic properties of DNA that make electrostatic adsorption unreliable for AFM measurements is the fact that muscovite mica, which is one of the most used AFM substrates on biological samples, has net negative charge, just like DNA. Mica exhibits this behaviour because of the presence of hydroxyl ($OH^-$) groups on its structure while the reason why DNA has negative charge is related to its structure as well, which is comprised by not only the nucleotide bases and the sugar residues, but also by a phosphate backbone $(PO_4)^{3-}$. This backbone confers negative charge to DNA due to the existence of one unlinked oxygen atom carrying one unpaired electron. Various methods that allow surpassing this issue have been proposed. The most common uses divalent cations, such as nickel ($Ni^{2+}$) or magnesium ($Mg^{2+}$), as binders between the unlinked oxygen atoms in a phosphate group and one hydroxyl group on the mica structure. This binding promotes the anchoring of the DNA to the substrate and keeps it relatively immobilized for AFM measurements, independently of the chosen observation media[117,118].

The buffer used in the preparation of DNA was HEPES buffer - 4-(2-hydroxyethyl)-1-piperazineethanesulfonic acid - which is a regularly used buffer in biological and biochemical experiments. HEPES has affinity with biological samples and molecules, and also presents a

structure stabilization effect on these targets, by maintain the pH of the solutions inside the interval of values that match the characteristics inside cells[119].

The reason why nickel chloride and HEPES buffer were selected is because together they constitute the most common approach to DNA binding for AFM observation, which was described first by Hansma *et al.*[120]. For the anchoring of DNA, it was used a protocol recommended by an AFM company, NT-MDT, whose standard procedure involves HEPES and nickel[81]. Details of the preparation can be consulted in Appendix I.a.vi.2. Since that in initial measurements good stabilization was intended over maintaining any biological activity, the nickel chloride concentration used was usually the highest recommended, with several experiments suggesting that this was the best approach to promote good AFM preparation.

Other methods of DNA anchoring preparation also exist and are thoroughly described in the literature. The most common, after divalent cations, is the functionalization of mica with 3-aminopropyltriethoxysilane or APTES. This molecule can covalently bind to surfaces like mica or silicon, allowing the anchoring of DNA due to the positive charge of its amine group. This method produces results resembling those produced with the first method, however, due to stronger anchoring, DNA molecules often appear more twisted[121,122]. If the objective of the measurement is to study DNA condensation mechanics, poly-L-lysine solutions can be used to functionalize mica, since they favour the appearance of DNA as condensed molecules over the stretched effect observed with other methods. Poly-L-lysine binds electrostatically to both mica and DNA, allowing for DNA molecules to converge around sites containing this polymer[123]. In case the object of study are linear DNA molecules, the thiolation of the sequence is a very good alternative because through the use of a gold film as substrate, it becomes possible to anchor the DNA to the gold by the thiol group, while leaving the rest of the molecule unbound and free to interact with its surroundings[124]. Obviously, more methods exist and an excellent review by Lyubchenko can be consulted to find some more techniques, but these focus more on specific types of interaction in DNA conjugates or with other biomolecules or on preparations that favour the DNA molecule to adopt certain shapes or conformations[75].

## 6.3. Results of DNA measurements

### 6.3.1. Plasmid conformation and first comparison between topography and phase acquisition

Initial studies had the sole objectives of evaluating if the preparation was fit to produce the DNA structures intended to be observed and to do analysis like determining characteristics like the height and width of the chain. After these, the objective was then to see if high resolution tips, especially the modified, allowed to attain enough resolution to discern the pitch of the chain, which lies on the verge of the AFM horizontal resolution limit.

Liquid measurements performed using Olympus TR800PB cantilevers produced images of very poor quality but with enough resolution to confirm the existence of DNA in the sample, as can be seen in Figure 6.1. Height of the molecules in liquid ranged between 0.35 and 0.7 nanometres. The low quality of the images is probably related to the fact that the radius of DNA is sixteen times smaller than the tip radius of these cantilevers, rendering images blurry and nonlinear between fast scan direction lines.

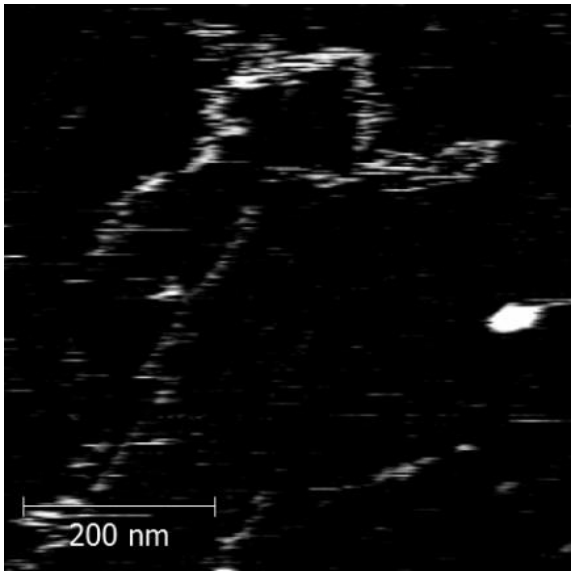


**Figure 6.1 - Topographic image of DNA molecule acquired in liquid with Olympus TR800PB probe.**

Air measurements were performed, as in previous experiments, in order to establish the capacity to replicate results in liquid. Images were obtained with two set of cantilevers, the average resolution AC160TS and sharper Olympus SSS-NCH, including the backside modified ones. Soon, it was clear that the preparation method elected for DNA measurements was producing the expected results, since images were clear when imaging with the required scan sizes: even with the medium resolution cantilevers it was relatively straightforward to determine that most of the plasmids were intact, appearing with the classic circular shape normally associated with them or twisted around each other, seldom exhibiting loose ends (Figure 6.2). It should be noted that although DNA resembles a cylindrical structure with equal diameter throughout all sectioning planes, tip convolution effects will lead to height values different than width values. Therefore, in this dissertation, height is referred as the diameter of DNA measured on the *z* axis and width as the diameter measured on the *x0y* plane (Figure 6.3).

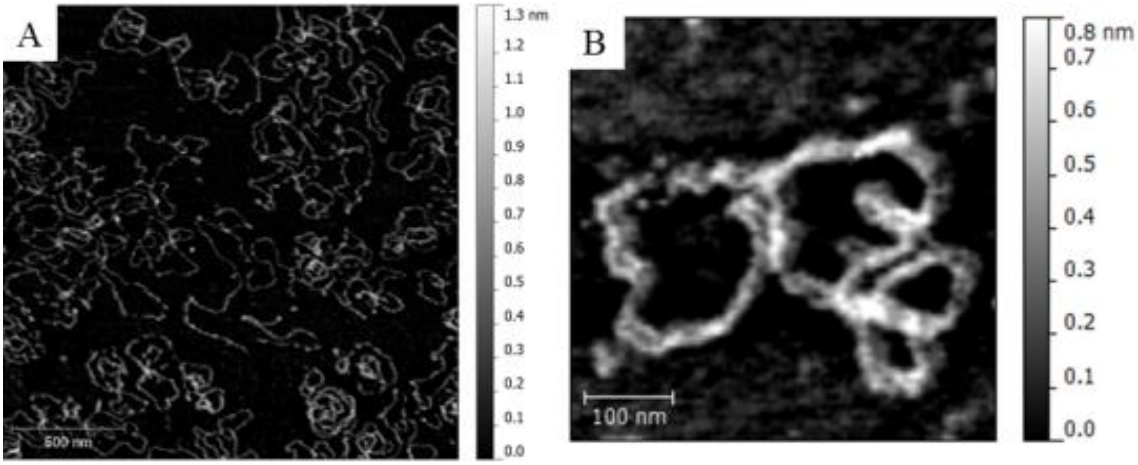


**Figure 6.2 - Topographic image of several HRPII plasmids (A) and detail of one of these molecules where the circular configuration can be seen (B).**

A first battery of measurements was performed using the AC160TS cantilever, from which several images were collected which clearly showed circular plasmid DNA molecules on the substrate. These images allowed for the first zoomed in picture of single plasmids and to document how the different channels of acquisition behaved. It was soon found out that although the height channel was very informative of the location of the DNA molecules against the background, its boundaries were not as clearly defined as wished, not allowing for clear measurements of width and sometimes to discern the terminal areas of the molecules. However, at this magnification it was possible to confirm the utility of phase imaging, since this input channel had a noteworthy resolution even with this tip (Figure 6.4), clearly defining the molecule boundaries and allowing to measure its dimension.

As a conclusion of these preliminary results, AFM was able to produce clear images and to display DNA in a way similar to what appears in publications related to the same type of studies. Using the nickel chloride mode of adhering DNA to the substrate, the DNA molecules appear as elongated strings throughout the scan area with very few situations of aggregation of the chains around themselves like it would be expected to happen if, for example, the anchoring had been done using APTES or poly-L-lysine. These compounds trigger DNA to exhibit a much more condensed state, leading to the appearance of aggregated structures that, while being fit for another purposes like force spectroscopy, wouldn't aid with the objectives of this dissertation.

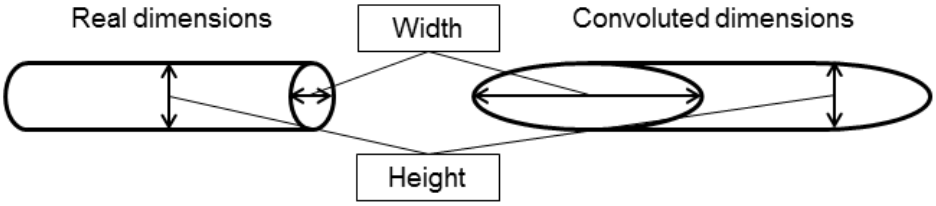


**Figure 6.3 - Schematic on the reason why DNA, being a cylindrical molecule, appears with different values when acquired on the *z* axis (height) and on the *x0y* plane (width) due to convolution effects.**

### 6.3.2. Morphology and dimensions of DNA: width vs. height, topography vs. phase, high resolution imaging and plasmid sequence length prediction

The analysis of a first batch of images created using AFM probes with average resolution gave the first insights about how the AFM perceived the DNA molecule and how tip convolution played a role in the perceived diameter of the molecule. When measured on the *x0y* plane with AC160TS probes, the average width of DNA molecules was calculated to be 16.16 ± 1.4 nm, while the measurement on the z axis showed values of 0.55± 0.2 nm. On the other hand, the values measured with the SSS-NCH probes gave width values of 12.67 ± 1.37 nm and heights of 0.87 ± 0.15 nm. These values were measured at half height of the DNA molecule, as recommended by West *et al.*[109]

However, as mentioned before, phase imaging can be used with any type of alternate contact probe, enabling the acquisition of dimension data that may be sharper than that acquired by topographic mode, as illustrated by Figure 6.4. Using this channel of acquisition, which only allows to measure on the *x0y* plane, the molecule's boundaries were more defined, shortening the measured diameter in the AC160TS probes to an average value of 14.49 ± 0.82 nm and the SSS-NCH's to 10.02 ± 0.94 nm . These results, although still far from realistic, do show the reliability that phase imaging can offer when working with biomolecules.

Only after obtaining confirmation that DNA adsorption was working as intended, and obtaining the first results on DNA dimensions, it was decided to make attempts at producing images using the enhanced probe. The images produced showed the same structures as the medium resolution tips, but with the enhanced probe, DNA molecules weren't as blurry as in the first batch of measurements, but instead showed remarkable resolution, even on the

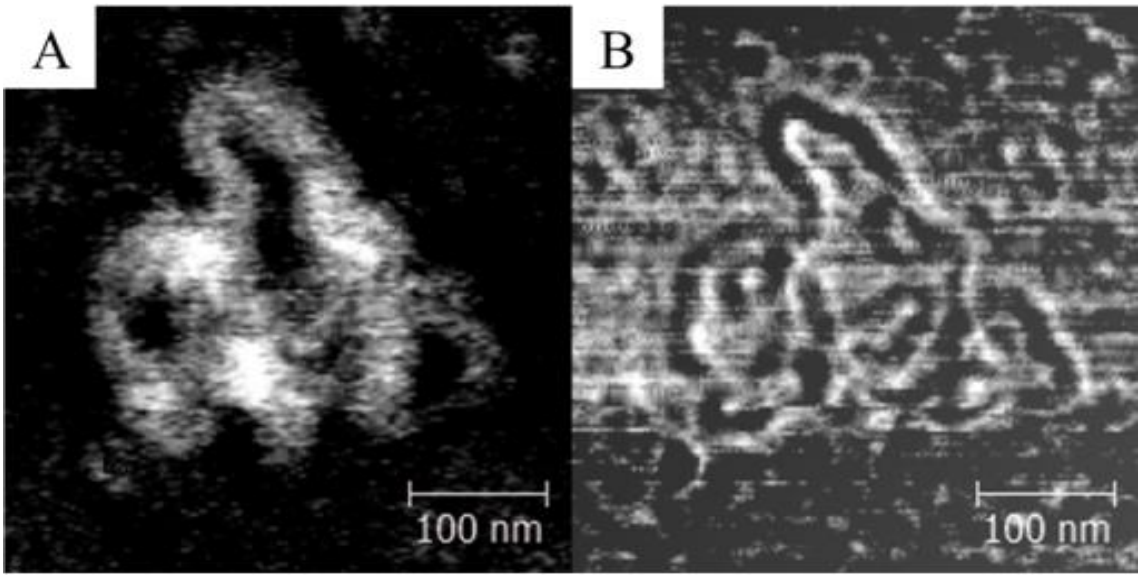


**Figure 6.4 - A clear difference in the sharpness of the DNA boundaries can be seen when comparing between topographic acquisition (left image) and phase acquisition (right image).**

topographic channel, showing clearly defined features and edges even in scans well below a scan area of one square micrometre. Overall, the images were very sharp and of high quality, what led to the first attempts of producing measurements with ångstrom resolution.

Several images of DNA molecules were captured while working on the limit of the cantilever independent resolution of the AFM, *i.e.*, the resolution value dependant solely on the AFM electronics and not on tip geometry, which is roughly 0.3 nanometres. It was possible to observe a stretched DNA molecule almost parallel to the probe raster direction (called the fast scan direction), a privileged position due to allowing the tip to scan along the top of the DNA molecule without even nanometric variations in height. This allowed to establish the existence of a structural periodicity in the molecule.

At this resolution, the measured dimensions of the DNA molecule were also as sharp as it was possible to acquire throughout all experiments. In the smaller scan area measurements, especially 150x150 nanometre scans, it was possible to produce images at the resolution limit of the AFM, where, outstandingly, the phase channel was still able to produce results that are sharper than the topographic channel by approximately 23%: 5.27 ± 0.4 nm for topographic acquisition and 3.95 ± 0.26 nm for phase acquisition.

Nevertheless, the most striking feature was the existence of the mentioned structural periodicity throughout the DNA molecule that can be seen in Figure 6.5, as subtle crests. In order to study the pitch distance of those structures, a height profile longitudinal to the molecule was done in two selected areas (Figure 6.7). The pitch distance values obtained were used to calculate the mean value of pitch distance, which was of 2.23 ± 0.29 nm, and also to build a box-plot with all the data gathered from that measurement (Figure 6.6).

The length of the HRPII plasmid was also approximated in an attempt to calculate the amount of base pairs through image analysis[125]. Three plasmids which showed more stretched structures than the average, since that coiling and aggregations can influence results, were selected for this attempt. However, even the most stretched plasmids exhibited some locations in which DNA was condensed. Through summing the length of the partial fragments, three plasmids were approximated to have lengths of 1825, 1834, and 2036, what was converted to

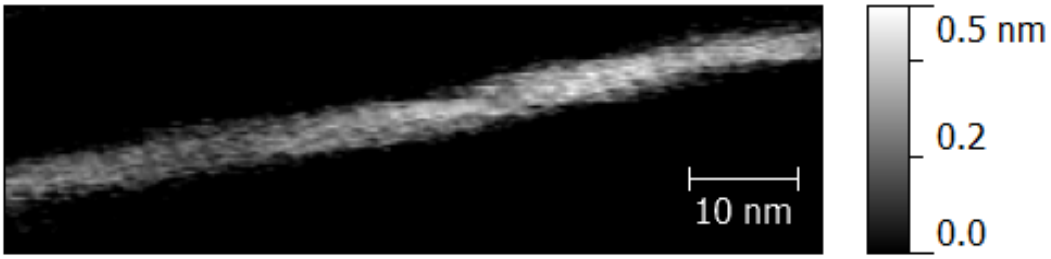


**Figure 6.5 - Topography of a DNA molecule where a pattern repetition can be observed.**

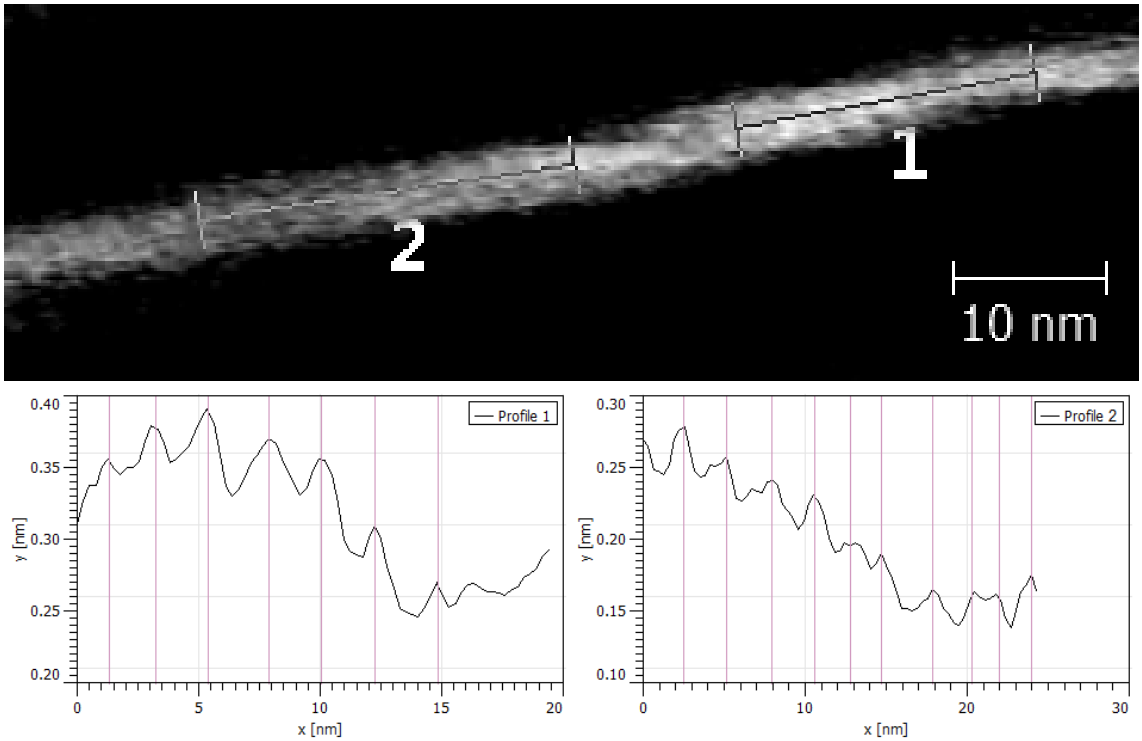


**Figure 6.7 – Images of a DNA molecule with the areas selected for pitch distance studies marked. These were used to produce the height profiles and the box-plot graph.**

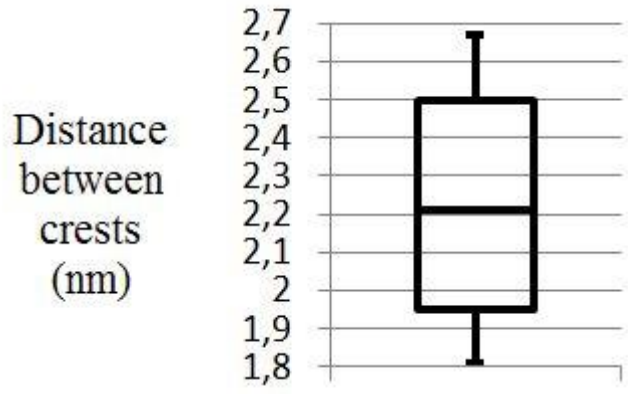


**Figure 6.6 – Box-plot of the distance between crests measured on the DNA molecule.**

base pairs by dividing such values by a factor of 0.33, equivalent to the relation between the amount of nucleotides that fit in a nanometre. These results suggested that these HRPII plasmid had a sequence length of 5530, 5558 and 6170 base pairs.

## 6.4. Discussion of DNA results

Several DNA molecules dimensions were obtained from scans done with different AFM probes. Given this difference, it was decided to evaluate the dimensions that were supposed to be obtained with each tip related to its geometry by application of the equation of Bustamante *et*

*al.* (Equation 3.2 at page 32)[*]. Therefore, in perfect conditions, a DNA molecule interrogated with an AC160TS probe would appear to have at least 13.4 nanometres. Given the average width value calculated being 16.16 ± 1.42 nm for width measurement done on topographic images and 14.49 ± 0.82 nm for measurements done on phase images, it can be concluded that the results are close to the expected by mathematic determination.

The use of the SSS-NCH probe dropped the expected minimum width by application of the same equation to roughly 8 nanometres. With calculated widths through topography acquisition of 12.66 ± 1.37 nm and 10.02 ± 0.79 nm for width calculated with the phase channel, the results were also within the expected range of results, although it was expected to have the topographic width value nearer to 10 nanometres. Values acquired with the modified SSS-NCH probe are also along the expected, especially those in phase imaging. Not only the topography dependent width was calculated as 5.27 ± 0.4 nm and the phase dependent width as 3.95 ± 0.26 nm, as it was possible to observe a periodicity in the high magnification image produced, which can be associated with the major groove of the DNA molecule (Figure 6.5). Overall, the measured values for DNA width fell between the expected values and the values found in the literature, which ranged from roughly 15 nanometres at square micrometre scan ranges to values close to 5 nanometres at small scale imaging.

Height values that were acquired throughout all the used probes didn't also match the textbook value of 2.5 nanometres for the width. Instead, average values of 0.55 and 0.87 nanometres were collected, what seems manifestly wrong. However, similar results have been reported, where it was verified that the mechanical forces applied to biomolecules such as proteins and DNA are enough to frequently compress them to one third of the real height and also that DNA height has been routinely reported on other experiments to be as low as 0.1, up to 1.5 nanometres[74]. This effect is especially noted if measurements are performed in liquid or if the sample is simply hydrated[90].

Critically analysing all the measured widths, the values obtained are in accordance with the literature in which DNA width was also studied. In 1994, Thundat *et al*. tried measuring DNA width in which similar anchoring techniques and obtained, with probes similar to the AC160TS, values of width between 21.9 and 18.7, although in some situations they claim to have measured DNA molecules with a 9 nm width[126]. With the first attempts at high resolution imaging of the DNA periodicity, which can be compared to the one attempted in this dissertation, the width values were between 4 and 8 nanometres, with some bordering the 3 nm, just as was verified in the experiments using the SSS-NCH modified probe [127]. Other attempts at

[*] $w = \frac{4(Rp+Rs)\sqrt{(Rs(Rp-Rs)}}{Rp}$, where *Rp* is the radius of the probe and *Rs* the radius of DNA.

measuring the DNA width, such as those by Maeda *et al.* or Hansma and Revenko have consistently reported values between 10 and 12 nanometres, very close to those obtained herein[128,129]. As final mean of comparison, Winzer *et al.*, in a study about correction of convolution, have studied the measured width and height of DNA with several probes. Their measured widths of DNA fell between 10.6 nm and 4.2nm and the measured heights between 0.4 nm and 1.1 nm. Gathering all this data, it becomes clear that the average widths measured during the laboratory work of this dissertation are up to par with most published literature that concerns DNA imaging with AFM[74].

The use of the phase channel was also demonstrated to be crucial in aiding in the imaging and measurement of nanometric structures, especially with lower resolutions probes, where the difference in the quality of phase to topographic imaging was very notable: in situations in which topography showed nothing else than an aggregate of wires, phase imaging made it possible to distinguish their structure and orientation. This affirmation is backed by recent studies focusing subnanometre phase imaging of DNA[130]. Establishing these differences is important since it shows the potential that AFM still holds for the future of biological imaging. Hopefully in the near future, the development of equipment and protocols that allow to routinely image at this scale will, ultimately, allow for visual differentiation of the different components, such as phosphate backbone or base pairs, of DNA and perhaps even set the ground needed for visual sequencing.

Comparing the values measured with average resolution probes, high resolution probes and modified high resolution probes, it can be concluded that there is a tendency for the quality of the image to improve, what shows that the area of study and expertise related to probe modifications can be explored in the future in order to push the limits of operation of the AFM, as demonstrated throughout Chapter 4, when probe modifications were approached. In the 150x150 nm images, the resolution was brought to the values after which the AFM would not have the capacity of resolving any further, and the fast scan rate was also slowed down to allow the probe to hover the sample at slower rates, such as 0.66 Hz and eliminate some edge artefacts that might still exist. In the end, the improvement in the resolution and ability to measure and document the behaviour of these biomolecules was improving as low resolution AFM probes were traded by higher resolution ones, which in turn were modified to enhance photodiode detection and which in its own turn were brought to operate on the verge of the AFM's ability to image with consistence. Figure 6.8 shows the average measured DNA width in the different situations mentioned (different probes and channels of acquisition) and compares them between each other, making it easy to see the effect of improving the quality of the AFM probes used in these experiments throughout both channels. Nevertheless, it comes to a point where no further

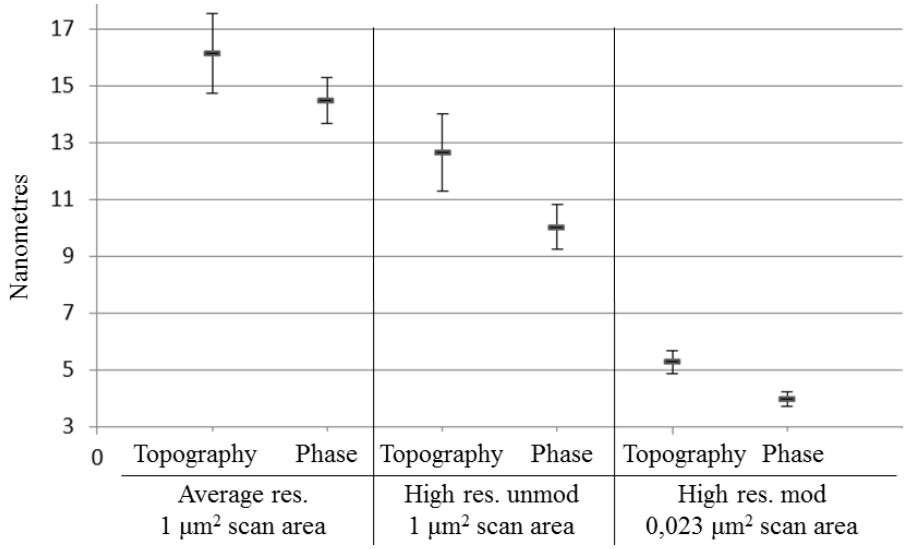


**Figure 6.8 – Average width values measured for the different probes used in the experiment in nanometres. 'Average res.' refers to AC160TS probes, 'High res. unmod' to the unmodified SSS-NCH and 'High res. mod' to the gold-palladium coated SSS-NCH. Topography and phase refers to the channels in which the measurements were obtained.**

improvement is possible because the factor limiting resolution becomes the AFM constituents themselves and not the probes or the sample preparation.

Concerning the length prediction of the plasmids, although three plasmids are not statistically significant, the results obtained can be compared with the predicted sequence length of the HRPII plasmid: 6438 base pairs, what translates to 2205 nanometres[131]. The results showed a discrepancy from the real value of 17.2% (1825 nm), 16.8% (1834 nm) and 7.8% (2036 nm). Although this method cannot calculate the number of base pairs of a DNA molecule with high precision, it is possible that with more statistical data the mean value could shift to values nearer the reality. Nevertheless, the method may be accurate enough to differentiate between two types of plasmid in the same sample or different linear sequences.

## 6.5. Comparison between single (ssDNA) and double stranded DNA (dsDNA) imaging under AFM

### 6.5.1. Difference between ssDNA and dsDNA and preparation for AFM

Structural differences between single stranded and double stranded DNA molecules were also studied under the AFM. This was achieved by heating the DNA samples in accordance to the principle of DNA melting, allowing double-stranded DNA (dsDNA) to become single stranded (ssDNA), when heated at or above its melting temperature ($T_m$). Such melting occurs because the hydrogen bonds between complementary nucleotides are weaker than the covalent bonds between sugar residues and phosphates or nucleotides, meaning that there is a specific temperature in which it is known that hydrogen bonds will be unable to resist the instability generated by the heating, while the other bonds in the DNA molecule will endure

the treatment, resulting in the denaturation of the DNA molecule but originating two new molecules, each with a phosphate backbone and the unpaired nucleotides[132,133].

A heating treatment was introduced in this experiment in order to denature the dsDNA into the two unpaired strands (Appendix I.a.vi.3). Besides the heating of the DNA solution over the melting temperature of DNA, the mica substrate which was going to receive it solution for imaging was also heated for the same amount of time. This way when the heated solution was moved to the mica, it would not suffer any effects from the temperature shock, lowering the chances of the nucleotides starting to pair with each other and aggregating before the chains were anchored to the mica via nickel chloride.

Double stranded DNA chains are stable at room temperature because of base pair homology and that is one of the reasons why AFM measurements of double stranded DNA produce images of molecules resembling wires: because there is a high, if not total homology all along the two DNA strands that make one DNA molecule. However, when the two strands are brought apart by any kind of treatment, they will randomly attempt to pair with any other nucleotide sequences with a given amount of homology. In practice, this means that when a double strand DNA molecule is melted, the reorganization of the resulting single strands will be chaotic and a lot less organized in general than double stranded chains when measured under an AFM. This proposition is also supported by the existing literature on studies of the morphology of single and double stranded DNA molecules under the AFM, in which a clear difference between these two states can be seen[134–136].

### 6.5.2. Results and discussion of ssDNA imaging

While double stranded DNA appeared in the previous experiments with the morphology generally associated with a tubular structure, single stranded DNA chains seem to converge together and aggregate with each other, generating far less organized structures resembling, for

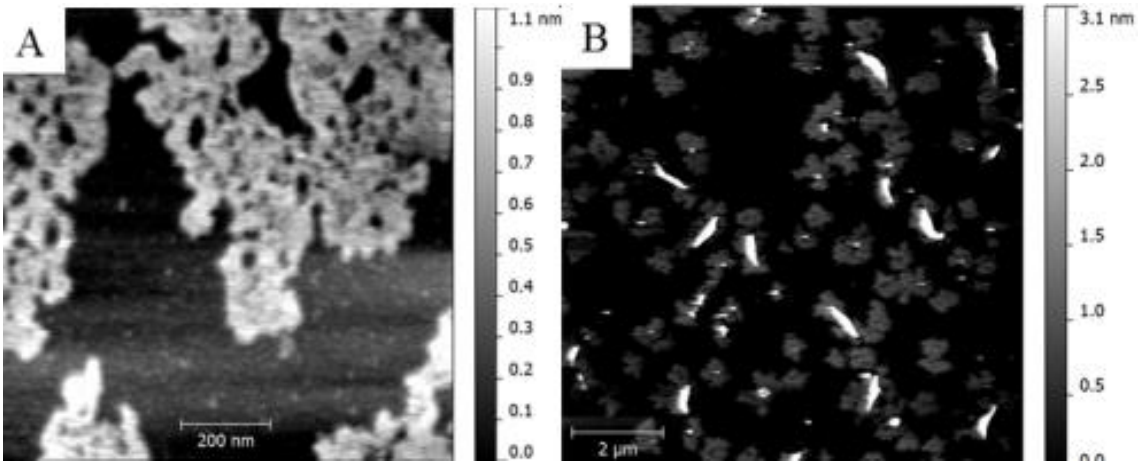


**Figure 6.9 - Topographic images of aggregated ssDNA molecules as a result of DNA melting and intra and inter-strand homology. In A, a detail of the condensed structure can be seen while in B several DNA aggregates can be observed.**

example, thread balls or curled wires due to the interaction between nucleotides sequences contained in the same strand forcing the strand to bend and twist around itself, as seen in Figure 6.9. Images acquired showed the absence of any structures as the ones observed under the AFM in the previous section, but instead showed an overwhelming presence of globular structures resembling condensed DNA molecules. This shows that ssDNA molecules, instead of appearing as unreactive as dsDNA strands did, exhibit a more reactive behaviour between themselves and other ssDNA strands, forming condensed DNA structures as reported by Adamcik *et al*[134].

In images presented here, the DNA seems to be in an even more condensed state than what is seen in the literature, what possibly relates with the fact that these studies used linearized DNA, while the genetic material used in this dissertation was plasmid DNA. This means that although the DNA strands melt away from each other, the unpaired chain has less mobility than a linear sequence, leading to the appearance of highly condensed DNA structures in comparison to other studies, especially those using linear strands[137,138]. It was also noted as a curiosity that, by mistake, some of these experiments were done without filtering the buffer solutions prior to inserting the DNA in them. This does not affect the DNA in any way since preliminary DNA measurements were done skipping filtering and were shown to not affect the

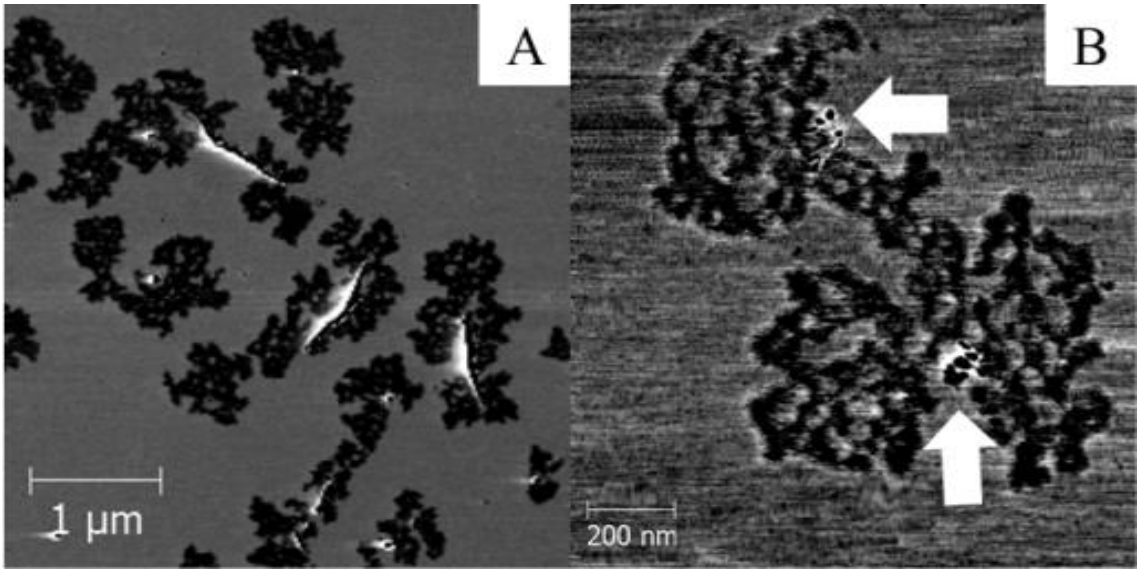


**Figure 6.10 Phase imaging of ssDNA condensing around contaminants. These appeared both as long and thin objects with boundaries in white (A) and globular objects (B, pointed by arrows).**

measurements. However, it was seen that single stranded DNA showed the interesting behaviour of aggregating around these particles. It can be guessed that this relates to surface characteristics they exhibit which facilitates the convergence of the molecules around them, as happens in Figure 6.10. The contaminants actually appear to anchor DNA in a way similar to poly-L-lysine[121].

## 6.6. Measurements of plasmid DNA undergoing EcoRV digestion

### 6.6.1. Overview on restriction enzymes, on EcoRV and objective

Restriction enzymes or restriction endonucleases are some of the most well studied enzymes in biology due to having the ability of recognizing specific DNA sequences and cleaving the DNA molecule in those locations, a capacity that is believed to have evolved due to the need of organisms in defending themselves from foreign DNA sequences inserted in their cells, such as virus, constituting, therefore, a defence mechanism[139]. The capacity of recognizing specific sequences made these endonucleases one of the most used molecular biology tools, especially in gene cloning due to their ability of cutting open a cloning vector, like a plasmid, in order to assist in the insertion of a DNA sequence to be cloned. They can also be used for other purposes like assisting in the construction of restriction maps or any other molecular biology or biochemical technique that requires cutting DNA in specific locations[139–141].

Due to the characteristics mentioned above, these enzymes are routinely used in research and industries and, as today, the behaviour and reaction properties of most is well studied, especially from the biochemical standpoint[142–146]. Some studies of endonuclease activity observed with the aid of AFMs have already been published. However, many focus on confirming the binding of the enzymes and not so much on the event of DNA cleavage on itself. A more detailed experiment could document in sequence the enzyme binding, the conformational change brought upon the DNA molecules and the cleavage moment, since the only practical way to successfully do so requires last generation AFMs, with the ability to raster a 256x256 or 512x512 image in a matter of seconds. More common pieces of equipment, especially the one used in these experiments, may require up to ten minutes to complete a scan in these conditions.[*]

Nevertheless, the objective of this study was precisely to try to image these events leading to DNA cleavage by an endonuclease in succession but at a larger scale because it was expected that the absence of a liquid medium to facilitate mobility and reaction of an endonuclease that would be specifically selected for purpose of this study, would allow to spot differences between phases of the reaction.

The selected enzyme was EcoRV, a type II restriction endonuclease first isolated from *E. coli* strains, and determined to cleave the palindromic sequence of 5'-GATATC-3' between the 3$^{rd}$ and 4$^{th}$ nucleotide, cleaving the opposite phosphate backbones between both complementary sequences and generating blunt ends. The determining factor in selecting this

[*] The AFM operation at the scales required was done at between 0.7 and 1.3Hz (1 scan line each 1.33 and 0.66 seconds respectively). This means that a 256x256 scan would take between approximately 169 and 340 seconds

enzyme, apart from the existence of a cleavage site in the HRPII plasmid – in fact, there are two -, was the fact that EcoRV is will bind and cleave the DNA on specific sites without the need of ATP activation and that its cleavage mechanism comprises a conformational change in DNA by bending it roughly 50 degrees during the cleavage reaction[131,143,146]. This peculiarity meant that, adding to the interest of visualizing the entire cleavage reaction in whatever medium and mode of operation, this endonuclease would produce an effect on the DNA molecule that hopefully could be visually confirmed during the measurements, offering empirical evidence of the conformational changes forced onto the DNA by the binding of the protein to the cleavage site.

The fact that there is no need for ATP activation is also a key aspect in the choice of this enzyme because this allows the reaction to occur spontaneously, *i.e.*, without the need to add another buffer with the purpose of prompting the reaction to occur. The need to do so would be counterproductive because this would mean one more substance which could possibly affect a high magnification measurement, when the objective is making sure that when the sample is ready to be analysed goes under the AFM probe, the chances of contaminations or the existence of variables that can interfere with image acquisition are as low as possible[142].

### 6.6.2. Preparation of the DNA-EcoRV measurement

The DNA was prepared following the same procedures as in previous experiments (Appendix I.a.vi.2): fifty microlitres of DNA were deposited on the mica, what comprises an average mass between 5 and 10 ng of DNA. Since EcoRV was originally suspended with a concentration of ten thousand units* per millilitre (ten units per microlitre), it was diluted to bring it to a value closer to the one required to digest, over the course of at least one hour, such quantity of 5-10 ng of DNA. This was achieved by diluting the enzyme to a final ratio of 1 to 1000, producing a solution with approximately 0.01 units of enzyme per microlitre.

At a temperature of 37ºC and perfect conditions of mobility, which are not met during the measurements, it would take roughly one hour to react with the overwhelming majority of the DNA molecules on the mica. However, in this experiment that is not correct because it was expected that the drying procedure before each set of measurements would lower the activity of the enzyme by dehydrating the sample and also by affecting the ability of the enzyme in scouting throughout the nucleotides of one plasmid and mobility to other molecules. This meant that the measurement could go on for more than one hour before the vast majority of the plasmids were cleaved. On the other hand, the HEPES buffer originally introduced to stabilize DNA, is known to also stabilize proteins and could play a role in countering some of these destabilization effects[119].

* One unit is the enzyme activity needed to cleave one microgram of DNA over one hour at 37 ºC in digestion buffer.

Initially, it was attempted to dry the EcoRV solution on the mica without rinsing it with water, but this method proved to be unreliable due to the existence of glycerol and/or 2-mercaptoethanol in the digestion buffer of the enzyme. Glycerol is far more viscous than water, meaning the force needed to dislocate it and facilitate drying is higher than the one required to dry the DNA solution. On the other hand, 2-mercaptoethanol has a low vapour pressure, making it hard to evaporate[147,148]. Therefore, although the substrate appeared to be dried, during the preparation of the AFM engage on the sample, it was noted that the surface had a viscous and oily appearance. This renders measurement impossible due to the fact that if the substrate had a layer that could be spotted using the AFM optical microscope (roughly 1mm of area under the objective) and it was more viscous than water, the tip oscillation amplitude and the respective drive voltage would not be enough to collect a quality image since the tip would not be able to penetrate through such contamination layer.

The attempts to measure through the layer showed signals of oscillation interferences, normally associated with the existence of liquid around the AFM probe, meaning it was impossible to detect the surface of the sample in such conditions, what lead to the introduction of a rinsing step before the DNA-EcoRV solution was observed in the equipment.

The sample was removed from the AFM after each hour of measurement and a fifty microlitre drop of EcoRV solution was again deposited on it and dried. This allowed to not only slowly accelerate the rate of cleavage, which is believed to have been slowed by the non-optimal temperature and reaction conditions, but also to raise the quantity of EcoRV in submicrometric scans, in which they were too scarce to be easily detected. Also, the addition of a liquid medium for five minutes between the scans helped in increasing the mobility of the enzymes which were already in the sample, and also allowed DNA strands to move more freely, what helped to assess if the molecules were being cleaved and becoming linearized, since the probability that they would stand in the same place without moving was reduced. The sheer raise in the number of EcoRV would also possibly allow to image enzymes, both associated and possibly reacting with the DNA, and in an unbound state, laying on the substrate.

Also before presenting the results, it is important to note that although the 50 degree bend during the cleavage reaction is transversal to all EcoRV reactions, there are situations in which it would be impossible to observe this phenomenon when both DNA and this endonuclease conjugate. The simplest reason is that EcoRV may be scouting through the strand in an attempt to find the sequence that triggers the cleavage mechanism. However, it can happen that the reaction conjugate forms in such a way that the enzyme unit rests on top of the DNA, making the bend unnoticeable since it would occur below the enzyme and away from probe interrogation. In theory, this disposition is the most probable to occur because the nickel

chloride anchoring, plus the absence of a liquid environment, which could facilitate movement and assist in the promotion of enzymatic activity by acting as molecular lubricant. This does not mean that it is impossible to image the desired bend, but that hypothetically, this contributes to a higher stiffness and unreactivity of the system because, for EcoRV to bind on the side with DNA, it is possible that the nickel chloride link must be broken. Only in situations where the enzyme can slide against the DNA, can the desired physical effect be observed[149].

### 6.6.3. Results of the DNA-EcoRV reaction

These results were obtained throughout three hours in which at the start of the second and third hour, the sample was removed from under the AFM and another 0.01 units of enzyme were dropped onto the substrate. This increased the EcoRV/DNA ratio to two and three, respectively.

The acquired images showed structures that are, without any doubt, EcoRV endonucleases, besides from DNA molecules, which appeared both with the circular configuration associated with plasmids and linearized due to enzymatic cleavage. These were detected both on the substrate but away from DNA molecules, meaning they were not catalysing any reaction, and also bound to DNA molecules, as can be observed in Figure 6.11. In this last situation, both molecules with an EcoRV bound to it but without any cuts in its structure, and also plasmid DNA which appears to have been cleaved together with EcoRV units were observed.

Concerning morphology, EcoRV units under the AFM resemble a globular structure. Some images produced show that the enzyme appears to have a rough, bulged macro structure that can be differentiated using an AFM like in Figure 6.12, in which both topographic and phase imaging show that surface of the enzyme is not flat and appears to have some complexity.

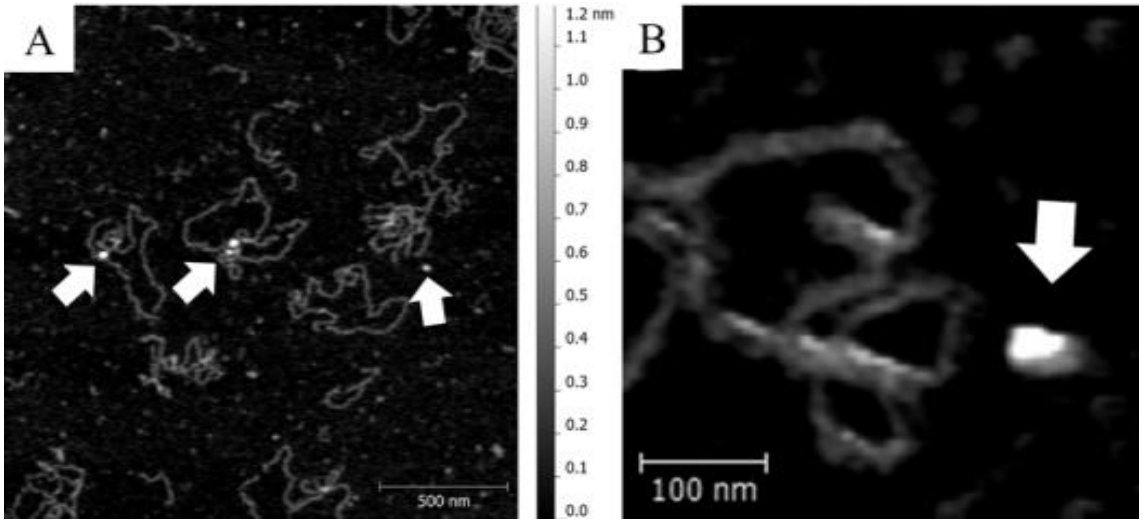


**Figure 6.11 Topographic images of DNA plasmids and EcoRV units, marked as white arrows. As can be seen by the lower magnification (A) and higher magnification image (B), EcoRV units appear as bright dots which can be both associated with DNA or unbound on the substrate.**

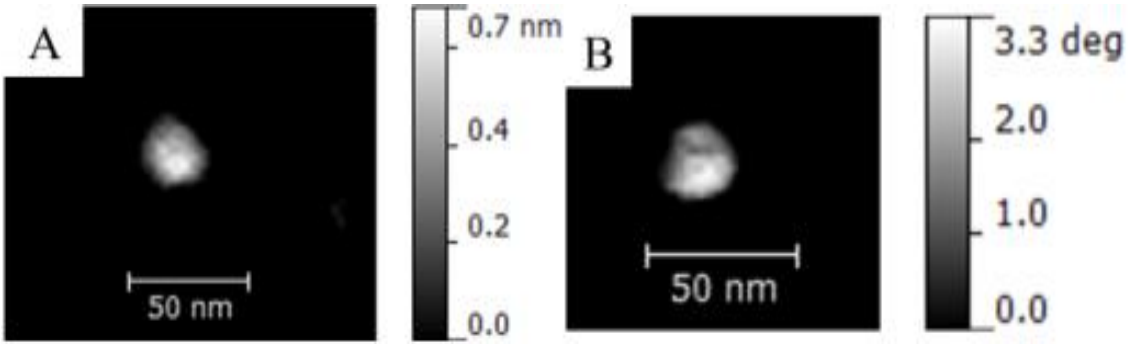


**Figure 6.12 EcoRV units seem to have rough surfaces, both when measured in the topographic channel (A) and in the phase channel (B). Background was removed to aid in the observation of differences on the EcoRV unit, shortening the height scale in the process.**

It is especially noteworthy that there are some differences in the same unit when comparing both channels of acquisition, what possibly relates with the existence of different structural subunits.

The measured dimensions of the enzyme, given its nanometric size, are bound to be influenced by tip convolution artefacts just as happened with DNA, which appeared as having less than the 2.5 nm of diameter, a phenomenon already mentioned in the discussion of the DNA measurements. In the images produced during this experiment, DNA frequently presented itself with diameters of roughly 15 nanometres when measured on the *x0y* plane and heights of roughly 0.5 nanometres, which is also in agreement with the previous chapters. On the other hand, EcoRV units were measured to have between 30 and 40 nanometres of width, with heights ranging between 1 and 2 nanometres.

Given what was learnt about tip convolution effects as well as the diameter and height difference between what was measured for DNA and the real dimensions of this molecule, it can be expected for EcoRV to surely be smaller in general, having width values below the 10 nanometres because when using the DNA strands as calibration feature, it was observed that, in average, EcoRV units appeared to be between two and four times taller than those, leading to the prediction that the real structure of an EcoRV unit should be a spherical or ovoid structure with widths between 3 and 8 nm.

It was also noted that in some situations, structures too large to be EcoRV units were seen. Topographic imaging showed the existence of complex structures, what was confirmed by phase imaging, as seen in Figure 6.13, something that is coherent with the possibility that the enzymes when not reacting or denatured, may aggregate.

On Figure 6.14, an endonuclease that appears to have just reacted with a DNA molecule can be observed. In this figure, the location of the DNA molecule is easily spotted coming down from the top right corner of the scan area, and disappearing below an EcoRV unit. However, the continuity of this strand is interrupted: no DNA strand comes out of the other side of the

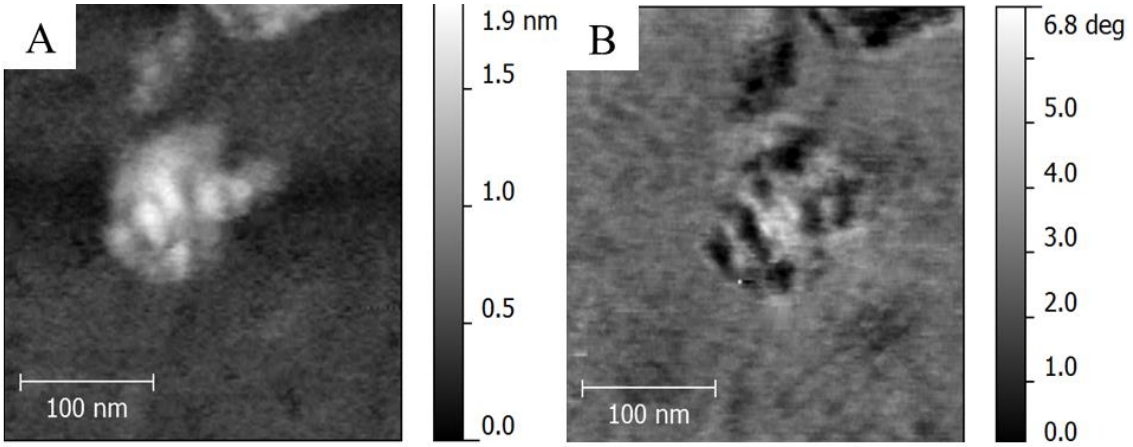


**Figure 6.13 Topographic (A) and phase (B) imaging of an EcoRV aggregate resting against the substrate.**

endonuclease. Another end of a DNA molecule appears 20 nanometres away from this enzyme, what suggests that before the area was scanned with the AFM probe, that specific endonuclease had recognized a target sequence in that location, cleaved it, and that the resulting ends of the DNA molecule stood around the EcoRV unit.

Concerning the attempts to image the endonuclease reaction, several images were produced and analysed, especially in the samples where the EcoRV/DNA ratio was higher. In spite of the limitations related with orientation mentioned in the preparation chapter, it was possible to observe rare situations in which some DNA-EcoRV conjugates exhibit a subtle bend along the enzyme structure, such as in Figure 6.15, and which were measured to be of roughly 42.9 ± 3 degrees.

Over the course of the three hours in which these sets of images were produced, it was also visually confirmed that the amount of linearized plasmids and DNA fragments forming was rising. Although not so obvious during scans probably due to the inexistence of a liquid environment, rendering molecules more immotile, these fragments because quite easy to spot

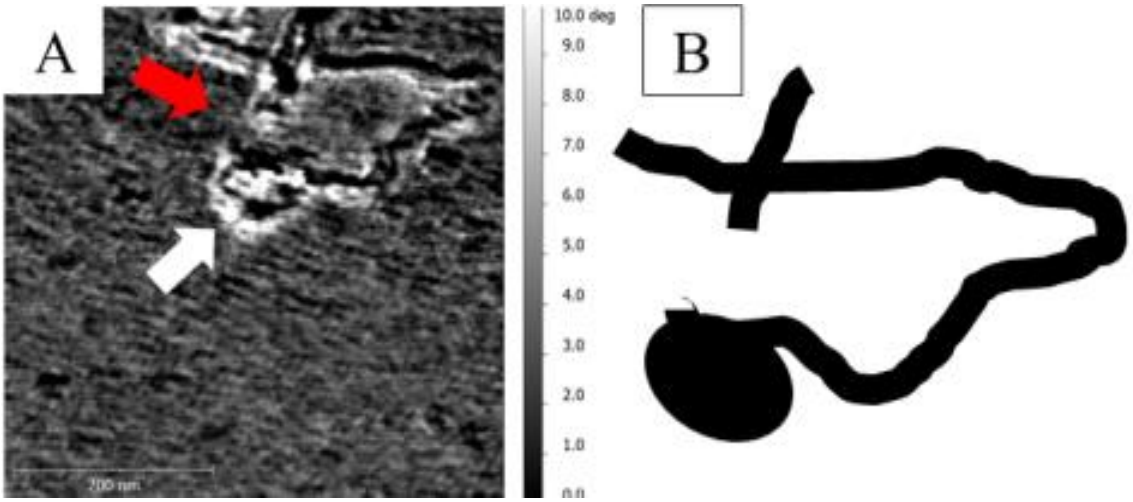


**Figure 6.14 – Phase image (A) and diagram (B) of the DNA-EcoRV conjugate. The red arrow in the phase image marks the zone where DNA was cleaved and the white one the location of the EcoRV unit.**

after each time a new drop with EcoRV solution was left to react for some minutes, possibly by improving mobility by creating a short window of opportunity in which the reaction medium was liquid, allowing some DNA molecules to drift over the surface, shift orientation or just detach from the original position, making it remarkably easy to point the location of plasmids that had suffered restriction enzyme digestion.

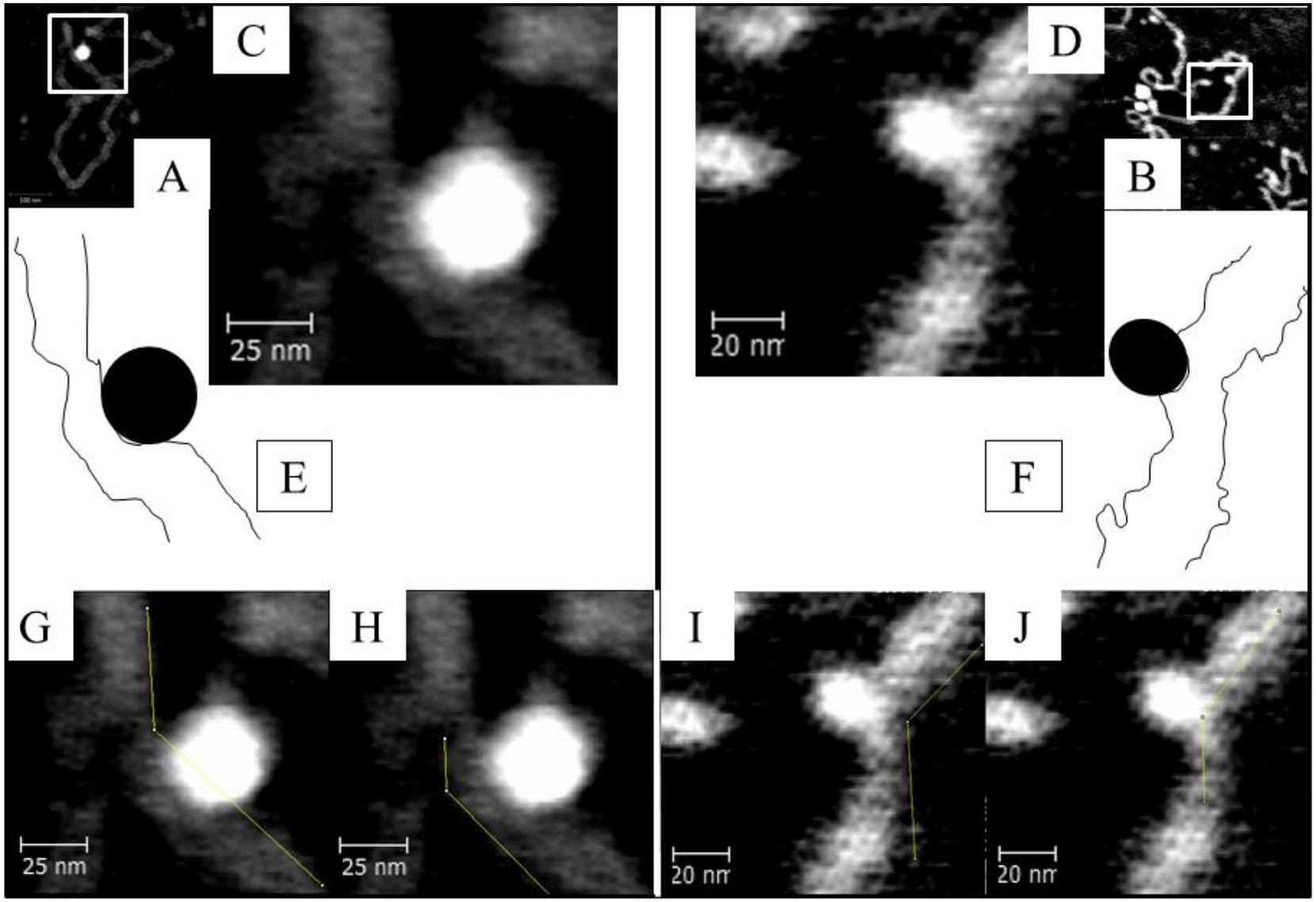


**Figure 6.15 – Examples of possible DNA-EcoRV cleavage complexes. The squared area in images A and B shows the areas which generated images C and D. Bend angle measurements were done in these, as represented by the yellow lines in images G, H, I and J. Images. E and F represent schematics of these complexes.**

## 6.7. Discussion

AFM EcoRV measurements were successful in giving information on morphology, dimensions, behaviour and interactions with DNA. The enzymes were imaged connected to DNA, in situations in which there were no cuts in the strands, what is possible if the endonuclease was scouting the DNA molecule in search for the target sequence. However, there were some situations in which EcoRV appears conjugated with a DNA strand which was cut in an adjacent position. Overall, several plasmids went from a circular configuration, to becoming linearized. Especially after the third hour of observation, smaller fragments appeared, what is backed by previous restriction mapping of the HRPII plasmid, which indicates two cleavage sites, one of the reasons why both this enzyme and plasmid were chosen[131].

On the subject of the bend produced by the reaction, in some situations where DNA and EcoRV were bound, there was a DNA bend of 42.9 ± 3 degrees. This is in agreement with the existing literature, which cites a 50 degree bend as a fundamental mechanism in the cleavage reaction of this endonuclease[143]. Actually, while the formation of the specific complex generates a bend of roughly 50 degrees, it is known that in case of non-specific binding (such as when scouting the molecule) no kink should be observed[142]. However, in order to confirm this observation, further studies would be necessary in order to collect more data and evaluate if the bends reported are in fact related to the formation of cleavage conjugates. The use of plasmid DNA for this experiment can also be changed in favour of smaller and linear DNA molecules in the future, which, unlike plasmid DNA, would tend to stay straighter during scans. This allows studying this phenomenon in conditions that favour its detection. To conclude, the data, especially due to the amount of collected angles, is not statistically relevant and therefore does not allow concluding that the bend is generated by the cleavage mechanism, but serves as an indication that AFM is a suitable technique to detect this phenomenon.

The enzyme also appears to not undergo any conformational changes in any situation. Whether linked to DNA molecules, scouting or cleaving the molecule, or when on an unreactive form, laying on the mica, EcoRV units always exhibited the same structure.

Because of the known dimensions of single proteins, and predicting that the structure of the enzymes would probably be spherical or elliptical, it was expected for measurements to suffer some tip convolution effects, especially because the AFM probes used in standard conditions are not of the highest resolution. Nevertheless, this allowed proposing approximate dimensions of EcoRV by making a comparison between the measured and the real values of the DNA height[105].

Concerning morphology, the enzyme was shown to exhibit a macro structure with a rough surface, with several bulges and bumps on its surface, both in its active and free forms. Using the Protein Data Bank (PDB)[*], a comparison between the published structure of the EcoRV endonuclease and the structure and morphology observed under the AFM, could be established. The fact that both the dimensions and shape of the enzyme could be seen through the topographic and phase channels, in spite of the average resolution of the probes, proves that this endonuclease does not have a flat surface. Instead, the EcoRV unit exhibits several bulges coherent with the existing references which have catalogued the existence of different protein domains connected to each other, together forming the enzyme unit. The dimensions of EcoRV are referred on PDB as having three main axes with lengths of 4.8 nm, 4.84 nm and 6.36 nm, what falls under the dimensions proposed above: an enzyme having axis larger than three nanometres and smaller than eight[150,151]. However, the level of resolution attained by x-ray crystallography, the main technique used to map proteic domains in structural biology studies, is still much higher than what can be attained by AFM. Nevertheless, if there were no protein domain maps or any previous knowledge of the structure of EcoRV, these experiments would be enough to, at least, show that this endonuclease a complex structure, made up of different domains that establish bonds between each other, forming a compact structure.

[*] http://www.rcsb.org

# 7. Conclusions

The main objective of this dissertation was to demonstrate the potential of atomic force microscopy as a fundamental tool to study and interpret biological phenomena at the nanoscale, and also as a means to analyse and obtain information from bionanotechnological systems. With this purpose in mind, AFM probe modifications were initially focused as a means to increase the resolution when it depends exclusively on the probe, or as a means to shield them from oxidizing or reducing conditions.

All AFM probe coating modifications were done using a gold-palladium mixture. Coating modifications of the probes' reflective side to increase the generated voltage on the photodiode were studied. Observations indicated that photodiode voltage improved by between 10 and 15% and images were sharper than those obtained using unmodified silicon probes throughout all channels of acquisition. Tip coatings were also explored in order to extend the possibility of using silicon probes in liquid operation at more extreme pH values, by protecting the tip from redox reactions. While it could be shown that these probes potentially have slightly enlarged radius compared to unmodified versions, this fact should only affect resolution significantly below micrometric scan areas. Nanofabrication by focused ion beam milling was also approached as a mean of sharpening probes. Triangular probes were sharpened from having side walls with roughly 60 degrees to nearly 90 degrees. Measurements with modified and unmodified probes showed considerable improvements when operating with focused ion beam milled probes. These showed improved lateral resolution and less tip convolution effects, especially above micrometric scales, leading to more realistic measurements. The reflective side coated probes were used in high magnification imaging, where they produced consistently better results than images acquired with unmodified probes under the same conditions.

The behaviour of several biomolecules, such as DNA or proteins in different situations, was also documented. Insight on the nature of AFM's operation and methods of acquiring data was also gathered, something fundamental to understand artefacts and how they affect measurements. Experiments also underlined that while producing low magnification images in air is possible just after some days of training, imaging at high magnification scales, especially in liquid media, requires a solid understanding of the fundamentals of operation of an AFM in order to be able to decode the outputted data and to adapt scan conditions and parameters to assure the highest quality in results..

Insulin was used in initial studies of replicability of AFM operation in air and in liquid, with images of insulin liquid being similar to those obtained in air. Similarly, it was possible to distinguish morphological features such as the torsion of the insulin fibrils in both media. Dimension measurements of insulin fibrils, such as width, height and torsion pitch are very

similar to published references and even allowed to extrapolate some of the synthesis conditions, illustrating the potentiality that being able to see and document these microscopic structures at nanometric scale may hold.

Gold nanoparticles with ca. 14 nm in diameter and functionalized with biomolecules were also studied. Small modifications, such as the use of vacuum or desiccators together with the published sample preparation, were developed and were successful in improving the quality of measurements of these samples. For functionalization studies, two batches of functionalised nanoparticles were used: while both had a mercaptoundecanoic acid (MUA) ligand, one of the batches was also conjugated with bovine serum albumin (BSA) protein adsorbed to the MUA capping. AFM measurements had the objective of proving that the protein capping was enough to provoke an average nanoparticle diameter shift when larger functionalization agents were used. After comparing both batches of nanoparticles, the results indicated that the objective was successfully completed, with the most used and quoted as faithful method (individually detecting the diameter of all the nanoparticles in an image and plotting the diameter dispersions in dependence of the type of functionalization) showing differences in the mean diameter of both batches of roughly two nanometres.

Concerning DNA, its molecules appeared in images as expected - a string like structure – and its measured dimensions match what is described in the literature. Although in several images the width was clearly over the described 2.5 nm while height could be below this value, these differences were also observed in studies spawning several years and operation using different AFM probes. Width values are explained by tip convolution effects while smaller height values by compression of the DNA molecule and a background rise due to buffer contaminants. High resolution imaging of DNA using modified probes also made possible to sharpen measured dimensions to near real values consistently and to detect and image the major groove periodicity in air. The sample preparation used for the observation of DNA was successful in air, anchoring the DNA in place, and avoiding the formation of overly condensed structures similar to curled wire, often associated with other methods. This aided in the acquisition of images of individual molecules, allowing visualization of plasmid disposition and how it arranged itself against the substrate. When done in liquid, the quality of the images was low due to the enlarged radius of the tip in initial tries or due to incompatibility between a state of the art biology probe and a not so recent material science oriented AFM. This incompatibility is clear when it is considered that the laser width of this AFM is approximately 80 µm while these probes were 40 µm in length and 16 µm in width, what introduces sensitivity issues and light artefacts, ultimately leading to acquiring bad quality images. Single stranded DNA was also generated and imaged, where it was possible to document how DNA molecules form

aggregated structures resembling entangled wires after they are melted, due to the establishing intra- and inter-molecule base pair homology.

The DNA-EcoRV endonuclease reaction measurements were performed in air, where the enzyme ability to react is diminished so it was decided to add steps in which a liquid medium containing reaction buffer could favour reaction. Measurements showed the morphology of the enzyme as well as the formation of cleavage complexes, in which the fifty degree bend associated with this specific conjugate could be documented in some situations. However, given the reduced amount of conjugates measured, it cannot be said that the bends unequivocally arise from the DNA-EcoRV conjugate and further studies would be required to defend this assertion. Linearization of the plasmids throughout all images show incontestable proof that plasmid cleavage occurred during the experiment

Gathering all the experimental work done and after analysing the results, it can be said that the vast majority of the objectives of this dissertation were fulfilled, since that the initially proposed objectives were met, ranging from successful probe modifications to imaging of biological conjugates. The only objective that wasn't fulfilled to the point it was desired was operation in liquid. Although the training in it was complete and the knowledge needed to operate in this medium was acquired, plans to engage in more demanding and high resolution imaging had to be abandoned due to physical limitations imposed by the AFM and the probes available at the time.

# 8. Future prospects

The most interesting key concepts that were addressed in this dissertation, which will surely merit development on the field of bionanotechnology in the future, are liquid media operation and AFM probe modifications.

The future of liquid AFM - that does not depend on the obvious technological progression over time in which more efficient, trustworthy and sensitive electronic components or higher frequency processors are designed, devised and released to the market - relies on continuing to study and experiment on best types of liquid media and buffers. These can be chosen taking into account the object of study as well as substrate choice and functionalization, in order to aid in the anchoring of the object of study and avoid the chances of considerable movement during the scan (fundamental to produce high resolution images), but without locking the objects of study in such a way it becomes impossible for it to react with its surroundings.

On the other hand, AFM probes, as one of the defining element of atomic force microscopy, are another target for an approach aiming at improving resolution, the nature of data acquisition and, by extension, the quality of the results. Modifications following the same line of work as those presented in this essay are something that merits more studies in the future, just as the fabrication and types of AFM probes will need to advance in order to attain even greater resolutions and the ability to analyse the properties of an object of study. The focused ion beam approach is interesting because, in future equipment its resolution can perhaps even get to smaller values, which can be explored in milling modifications similar to the ones described above, in order to generate probes that over time tend to become virtually impossible to generate measurements plagued by tip convolution effects.

At the moment, the manual production using FIB technology is not so cost advantageous since that commercial high resolution tips cost along the lines of 75 dollars per piece, while the operation of a FIB gun for one hour (limited by the ion source lifetime) can rise to 90 dollars per hour. However, the choices of modification sometimes compensate because this way the probes can be fabricated on demand and with specific characteristics. If there was need for a conductive AFM probe with 3 nm of radius but there’s nothing available for that purpose, such probes could just be left to be fabricated automatically during a two hour break and, upon returning to the laboratory, any imperfections that may stand out can quickly be dealt with, leaving the operator with a custom AFM probe ready for operation.

Finally, the resonance frequency of an AFM probe when operating in alternate and non-contact modes also affects the resolution and precision of the measurements. It can be said that

an hypothetical AFM probe operated at a given resonance frequency will, in theory, have the ability to produce images with higher resolution than if it is operated at frequencies below this value. The evolution of the usual resonance peaks of commercial AFM probes over the years, from values such as dozens of kilohertz to megahertz, in nowadays non-contact modes of operation that use state of the art probes, arises from this. It is therefore obvious that the tendency in the near future will also rest on the development of probes that, with the same drive voltages, can deliver results at higher natural harmonic frequencies of operation. Nowadays, it is possible to do sample measurements at higher frequencies than the usual small hundreds of kilohertz - especially 300 KHz - in which the commercial available average resolution alternate contact AFM probe usually produces the best results - by manually tuning the AFM probe to be oscillated at harmonics of the natural frequency. However, in some situations the drive voltage required is not enough to produce a tuning with enough quality to detect the sample satisfactorily.

To finish this dissertation and after all the laboratory work with the AFM, I believe that exploring and developing liquid media operation, especially with regards to substrate functionalization and sample preparation will have to be further studied in order to open the possibility of single molecule studies in those media of operation. Also probe modifications, not only from the top-to-bottom approach presented herein, but especially from bottom-to-top approaches, such as functionalization with specific molecules and nanostructures, are already becoming a great mean to assist in the collection of novel information. While being a very interesting approach to further the application of microscopy applied to biology and biology related structures and/or phenomena in general, these will also allow to broaden the type of information that can be acquired from a given sample.

Given today's and the near-future interest and demand of equipment, protocols and machinery able to deliver satisfactory analysis of novel nanotechnological devices, the (even more) important asset that the AFM is and will become comes as something obvious and predictable. This statement is especially strong when considering bionanotechnological and nanotechnological structures and devices, as well as the possibility of modifying them by, for example, nanolithography, nanoindentation or nanoassembly. To conclude, the AFM has the possibility of doing this and more, especially keeping in mind that, unlike electron microscopes or scanning tunnelling microscopes which could demand extensive sample preparation, AFMs allow the study of samples with virtually no preparation, while merging the possibility of outstanding resolution with a variety of non-destructive but equally informative techniques.

# 9. References


1. Corliss, J. A Salute to Antony van Leeuwenhoek of Delft, Most Versatile 17th Century Founding Father of Protistology. *Protist* **153,** 177–190 (2002).

2. Wilson, E. *The Cell in Development and Inheritance*. (Macmillian, 1928).

3. Bordenave, G. Louis Pasteur (1822-1895). *Microbes and infection / Institut Pasteur* **5,** 553–60 (2003).

4. Roingeard, P. Viral detection by electron microscopy: past, present and future. *Biology of the cell / under the auspices of the European Cell Biology Organization* **100,** 491–501 (2008).

5. Beck, A. Unknown health impact of nanotech worries some. *Reuteurs* (2007). at <http://www.reuters.com/article/2007/11/14/us-nano-idUSN1221261620071114>. Acessed 14 September 2013.

6. NanoAction Project. *Principles for the Oversight of Nanotechnologies and Nanomaterials*. (2007).

7. Coco, M. & Bainbridge, W. *Nanotechnology: Societal Implications - Maximizing Benefits for Humanity*. (National Science Foundation, 2003).

8. Yao, N. & Wang, Z. *Handbook of microscopy for nanotechnology*. (Springer, 2005).

9. Buratto, S. Near-field scanning optical microscopy. *Current Opinion in Solid State & Material Science* **1,** 485–492 (1996).

10. Lipson, S. Why is super-resolution so inefficient? *Micron* **34,** 309–312 (2003).

11. Kuznetsova, Y., Neumann, A. & Brueck, S. R. Imaging interferometric microscopy-approaching the linear systems limits of optical resolution. *Optics express* **15,** 6651–63 (2007).

12. Zhang, Y.-J., Zheng, C.-W. & Xiao, H.-C. Improving the resolution of a solid immersion lens optical system using a multiphase Fresnel zone plate. *Optics & Laser Technology* **37,** 444–448 (2005).

13. Jinschek, J. R. & Helveg, S. Image resolution and sensitivity in an environmental transmission electron microscope. *Micron* **43,** 1156–68 (2012).

14. Smith, D. J. The realization of atomic resolution with the electron microscope. *Reports on Progress in Physics* **60,** 1513–1580 (1997).

15. Goldstein, J., Newbury, D., Joy, D. & Lyman, C. *Scanning electron microscopy and X-ray microanalysis*. (Kluwer Academic/Plenum Publishers, 2003).

16. Müller, S., Aebi, U. & Engel, A. What transmission electron microscopes can visualize now and in the future. *Journal of structural biology* **163,** 235–45 (2008).

17. Thach, R. & Thach, S. Damage to biological samples caused by the electron beam during electron microscopy. *Biophysical journal* 204–210 (1971).

18. Aassime, a. *et al.* Anti-charging process for electron beam observation and lithography. *Microelectronic Engineering* **110,** 320–323 (2013).

19. Cazaux, J. e-Induced secondary electron emission yield of insulators and charging effects. *Nuclear Instruments and Methods in Physics Research Section B: Beam Interactions with Materials and Atoms* **244,** 307–322 (2006).

20. Bell, D. & Erdman, N. *Low voltage electron microscopy: Principles and applications*. (Wiley, 2012).

21. Mallon, J. & Whelan, P. F. Calibration and removal of lateral chromatic aberration in images. *Pattern Recognition Letters* **28,** 125–135 (2007).

22. Marks, L. What Are the Resolution Limits in Electron Microscopes? *Physics* **6,** 82 (2013).

23. Khursheed, A. Ultimate resolution limits for scanning electron microscope immersion objective lenses. *Optik - International Journal for Light and Electron Optics* **113,** 67–77 (2002).

24. Bogner, A., Jouneau, P.-H., Thollet, G., Basset, D. & Gauthier, C. A history of scanning electron microscopy developments: towards "wet-STEM" imaging. *Micron* **38,** 390–401 (2007).

25. Bloebaum, R. D., Skedros, J. G., Vajda, E. G., Bachus, K. N. & Constantz, B. R. Determining mineral content variations in bone using backscattered electron imaging. *Bone* **20,** 485–90 (1997).

26. Munroe, P. R. The application of focused ion beam microscopy in the material sciences. *Materials Characterization* **60,** 2–13 (2009).

27. Kim, C.-S., Ahn, S.-H. & Jang, D.-Y. Review: Developments in micro/nanoscale fabrication by focused ion beams. *Vacuum* **86,** 1014–1035 (2012).

28. Davies, S. & Khamsehpour, B. Focused ion beam machining and deposition for nanofabrication. *Vacuum* **47,** 455–462 (1996).

29. Giannuzzi, L. & Stevie, F. A review of focused ion beam milling techniques for TEM specimen preparation. *Micron* **30,** 197–204 (1999).

30. Binnig, G. & Rohrer, H. Scanning tunneling microscopy. *IBM Journal of research and development* **126,** 236–244 (1983).

31. Stadelmann, T. Antidot superlattices in InAs-GaSb double heterostructures: transport studies. (2006). Thesis submitted for the degree of Doctor of Philosophy, Oxford College.

32. West, P. *Introduction to atomic force microscopy*. (Published at www.paulwestphd.com/book.html, 2006).

33. Eaton, P. & West, P. *Atomic Force Microscopy*. (Oxford University Press, 2010).

34. Kindt, J. H., Fantner, G. E., Cutroni, J. a & Hansma, P. K. Rigid design of fast scanning probe microscopes using finite element analysis. *Ultramicroscopy* **100,** 259–65 (2004).

35. Sulchek, T. *et al.* Parallel atomic force microscopy with optical interferometric detection. *Applied Physics Letters* **78,** 1787 (2001).

36. Gotszalk, T., Grabiec, P. & Shi, F. Fabrication of multipurpose AFM/SCM/SEP microprobe with integrated piezoresistive deflection sensor and isolated conductive tip. *Microelectronic Engineering* **42,** 477–480 (1998).

37. Butt, H.-J., Cappella, B. & Kappl, M. Force measurements with the atomic force microscope: Technique, interpretation and applications. *Surface Science Reports* **59,** 1–152 (2005).

38. Cappella, B. & Dietler, G. Force-distance curves by atomic force microscopy. *Surface Science Reports* **34,** 1–104 (1999).

39. Jiang, P., Xie, S., Pang, S. & Gao, H. The combining analysis of height and phase images in tapping-mode atomic force microscopy: a new route for the characterization of thiol-coated gold nanoparticle. *Applied Surface Science* **191,** 240–246 (2002).

40. Hafner, J. H., Cheung, C. L., Woolley, T. & Lieber, C. M. Structural and functional imaging with carbon nanotube AFM probes. *Progress in biophysics and molecular biology* **77,** 73–110 (2001).

41. West, P. & Starostina, N. in *Pacific Nanotechnology Training Manual* 1–12 (Pacific Nanotechnology, 2002).

42. Gu, G.-Y. & Zhu, L.-M. Motion control of piezoceramic actuators with creep, hysteresis and vibration compensation. *Sensors and Actuators A: Physical* **197,** 76–87 (2013).

43. Russell, P., Batchelor, D. & Thornton, J. SEM and AFM: complementary techniques for high resolution surface investigations. *Bruker* (2001). at <www.bruker.jp/axs/nano/imgs/pdf/AN046.pdf>

44. Bloo, M. L., Haitjema, H. & Pril, W. O. Deformation and wear of pyramidal, silicon-nitride AFM tips scanning micrometre-size features in contact mode. *Measurement* **25,** 203–211 (1999).

45. Jalili, N. & Laxminarayana, K. A review of atomic force microscopy imaging systems: application to molecular metrology and biological sciences. *Mechatronics* **14,** 907–945 (2004).

46. Martin, Y., Williams, C. C. & Wickramasinghe, H. K. Atomic force microscope–force mapping and profiling on a sub 100-Å scale. *Journal of Applied Physics* **61,** 4723 (1987).

47. Korayem, M. H., Kavousi, a. & Ebrahimi, N. Dynamic analysis of tapping-mode AFM considering capillary force interactions. *Scientia Iranica* **18,** 121–129 (2011).

48. Hansma, P. & Cleveland, J. Tapping mode atomic force microscopy in liquids. *Applied Physics Letters* **2,** 18–20 (1994).

49. Bustamante, C., Rivetti, C. & Keller, D. J. Scanning force microscopy under aqueous solutions. *Current opinion in structural biology* **7,** 709–16 (1997).

50. Ando, T., Uchihashi, T. & Fukuma, T. High-speed atomic force microscopy for nano-visualization of dynamic biomolecular processes. *Progress in Surface Science* **83,** 337–437 (2008).

51. Gaczynska, M. & Osmulski, P. AFM of biological complexes: what can we learn? *Current opinion in colloid & interface science* **13,** 351–367 (2008).

52. Garcia, S. *et al.* Cutinase activity in supercritical and organic media: water activity, solvation and acid–base effects. *The Journal of Supercritical Fluids* **35,** 62–69 (2005).

53. Jiang, Q. *et al.* DNA origami as a carrier for circumvention of drug resistance. *Journal of the American Chemical Society* **134,** 13396–403 (2012).

54. Serry, F. Improving the accuracy of AFM force measurements: The thermal tune solution to the cantilever spring constant problem. *Application Notes. Veeco Instrument Inc.: Santa Barbara* (2005).

55. Ohler, B. Cantilever spring constant calibration using laser Doppler vibrometry. *The Review of scientific instruments* **78,** 063701 (2007).

56. Fuierer, R. in *Procedural Operation "Manualette"* (Asylum Research) (2009).

57. Boothroyd, D. Atomic force microscopy set to answer fundamental questions in a range of fields. *newelectronics* (2013).

58. Giessibl, F. J. AFM's path to atomic resolution. *Materials Today* **8,** 32–41 (2005).

59. Radmacher, M., Cleveland, J. P., Fritz, M., Hansma, H. G. & Hansma, P. K. Mapping interaction forces with the atomic force microscope. *Biophysical journal* **66,** 2159–65 (1994).

60. Carvalho, F., Martins, I. C. & Santos, N. C. Atomic force microscopy and force spectroscopy on the assessment of protein folding and functionality. *Archives of biochemistry and biophysics* **531,** 116–27 (2013).

61. Linke, W. a & Grützner, A. Pulling single molecules of titin by AFM--recent advances and physiological implications. *Pflügers Archiv : European journal of physiology* **456,** 101–15 (2008).

62. Borgia, A., Williams, P. M. & Clarke, J. Single-molecule studies of protein folding. *Annual review of biochemistry* **77,** 101–25 (2008).

63. Liu, H., Fu, S., Zhu, J. Y., Li, H. & Zhan, H. Visualization of enzymatic hydrolysis of cellulose using AFM phase imaging. *Enzyme and Microbial Technology* **45,** 274–281 (2009).

64. Kim, J. M., Jung, H. S., Park, J. W., Lee, H. Y. & Kawai, T. AFM phase lag mapping for protein–DNA oligonucleotide complexes. *Analytica Chimica Acta* **525,** 151–157 (2004).

65. Shukla, V. K. & Kumar, S. Investigations of environmental induced effects on AlQ3 thin films by AFM phase imaging. *Applied Surface Science* **253,** 6848–6853 (2007).

66. Lekka, M. Atomic force microscopy: A tip for diagnosing cancer. *Nature nanotechnology* **7,** 691–2 (2012).

67. Brown, J. *et al.* Electrically conducting, ultra-sharp, high aspect-ratio probes for AFM fabricated by electron-beam-induced deposition of platinum. *Ultramicroscopy* **133C,** 62–66 (2013).

68. Chen, L., Cheung, C., Ashby, P. & Lieber, C. Single-walled carbon nanotube AFM probes: optimal imaging resolution of nanoclusters and biomolecules in ambient and fluid environments. *Nano Letters* **4,** 1725–1731 (2004).

69. Gan, Y. Invited Review Article: A review of techniques for attaching micro-and nanoparticles to a probe's tip for surface force and near-field optical measurements. *Review of Scientific Instruments* **081101,** (2007).

70. Berquand, A. & Ohler, B. Common Approaches to Tip Functionalization for AFM-Based Molecular Recognition Measurements. *Bruker* (2010).

71. Konoplev, B. G., Ageev, O. a., Smirnov, V. a., Kolomiitsev, a. S. & Serbu, N. I. Probe modification for scanning-probe microscopy by the focused ion beam method. *Russian Microelectronics* **41,** 41–50 (2012).

72. Menozzi, C. *et al.* Focused ion beam as tool for atomic force microscope (AFM) probes sculpturing. *Journal of Physics: Conference Series* **126,** 012070 (2008).

73. Zeiss. Auriga, your crossbeam workstation. *29 May 2012* (2012). at <http://microscopy.zeiss.com/microscopy/en_de/products/fib-sem-instruments/auriga.html>. Acessed 2 September 2013.

74. Winzer, A., Kraft, C., Bhushan, S., Stepanenko, V. & Tessmer, I. Correcting for AFM tip induced topography convolutions in protein-DNA samples. *Ultramicroscopy* **121,** 8–15 (2012).

75. Lyubchenko, Y. L. Preparation of DNA and nucleoprotein samples for AFM imaging. *Micron (Oxford, England : 1993)* **42,** 196–206 (2011).

76. Bustamante, C. *et al.* Circular DNA molecules imaged in air by scanning force microscopy. *Biochemistry* **31,** 22–6 (1992).

77. Ziou, D. & Horé, A. Reducing aliasing in images: a PDE-based diffusion revisited. *Pattern Recognition* **45,** 1180–1194 (2012).

78. Humphreys, G. & Pharr, M. in *Physically Based Rendering* (Morgan Kaufmann, 2004).

79. Joshi, M. V., Chaudhuri, S. & Panuganti, R. Super-resolution imaging: use of zoom as a cue. *Image and Vision Computing* **22,** 1185–1196 (2004).

80. Peled, A., Castro, J. & Weiss, W. J. Atomic force and lateral force microscopy (AFM and LFM) examinations of cement and cement hydration products. *Cement and Concrete Composites* **36,** 48–55 (2013).

81. Méndez-Vilas, A., Bruque, J. M. & González-Martín, M. L. Sensitivity of surface roughness parameters to changes in the density of scanning points in multi-scale AFM studies. Application to a biomaterial surface. *Ultramicroscopy* **107,** 617–25 (2007).

82. Smith, N., Kinion, D., Tesch, P. & Boswell, R. A high brightness plasma source for focused ion beam applications. *Microscopy and Microanalysis* **13,** 180–181 (2007).

83. D'Costa, N. P. & Hoh, J. H. Calibration of optical lever sensitivity for atomic force microscopy. *Review of Scientific Instruments* **66,** 5096 (1995).

84. Seeley, R., Stephens, T. & Tate, P. *Anatomy and Physiology*. (McGraw-Hill International, 2008).

85. Pettersson, T. & Konttinen, Y. T. Amyloidosis-recent developments. *Seminars in arthritis and rheumatism* **39,** 356–68 (2010).

86. Ivanova, M. I., Sievers, S. a, Sawaya, M. R., Wall, J. S. & Eisenberg, D. Molecular basis for insulin fibril assembly. *Proceedings of the National Academy of Sciences of the United States of America* **106,** 18990–5 (2009).

87. Kurouski, D., Dukor, R. K., Lu, X., Nafie, L. a & Lednev, I. K. Spontaneous inter-conversion of insulin fibril chirality. *Chemical communications (Cambridge, England)* **48,** 2837–9 (2012).

88. Kurouski, D., Deckert-Gaudig, T., Deckert, V. & Lednev, I. K. Structure and composition of insulin fibril surfaces probed by TERS. *Journal of the American Chemical Society* **134,** 13323–9 (2012).

89. Borsali, R., Pecora, R., Cohen-Bouhacina, T. & Maali, A. in *Soft Matter Characterization* (SpringerReference, 2008).

90. Jiao, Y. & Schäffer, T. E. Accurate height and volume measurements on soft samples with the atomic force microscope. *Langmuir: the ACS journal of surfaces and colloids* **20,** 10038–45 (2004).

91. Salunke, D. & Veerapandian, B. Structural transformations in protein crystals caused by controlled dehydration. *Journal of Biosciences* **8,** 37–44 (1985).

92. Kurouski, D., Dukor, R. K., Lu, X., Nafie, L. a & Lednev, I. K. Normal and reversed supramolecular chirality of insulin fibrils probed by vibrational circular dichroism at the protofilament level of fibril structure. *Biophysical journal* **103,** 522–31 (2012).

93. Seitz, O. *et al.* Preparation and characterisation of gold nanoparticle assemblies on silanised glass plates. *Colloids and Surfaces A: Physicochemical and Engineering Aspects* **218,** 225–239 (2003).

94. Georgiev, P. *et al.* Implementing atomic force microscopy (AFM) for studying kinetics of gold nanoparticle's growth. *Colloids and Surfaces A: Physicochemical and Engineering Aspects* **434,** 154–163 (2013).

95. Veigas, B. *et al.* Noble Metal Nanoparticles for Biosensing Applications. *Sensors* **12,** 1657–1687 (2012).

96. Tiwari, P. M., Vig, K., Dennis, V. a. & Singh, S. R. Functionalized Gold Nanoparticles and Their Biomedical Applications. *Nanomaterials* **1,** 31–63 (2011).

97. Ito, A., Shinkai, M., Honda, H. & Kobayashi, T. Medical application of functionalized magnetic nanoparticles. *Journal of bioscience and bioengineering* **100,** 1–11 (2005).

98. Baptista, P. *et al.* Gold nanoparticles for the development of clinical diagnosis methods. *Analytical and bioanalytical chemistry* **391,** 943–950 (2008).

99. Turkevich, J., Stevenson, P. & Hillier, J. A study of the nucleation and growth processes in the synthesis of colloidal gold. *Discussions of the Faraday Society* **11,** (1951).

100. Kimling, J. *et al.* Turkevich method for gold nanoparticle synthesis revisited. *The journal of physical chemistry. B* **110,** 15700–7 (2006).

101. Eaton, P., Doria, G., Pereira, E., Baptista, P. V. & Franco, R. Imaging gold nanoparticles for DNA sequence recognition in biomedical applications. *IEEE transactions on nanobioscience* **6,** 282–8 (2007).

102. Verslues, P. E., Agarwal, M., Katiyar-Agarwal, S., Zhu, J. & Zhu, J.-K. Methods and concepts in quantifying resistance to drought, salt and freezing, abiotic stresses that affect plant water status. *The Plant journal : for cell and molecular biology* **45,** 523–39 (2006).

103. Nanotechnology Characterization Laboratory of the National Cancer Institute. *Measurement of Nanoparticles Using Atomic Force Microscopy*. (National Institute of Standards and Technology, U.S. Department of Commerce, 2009).

104. Boyd, R. D., Pichaimuthu, S. K. & Cuenat, A. New approach to inter-technique comparisons for nanoparticle size measurements; using atomic force microscopy, nanoparticle tracking analysis and dynamic light scattering. *Colloids and Surfaces A: Physicochemical and Engineering Aspects* **387,** 35–42 (2011).

105. Klapetek, P., Valtr, M., Nečas, D., Salyk, O. & Dzik, P. Atomic force microscopy analysis of nanoparticles in non-ideal conditions. *Nanoscale research letters* **6,** 514 (2011).

106. Baalousha, M. & Lead, J. R. Characterization of natural and manufactured nanoparticles by atomic force microscopy: Effect of analysis mode, environment and sample preparation. *Colloids and Surfaces A: Physicochemical and Engineering Aspects* **419,** 238–247 (2013).

107. Gebregeorgis, A., Bhan, C., Wilson, O. & Raghavan, D. Characterization of Silver/Bovine Serum Albumin (Ag/BSA) nanoparticles structure: morphological, compositional, and interaction studies. *Journal of colloid and interface science* **389,** 31–41 (2013).

108. Rao, A. *et al.* Characterization of nanoparticles using Atomic Force Microscopy. *Journal of Physics: Conference Series* **61,** 971–976 (2007).

109. West, P. E., Olson, K. S., Mecartney, M. L. & Starostina, N. Tip Dilation and AFM Capabilities in the Characterization of nanoparticles. *Journal of Materials* **59,** 12–16 (2007).

110. Gomes, I. *et al.* Controlled adsorption of cytochrome c to nanostructured gold surfaces. *Journal of Nanoparticle Research* 1321 (2012).

111. Moreno-Herrero, F., Colchero, J. & Baró, a M. DNA height in scanning force microscopy. *Ultramicroscopy* **96,** 167–74 (2003).

112. UniprotKB. P02769 (ALBU_BOVIN). *Serum albumin precursor - Bos taurus (Bovine)* (2013). at <http://www.uniprot.org/uniprot/P02769>. Acessed 13 September 2013.

113. UniprotKB. P00004 (CYC_HORSE). *Cytochrome C - Equus Caballus (Horse)* (2013). at <http://www.uniprot.org/uniprot/P00004>. Acessed 13 September 2013.

114. Benedetti, C. E. *et al.* Plasmodium falciparum histidine-rich protein II binds to actin, phosphatidylinositol 4,5-bisphosphate and erythrocyte ghosts in a pH-dependent manner and undergoes coil-to-helix transitions in anionic micelles. *Molecular and Biochemical Parasitology* **128,** 157–166 (2003).

115. Garcia, M., Kirimoama, S. & Marlborough, D. Immunochromatographic test for malaria diagnosis. *The Lancet* **2,** 1549 (1996).

116. NZYTech. NzyTech, Lda. - Genes and Enzymes - NZYMaxiprep. *8 January 2013* (2013). at <https://www.nzytech.com/site/vmchk/DNA-RNA-Purification-kits/NZYMaxiprep>. Acessed 13 September 2013.

117. Sun, L., Zhao, D., Zhang, Y., Xu, F. & Li, Z. DNA adsorption and desorption on mica surface studied by atomic force microscopy. *Applied Surface Science* **257,** 6560–6567 (2011).

118. Argaman, M., Golan, R., Thomson, N. H. & Hansma, H. G. Phase imaging of moving DNA molecules and DNA molecules replicated in the atomic force microscope. *Nucleic acids research* **25,** 4379–84 (1997).

119. Baicu, S. C. & Taylor, M. J. Acid-base buffering in organ preservation solutions as a function of temperature: new parameters for comparing buffer capacity and efficiency. *Cryobiology* **45,** 33–48 (2002).

120. Hansma, H. G. & Laney, D. E. DNA binding to mica correlates with cationic radius: assay by atomic force microscopy. *Biophysical journal* **70,** 1933–9 (1996).

121. Savvateev, M. Preparation of DNA molecules for AFM measurements. *26 October 2008* (2008). at <http://www.ntmdt.com/spm-notes/view/preparation-of-samples-of-dna-molecules-for-afm-measurements>. Acessed 1 September 2013

122. Lyubchenko, Y. L. & Shlyakhtenko, L. S. AFM for analysis of structure and dynamics of DNA and protein-DNA complexes. *Methods (San Diego, Calif.)* **47,** 206–13 (2009).

123. Ivanova, E. P., Pham, D. K., Brack, N., Pigram, P. & Nicolau, D. V. Poly(L-lysine)-mediated immobilisation of oligonucleotides on carboxy-rich polymer surfaces. *Biosensors & bioelectronics* **19,** 1363–70 (2004).

124. Medalia, O., Englander, J., Guckenberger, R. & Sperling, J. AFM imaging in solution of protein-DNA complexes formed on DNA anchored to a gold surface. *Ultramicroscopy* **90,** 103–12 (2001).

125. Rivetti, C. & Codeluppi, S. Accurate length determination of DNA molecules visualized by atomic force microscopy: evidence for a partial B- to A-form transition on mica. *Ultramicroscopy* **87,** 55–66 (2001).

126. Thundat, T., Allison, D. P. & Warmack, R. J. Stretched DNA structures observed with atomic force microscopy. *Nucleic acids research* **22,** 4224–8 (1994).

127. Mou, J., Czajkowsky, D. M., Zhang, Y. & Shao, Z. High resolution atomic-force microscopy of DNA: the pitch of the double helix. **371,** 279–282 (1995).

128. Maeda, Y., Matsumoto, T. & Kawai, T. Observation of single-and double-stranded DNA using non-contact atomic force microscopy. *Applied surface science* 400–405 (1999).

129. Hansma, H. & Revenko, I. Atomic force microscopy of long and short double-stranded, single-stranded and triple-stranded nucleic acids. *Nucleic Acids …* **24,** 713–720 (1996).

130. Cerreta, A., Vobornik, D. & Dietler, G. Fine DNA structure revealed by constant height frequency modulation AFM imaging. *European Polymer Journal* **49,** 1916–1922 (2013).

131. Oliveira, M. Caracterização de um sistema de sobrexpressão para a Histidine-rich protein II de Plasmodium falciparum. (2012). Project essay f the Bachelor of Biochemistry course, Faculdade de Ciências e Tecnologia, UNL.

132. Rychlik, W., Spencer, W. J. & Rhoads, R. E. Optimization of the annealing temperature for DNA amplification in vitro. *Nucleic acids research* **18,** 6409–12 (1990).

133. Saiki, R. K. *et al.* Primer-directed enzymatic amplification of DNA with a thermostable DNA polymerase. *Science (New York, N.Y.)* **239,** 487–91 (1988).

134. Adamcik, J., Klinov, D. V, Witz, G., Sekatskii, S. K. & Dietler, G. Observation of single-stranded DNA on mica and highly oriented pyrolytic graphite by atomic force microscopy. *FEBS letters* **580,** 5671–5 (2006).

135. Hamon, L. *et al.* High-resolution AFM imaging of single-stranded DNA-binding (SSB) protein-DNA complexes. *Nucleic acids research* **35,** e58 (2007).

136. Hansma, H. G., Laney, D. E., Bezanilla, M., Sinsheimer, R. L. & Hansma, P. K. Applications for atomic force microscopy of DNA. *Biophysical journal* **68,** 1672–7 (1995).

137. Adamcik, J., Valle, F., Witz, G., Rechendorff, K. & Dietler, G. The promotion of secondary structures in single-stranded DNA by drugs that bind to duplex DNA: an atomic force microscopy study. *Nanotechnology* **19,** 384016 (2008).

138. Kowalczyk, S. W., Tuijtel, M. W., Donkers, S. P. & Dekker, C. Unraveling single-stranded DNA in a solid-state nanopore. *Nano letters* **10,** 1414–20 (2010).

139. Perona, J. J. Type II restriction endonucleases. *Methods (San Diego, Calif.)* **28,** 353–64 (2002).

140. Watson, J. *et al. Molecular Biology of the Gene*. (Cold Spring Harbor Laboratory Press, 2003).

141. Lewin, B. *Genes*. (Pearson Prentice Hall, 2003).

142. Pingoud, A. & Jeltsch, A. Structure and function of type II restriction endonucleases. *Nucleic Acids Research* **29,** 3705–3727 (2001).

143. Pingoud, a, Fuxreiter, M., Pingoud, V. & Wende, W. Type II restriction endonucleases: structure and mechanism. *Cellular and molecular life sciences : CMLS* **62,** 685–707 (2005).

144. Kovall, R. a & Matthews, B. W. Type II restriction endonucleases: structural, functional and evolutionary relationships. *Current opinion in chemical biology* **3,** 578–83 (1999).

145. Bujnicki, J. M., Radlinska, M. & Rychlewski, L. Polyphyletic evolution of type II restriction enzymes revisited: two independent sources of second-hand folds revealed. *Trends in biochemical sciences* **26,** 9–11 (2001).

146. Aggarwal, A. Structure and function of restriction endonucleases. *Current Opinion in Structural Biology* **5,** 11–19 (1995).

147. Morris, G. J., Goodrich, M., Acton, E. & Fonseca, F. The high viscosity encountered during freezing in glycerol solutions: effects on cryopreservation. *Cryobiology* **52,** 323–34 (2006).

148. Datskos, P. G. & Sauers, I. Detection of 2-mercaptoethanol using gold-coated micromachined cantilevers. *Sensors and Actuators B: Chemical* **61,** 75–82 (1999).

149. Pastré, D. *et al.* Specific DNA-protein interactions on mica investigated by atomic force microscopy. *Langmuir : the ACS journal of surfaces and colloids* **26,** 2618–23 (2010).

150. Protein Data Bank. RCSB Protein Data Bank - RCSB PDB - 2B0D Structure Summary. (2011). at <www.rcsb.org/pdb/explore/explore.do?structureId=2B0D>

151. Hiller, D., Rodriguez, A. M. & Perona, J. J. Non-cognate enzyme-DNA complex: structural and kinetic analysis of EcoRV endonuclease bound to the EcoRI recognition site GAATTC. *Journal of molecular biology* **354,** 121–36 (2005).

152. Nzytech. NZYMaxiprep. *8 January 2013* 3–4 (2013). at <https://www.nzytech.com/site/index.php?option=com_virtuemart&Itemid=26&file_id=1045&lang=en&page=shop.getfile&product_id=359>- Acessed 1 September 2013.

# I. Appendix

## a. Material and methods

### i. General information on equipment, operation and facilities

Atomic force, scanning electron and focused ion beam microscopy operations were done in the Laboratory of Nanofabrication of CENIMAT/I3N at Faculdade de Ciências e Tecnologia of Universidade Nova de Lisboa (FCT-UNL). The AFM operated was an Asylum Research MFP-3D Stand Alone (Figure I.1A) and the SEM-FIB was a dual beam Zeiss Auriga (Figure I.1B). 2D AFM images and analysis were generated with Gwyddion (gwyddion.net), 3D renderings and thermal captures were done in Igor Pro (Wavemetrics) and bend angle measurements on ImageJ (http://rsb.info.nih.gov/ij/). Some images had their scale range limited to aid in their visualization in the printed dissertation.

"Standard conditions" refers to the operation of the AFM in intermittent contact mode in air, using Olympus AC160TS (Olympus Corporation) rectangular silicon probes with aluminium reflex coating. These have advertised resonant frequency of 300 kHz, spring constant of 26 N/m and average tip radius of 9 nm ± 2 nm.

Nanoparticle functionalization, *E. coli* growth and cultivation as well as plasmid DNA extraction and isolation were done in the Bionano@Requimte laboratory, led by Prof. Dr. Ricardo Franco. An initial attempt at plasmid isolation was done at Pólo 1 of the Centro de Investigação em Genética Molecular Humana (CIGMH), led by Prof. Dr. Pedro Viana Baptista. Both facilities are located in FCT-UNL in the Chemistry and Life Science departments, respectively.

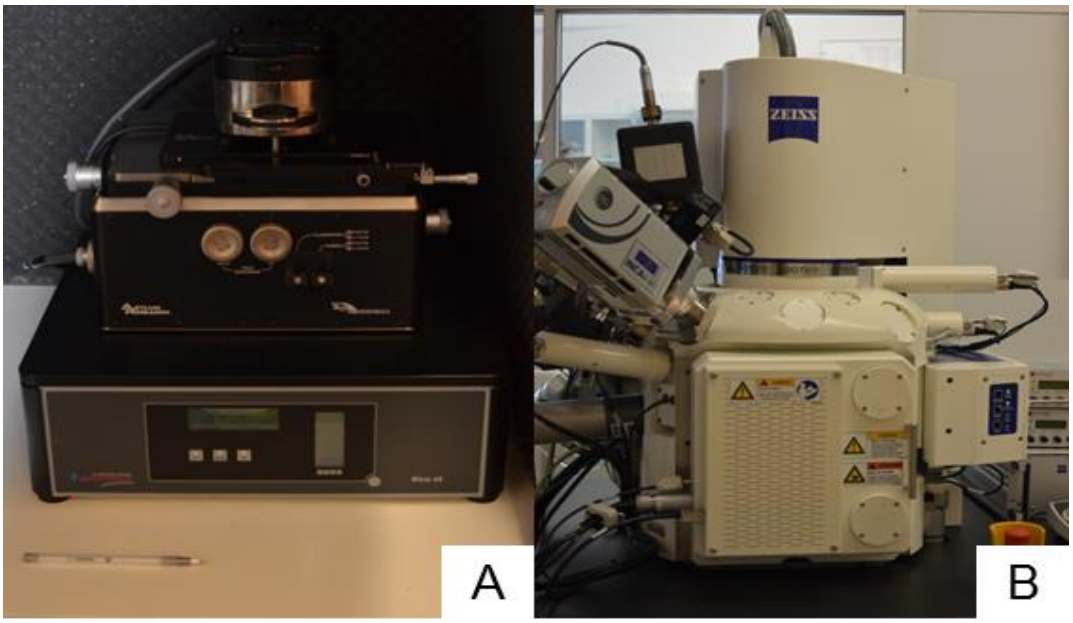


**Figure I.1 – Microscope equipment used in this dissertation's experiments: the AFM Asylum Research MFP-3D Stand Alone(A) and the dual beam SEM-FIB Zeiss Airuga (B).**

## ii. AFM probe index

**Table I.1 – Specifications of AFM probes used in this dissertation as advertised by manufacturers.**

| Manufacturer | Name of model | Freq.* (kHz) | Spring const. (N/m) | Tip radius (nm) |
|---|---|---|---|---|
| **Olympus** | AC160TS | 300 (100-200) | 26 (11-54) | 9 ± 2 |
| **Olympus** | BL-AC40TS | 130 (50-350) | 0.25 (0.05-1.2) | 9 ± 2 |
| **Budgetsensors** | ContAl | 13 ± 4 | 0.07 to 0.4 | <10 |
| **Olympus** | SSS-NCH | 320 (250-390) | 42 (21-78) | 3 ± 2 |
| **Budgetsensors** | Tap300Al | 300 ± 100 | 20 to 75 | <10 |
| **Olympus** | TR800PB | 68 (48-94) | 0.61 (0.29-1.27) | 42 ± 12 |

## iii. AFM probe modifications

### *1. Probe milling with FIB and imaging with modified probes*

AFM probe dimension modifications were done with the FIB (30 keV, currents ranging between 100 pA and 1nA). The probes selected were Budgetsensors ContAl (Innovative Solutions Bulgaria Ltd). Measurements to evaluate the modifications were done in the AFM in contact mode in scan areas with a side of 12 μm at 512x512 pixel resolution with a scan rate of 1 Hz. SEM images were acquired at 5 keV in SE channel.

### *2. Probe coating*

Probes were coated with a gold palladium mixture deposited in a Quorum Q150T ES by plasma arch discharge. 8 nm of material were deposited. The probes selected were Budgetsensors Tap300Al-G for the horizontal resolution experiments.

### *3. Measurement conditions*

Measurements to evaluate horizontal resolution were done in intermittent contact mode in scan areas with a side of 1 μm at 512x512 pixel resolution with a scan rate of 1 Hz. EDS images to verify coatings were collected in the SEM using a Inca X-act detector (Oxford Instruments). Backside coating was done in the same conditions but on an Olympus SSS-NCH. Measurements to evaluate the imaging capability of this probe are discussed in the DNA measurement section concerning the enhanced resolution probe (Chapter 0).

## iv. Insulin measurement conditions

Insulin samples on mica were donated by AtomicForce F&E GmbH (Asylum Research). One drop of 50 μl was dropped on the sample and on the AFM probe to form a liquid bridge in which tip-sample interaction occurred. Images were collected in standard conditions and also in liquid intermittent-contact mode, in which Olympus TR800PB probes were used.

* Free resonant frequency. Values in liquid are lower.

Measurements were done in scan areas with sides of 1 and 2 μm at 256x256 or 512x512 pixel resolution with a scan rate of 1 Hz.

## v. Material and methods of gold nanoparticle functionalization

### *1. Gold nanoparticle conjugate synthesis and functionalization*

Monodispersed gold nanoparticles were synthetized by the Turkevich method, generating particles with diameters of 13.9 ± 3.3 at 15.3 nM. The diameter value was determined by TEM (Figure I.2) by Dr. Pedro Quaresma of Instituto Superior Técnico of Universidade de Lisboa. AuNPs were reacted with MUA at a molar ratio of 5000 MUA to AuNPs and split in two groups, from which one was reacted with BSA, in order to become coated with this protein. Conjugates were stored at 3 nM. Zeta-potential studies of electrostatic adsorption of BSA to nanoparticles reported by the laboratory where nanoparticles were functionalized claimed that BSA saturation on the AuNP surface occurred at BSA:AuNP molar ratios of roughly one hundred. Freshly cleaved mica was selected as substrate and fifty microlitres of nanoparticle solution were pipetted onto it. Samples were left overnight in a desiccator in vacuum and different concentrations between 0.3 and 3 nM were tested for imaging.

### *2. Measurement conditions*

All images were acquired in standard conditions, with scan areas with sides between 300 nm and 10 μm, scan rates between 0.7 and 1 Hz at 256x256 pixel resolution. Measurements were done throughout several days under the same room conditions and preparation protocols, except where pointed.

### *3. Nanoparticle dimension measurements*

Nanoparticle dimension measurements were produced automatically by the Gwyddion software. The height points refer to the distance from the background average.

## vi. Material and methods of DNA related experiments

### *1. DNA plasmid extraction*

The organism selected to be used for the growth of DNA was an *E. coli* strain containing the HRPII (Histidine Rich Protein II) overexpression plasmid. Bacteria were grown in ampicillin rich LB-agar medium plaques in order to only favour the survival and growth of bacterial colonies which contained the HRPII plasmid (containing an ampicillin-resistance gene), and left to grow overnight at 37ºC. Isolated viable colonies were selected to inoculate 200 ml of LB growth medium divided by four 50 ml Erlenmeyers flasks (one as control) and left to grow overnight at 37ºC, with shaking at 210 rpm in an orbital incubator (Sanyo). The specific extraction protocol can be consulted in the NZYtech product brochure[152]. Following the

information given by the isolation kit manufacturer, the amount of DNA extracted was of roughly 1 mg, which was then diluted in 8 ml of molecular biology water, creating a DNA suspension with a predicted final concentration of 125 μg of DNA per millilitre. The DNA solution was divided into one millilitre kept at 4ºC and ready to be use at any time while the rest was kept at -20ºC.

### *2. DNA preparation for AFM measurements*

Anchoring of DNA was achieved by dissolving a DNA suspension in a buffer composed by 5 mM of HEPES and between 1 and 5 mM of nickel chloride, to a final concentration of 1μg of DNA per millilitre. The first DNA measurements were performed using an unknown bacterial plasmid as DNA source kindly donated by the Centro de Investigação em Genética Molecular Humana of FCT-UNL. All further measurements were done the HRPII plasmid. Both samples were treated with HEPES and nickel chloride on different concentrations but on the range of those mentioned. The resulting mixture was pipetted onto a freshly cleaved mica sheet and left to adsorb for five minutes. Measurements were done after this incubation period. In case of air measurements, the DNA solution was rinsed off using molecular biology water and dried using a gun of filtered nitrogen gas. In case of liquid measurements, it would be used straight for measurements. In some cases, a drop of molecular biology grade water was used to immerse the AFM probe.

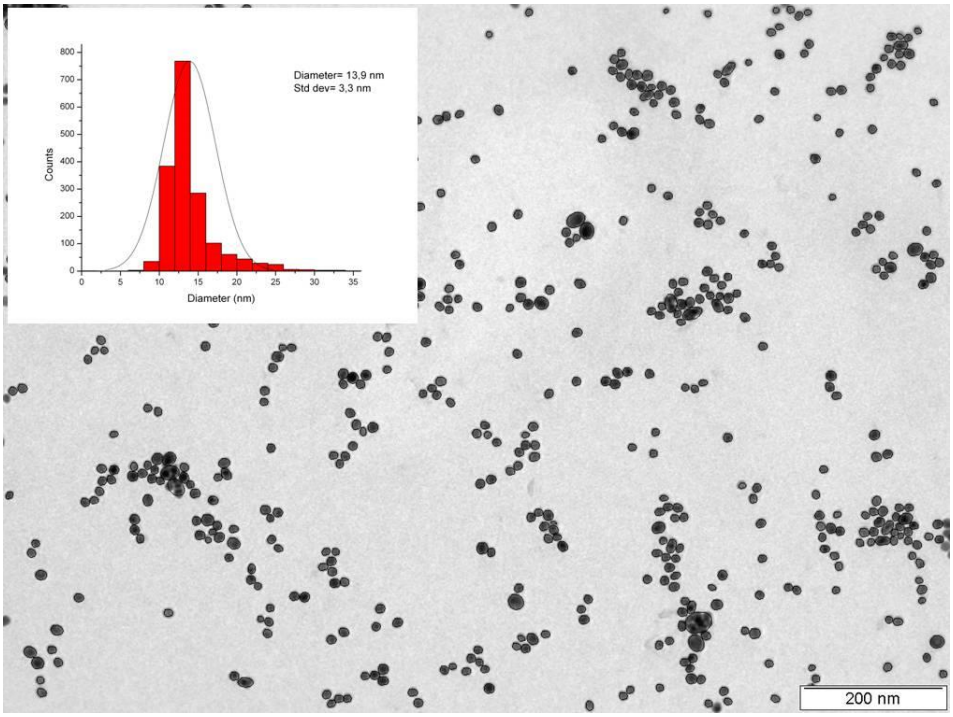


**Figure I.2 – Transmission electron microscope image of the gold nanoparticles before functionalization.**

### *3. Preparation of ssDNA*

Single stranded DNA was prepared following the same procedures as described in the section above. The heating treatment to trigger the melting of the dsDNA into ssDNA consisted in immersing an eppendorf with the DNA suspended in the HEPES-nickel chloride buffer in a water container at constant 95ºC. DNA was kept at these conditions between 5 and 10 minutes at the same time as the mica substrate on which it would be deposited was subjected to the same temperature. After this, DNA was deposited on the mica, rinsed with molecular biology grade water and dried with filtered nitrogen gas.

### *4. Preparation of DNA-EcoRV conjugates*

EcoRV endonuclease was purchased to Sigma-Aldrich in a storage and dilution buffer together with a digestion buffer. Each millilitre of endonuclease solution carries ten thousand units of endonuclease, with one unit being the amount of enzyme needed to completely cleave 1 µg of DNA over the course of one hour at 37º Celsius.

The DNA used in this experiment was prepared following the same procedure as described in subsection 2 of this section. The average mass of DNA deposited on the mica, since the quantity of solution dropped was 50 µl, can be approximated to be between 10 and 5 ng of DNA. EcoRV was diluted to 0.01 units per µl, what is equivalent to the amount needed to cleave 10 ng of DNA throughout one hour in perfect conditions. After the mica containing DNA on it was ready to be imaged, 50 µl of diluted enzyme solution were dropped on top of DNA and left to react for five minutes. After this, the substrate was dried using a filtered nitrogen

source and imaged. After one hour, the initial amount of EcoRV was doubled and after two hours it was tripled by adding 50 µl and leaving it to react for five minutes and drying it again.

### *5. Measurement conditions*

Attempts at liquid imaging of DNA molecule attempts were done with an Olympus TR800PB probe in intermittent-contact mode. Images were acquired in scan areas with sides between 500 nm and 2 µm, at scan rates between 0.7 and 1 Hz, and resolutions of 256x256, 512x512 and 1024x1024 pixels.

Air measurements were done in standard conditions as well as using Olympus SSS-NCH probes, some of which were modified with a gold-palladium coating on the reflective side. Images were acquired in scan areas with sides between 1 µm and 150 nm, at scan rates between 0.5 and 1 Hz, and resolutions of 256x256 and 512x512 pixels. Imaging of ssDNA structures was done in standard conditions in scan areas with sides between 1 to 10 µm, at scan rates between 0.7 and 1 Hz and resolutions of 256x256 and 512x512 pixels. Imaging of DNA-EcoRV samples was done in standard conditions, in scan areas with sides between 500 nm and 4 µm, at scan rates between 0.7 and 1 Hz and resolutions of 512x256 and 512x512.

### *6. DNA measurement method*

The DNA width was measured using profiles acquired throughout several images, which were acquired with the mentioned probes. The width was determined by obtaining a profile perpendicular to the molecule and evaluating the distance between the points at each side of the molecule profile that rested at half its maximum height. DNA height was measured by profiling as well, being the difference between the highest point in the profile and the background average.